Denoising and Demosaicking of Color Images

by

Mina Rafi Nazari

Thesis submitted to the
Faculty of Graduate and Postdoctoral Studies
In partial fulfillment of the requirements
For the Ph.D. degree in
Electrical and Computer Engineering

School of Electrical Engineering and Computer Science
Faculty of Engineering
University of Ottawa

Abstract

Most digital cameras capture images through Color Filter Arrays (CFA), and reconstruct the full color image from the CFA image. Each CFA pixel only captures one primary color component at each pixel location; the other primary components will be estimated using information from neighboring pixels. During the demosaicking algorithm, the unknown color components will be estimated at each pixel location. Most of the demosaicking algorithms use the RGB Bayer CFA pattern with Red, Green and Blue filters.

Some other CFAs contain four color filters. The additional filter is a panchromatic/white filter, and it usually receives the full light spectrum. In this research, we studied and compared different four channel CFAs with panchromatic/white filter, and compared them with three channel CFAs. An appropriate demosaicking algorithm has been developed for each CFA. The most well-known three-channel CFA is Bayer. The Fujifilm X-Trans pattern has been studied in this work as another three-channel CFA with a different structure.

Three different four-channel CFAs have been discussed in this research: RGBW-Kodak, RGBW-Bayer and RGBW- 5×5. The structure and the number of filters for each color are different for these CFAs. Since the Least-Square Luma-Chroma Demultiplexing method is a state of the art demosaicking method for the Bayer CFA, we designed the Least-Square method for RGBW CFAs. The effect of noise on different CFA patterns will be discussed for four channel CFAs. The Kodak database has been used to evaluate our non-adaptive and adaptive demosaicking methods as well as the optimized algorithms with the least square method.

The captured values of white (panchromatic/clear) filters in RGBW CFAs have been estimated using red, green and blue filter values. Sets of optimized coefficients have been proposed to estimate the white filter values accurately. The results have been validated using the actual white values of a hyperspectral image dataset.

A new denoising-demosaicking method for RGBW-Bayer CFA has been presented in this research. The algorithm has been tested on the Kodak dataset using the estimated value of white filters and a hyperspectral image dataset using the actual value of white

filters, and the results have been compared. The results in both cases have been compared with the previous works on RGB-Bayer CFA, and it shows that the proposed algorithm using RGBW-Bayer CFA is working better than RGB-Bayer CFA in presence of noise.

Acknowledgements

I would like to take this opportunity to thank my PhD supervisor, professor Eric Dubois, for his help and support throughout these years. His constant support, his advice in every steps of my degree and his deep knowledge helped me through this path. I would always be thankful for his supervision during my PhD degree.

Also I would like to thank all the committee members of my defense session, in addition to all my friends in the VIVA lab who have provided a friendly environment for research.

I would like to extend my gratitude to the kind staff of the engineering department at the University of Ottawa and my dear friends in the city of Ottawa.

I would like to thank my brother, for his kind support through my undergraduate and graduate studies. I was very fortunate to have him around during tough times of my PhD.

Last but not least, special thanks to my dear family which without their kind supports the completion of this work would not be imaginable.

Dedication

To my parents, my grandparents and my uncle, who always gave their unconditional love and support to me.

Table of Contents

List of Tables

List of Figures

Chapter 1

Introduction

1.1 Problem Statement

Imaging systems need three primary color coordinate values (tristimulus values) at each pixel location to reconstruct a full color image. Digital cameras usually capture images through a Color Filter Array (CFA). CFAs filter the incident light at each pixel sensor element with one of a certain number of color filters (usually three), and thus the captured image contains only one color component at each pixel, while the other components are missing. Through the demosaicking process, the missing color components at each pixel will be estimated and the full color image will be reconstructed.

CFAs vary based on their color filters, the number of sensor classes (different filters) in the CFA pattern, and their geometric structure. Most of the CFAs contain the three display primary colors (red, green and blue), while some others contain cyan, magenta and yellow. There are also some CFAs with an additional transparent filter. The arrangement of the color filters is different in each pattern, as well as the number of red, green, blue or other pixels in one period of the structure. The most common CFA is the Bayer structure containing two green pixels, one red and one blue in each template. See Figure 1.2 for some examples of CFA patterns.

Demosaicking refers to the process of reconstructing an image from incomplete samples.

The most basic demosaicking scheme relies on simple interpolation between neighboring pixel information within each class and its results are usually not adequate [2]. The performance of the demosaicking algorithm using different patterns and the robustness of the algorithm to noise are two major challenges in this field.

1.2 State of the art

Demosaicking algorithms and CFA design methods are both crucial steps to restore the image. In previous research, the demosaicking algorithms were mainly analyzed and implemented in the spatial domain. Demosaicking techniques in the spatial domain are categorized into two major groups. The first set of methods contains fixed interpolation techniques such as nearest neighbor, bilinear interpolation and bicubic interpolation on each color channel. Figure 1.1 shows the spatial multiplexing of sub-samples for the Bayer pattern. These methods usually provide satisfactory demosaicking results in smooth areas, but the results are not well estimated along edges or in high frequency areas. The second set of methods use inter-channel correlation with assumptions like smooth hue transition.

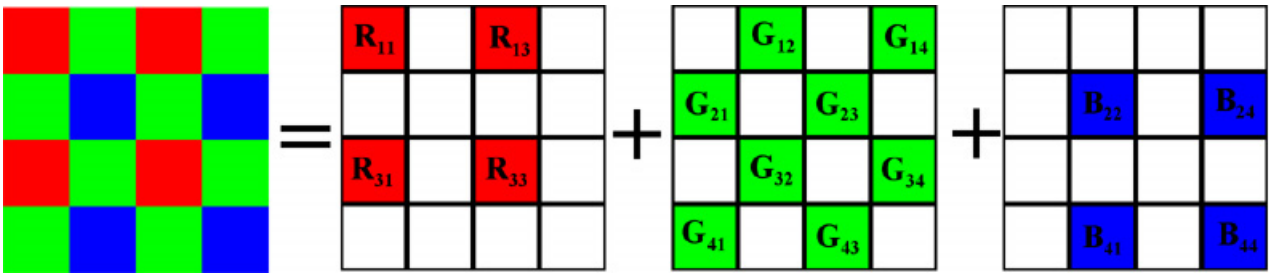

Figure 1.1: CFA spatial multiplexing of red, green and blue sub-samples for the Bayer pattern

As will be shown later, the CFA signal can be analyzed in the frequency domain, where it can be interpreted as the frequency division multiplexing of a baseband grayscale component called luma and color components at high spatial frequency referred to as chroma components. The number of chromas usually depend on the number of pixels/ filters in one period of the CFA pattern. The specific chroma in the low frequency band is called luma

or brightness component. The CFA signal can be modeled as a sum of one luma and a set of chromas at specific spatial frequencies. In the last decade, it has been demonstrated that the luma and chroma components are reasonably isolated in the frequency domain. Hence, demosaicking algorithms using a frequency domain representation became more competitive.

The most popular and simple CFA template is Bayer, and many existing demosaicking methods are working well on it. One of the best demosaicking methods for RGB-Bayer pattern in the frequency domain which outperforms other methods, is the adaptive least square luma-chroma demultiplexing method. In this method a set of least-square filters will be applied on an adaptive demosaicking method. The adaptive demosaicking algorithm for the Bayer pattern chooses one chroma component that locally has less overlap with luma, and reconstructs the other chromas adaptively. Some literature has proposed that using other patterns rather than Bayer might lead to better reconstruction results. Due to the overlapping effect between different channels in the CFA, some CFA structures might work better than Bayer. Some patterns have been proposed but they have not been fully studied, like the Fujifilm X-Trans pattern. Some others proposed and commercially implemented that use other color filters rather than red, green and blue might provide better signal to noise ratio.

Adding a clear filter instead of color filters to the CFAs has been proposed in some previous work. The clear or transparent filter is shown as panchromatic (P) or white (W) filter in different CFA patterns. Since color filters transmit only a fraction of the visible spectrum, they are more attenuated than panchromatic/white filter and it has been assumed that the panchromatic/white filters might have better signal to noise ratio. It has been proposed that adding panchromatic/white filters to the CFA results in better image quality or robustness to the noise. During the photo capturing process the photon noise will be introduced, and usually in lower light levels, signal to noise ratio will be lower. Through the white balancing process in digital cameras, the value of received noise in different color channels will be scaled differently. The value of scaled noise in the white channel is usually less than other color channels, so adding panchromatic/white filters to

the CFA might increase the overall signal to noise ratio in the image. Several patterns with clear filters have been proposed in literature, and the noise effect of these patterns needs to be fully studied.

1.3 Research hypothesis and objectives

Advanced demosaicking algorithms have been discussed in the literature for some three channel CFAs like Bayer. We propose that luma-chroma demultiplexing methods can be used to design good demosaicking methods for various other RGB CFAs such as Fujifilm X-Trans pattern.

Different types of four-channel RGBW CFAs have been introduced in previous work. The comparison between RGBW CFAs and the three-channel RGB CFAs, indicated that the quality of image and signal to noise ratio (SNR) were improved using the RGBW CFAs. We hypothesize that better overall image quality can be obtained for noisy camera sensor images using RGBW patterns, since the panchromatic/white filters pass more light, and therefore result in better signal to noise ratio. A basic demosaicking algorithm for different RGBW CFAs can be designed, and Luma-chroma demultiplexing methods can be used to design optimized demosaicking methods for noisy image with RGBW CFAs.

The objectives of this research are:

- To design demosaicking method based on the frequency domain analysis for three channel Fujifilm X-Trans pattern that have not been studied in the literature.
- To develop demosaicking systems for RGBW CFAs that demonstrate that RGBW CFAs have better performance in the presence of noise than RGB Bayer CFAs.
- To present a general method that can be used for luma-chroma demultiplexing with advanced RGB and RGBW CFA designs.

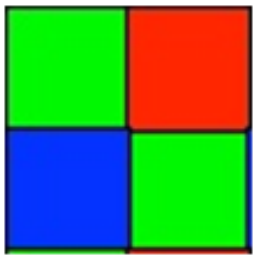

(a) RGB-Bayer pattern

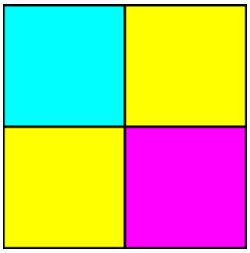

(b) CYYM pattern

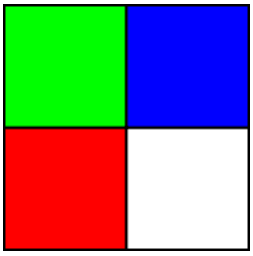

(c) RGBW-Bayer pattern

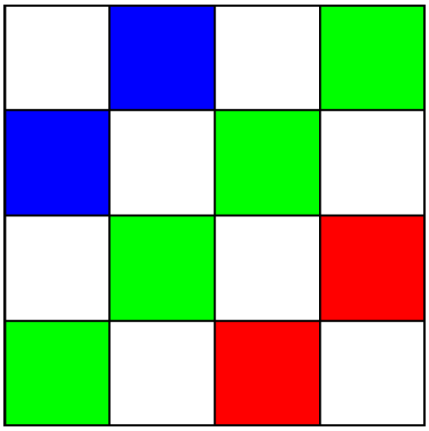

(d) RGBW-Kodak pattern

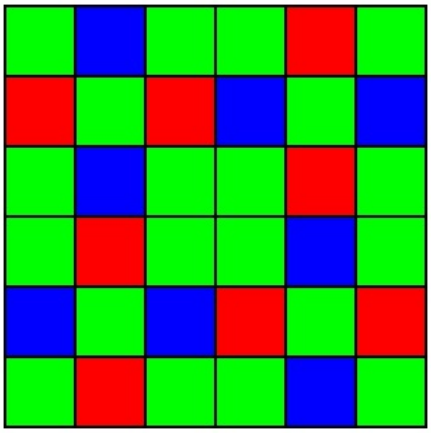

(e) Fujifilm X-Trans pattern

Figure 1.2: Sample CFA patterns

1.4 Proposed research

In this research, we decided to work on other proposed CFA patterns which had received little analysis and compare the results with Bayer. We want to study and optimize the reconstruction techniques for various new sampling structures, such as Fujifilm with three color components and different RGBW patterns with four color components. This study involves the design and optimization of appropriate non-adaptive and adaptive demosaicking methods. The noise effect on the RGBW patterns will be studied, and also the noise reduction step will be applied.

The Fujifilm cameras using different CFA patterns have been commercially successful, but there is little research on the performance of these structures. Due to the large number of RGB pixels in the Fujifilm X-Trans pattern [19], its complicated structure, its stated advantage and also lack of literature on this pattern, we were interested to work on it. It is a 6×6 pattern, and it contains 18 components in one period, so the overlap effect of the components in the frequency domain as well as designing an appropriate filter to extract each component, will be studied in this research. Hence, we modeled the demosaicking steps using the X-Trans Fujifilm pattern and simulated non-adaptive and adaptive demosaicking algorithms in Matlab software. A detailed optimization of filter parameters and the region of support has been addressed.

Peak signal to noise ratio (PSNR) and S-CIELAB are two validated metrics in this research area. Since other existing metrics have not been validated in this field, and our research does not consist of evaluation of different metrics, the reconstructed image quality is measured with these two metrics. So, the presented results in this research can be compared with previous demosaicking methods in terms of PSNR and S-CIELAB. Using these criteria, we will evaluate the amount of received noise, the false color artifact in the reconstructed image, and quality of the image in the sense of human vision perception.

Since the signal to noise ratio in color filters is lower than for clear filters, some other modified CFAs contain panchromatic/ white filters as well. The RGBW color filter arrays can improve the quality of the image, and improve the signal to noise ratio compared to the previous three-channel CFAs.

The simplest four-color CFA is RGBW-Bayer. Each R, G and B CFA pixel only captures one of the primary color component and white filters pass all three color components. The value of missing color components will be estimated with an appropriate demosaicking algorithm. A basic demosaicking scheme relies on linear interpolation of neighboring pixels color information [16].

As we mentioned, the color components are more isolated in the frequency domain, many demosaicking methods on the RGB Bayer pattern have been discussed in the frequency domain. Also, the least square method presented in [29],[18] optimized the chroma extraction step. The extracted chroma using least-square filter will reduce the false color effect in the reconstructed image. The least square method has been applied on the RGB-Bayer pattern in [29].

Different four channel CFAs have been studied and compared using interpolation methods in [2]. A new demosaicking algorithm based on [18] will be provided for RGBW Bayer, RGBW-Kodak and a 5×5 RGBW [45] in this research. Due to the specific structure of these CFAs and the number of different color filters, these three CFAs have been studied in this research.

The Kodak-RGBW [22] pattern has a large number of white filters and its adaptive and non-adaptive demosaicking algorithm will be discussed in this research. Furthermore, we have developed an adaptive demosaicking algorithm using the RGBW-Bayer pattern as a four-channel color filter array to enhance the quality of the display and signal to noise ratio value. The optimized least square method will be presented on this pattern as well. The additional filter array is spectrally nonselective and isolates luma and chroma information. The 5×5 RGBW CFA has been proposed in [45] and our demosaicking algorithm has been implemented on it. The results of these three patterns will be compared with the RGB-Bayer as well.

Often CFA images are noisy, and some demosaicking-denoising algorithms for RGB CFAs have been presented in literature. We would like to study the effect of demosaicking-denoising algorithm on RGBW CFAs in this research. A demosaicking-denoising algorithm will be proposed in this thesis, and the results will be compared with previous works.

The study on Fujifilm X-Trans pattern resulted a publication in International Conference of Image Processing (ICIP)-2014 [38], and the research conducted on RGBW-Kodak pattern has been published in SPIE/ IS&T Electronic Imaging-2015 conference [39]. The proposed demosaicking algorithms for different RGBW patterns have been published in SPIE/ IS&T Electronic Imaging-2016 conference [40].

1.5 Structure of the thesis

The rest of this thesis is organized as follows: Chapter 2 will review the related work in this area. Different CFAs will be discussed in Chapter 3 and appropriate adaptive and non-adaptive demosaicking algorithms will be presented in this section. The least square optimized demosaicking algorithm will also be presented in the same section. The experimental result using the proposed algorithm and the comparison between our method and the previous method will be carried out. An appropriate demosaicking algorithm using RGBW CFA for noisy images will be presented in Chapter 4. The conclusion and future work will be discussed in Chapter 5.

Chapter 2

Background and Related Work

There are two major issues regarding the quality of reconstructed color images from single-sensor digital cameras: CFA patterns and demosaicking algorithms. In this chapter different CFAs will be categorized based on their color filter types and placements. We will first explain the basic CFA formation and demosaicking algorithm steps. Different demosaicking algorithms that have been modeled in space and frequency domains will be introduced, and the state of the art demosaicking method will be reviewed. Finally, the effect of noise through the demosaicking process and the noise reduction methods will be discussed.

2.1 Representation of CFA formation

Virtually all the CFA patterns that are used or have been proposed are periodic; different periodic CFAs can be represented using specific lattices in the space domain, and the corresponding reciprocal lattices in the frequency domain. The general theory of CFA representation in the frequency domain has been described in [16], and the basis will be reviewed here.

In most cases, the CFA signal is sampled on a square lattice $\Lambda = \mathbb{Z}^2$ with reciprocal lattice $\Lambda^* = \mathbb{Z}^2$. We use the pixel spacing as the unit of length. A sublattice of lattice Λ shows the periodicity of the pattern. The following lattice Γ and it's corresponding

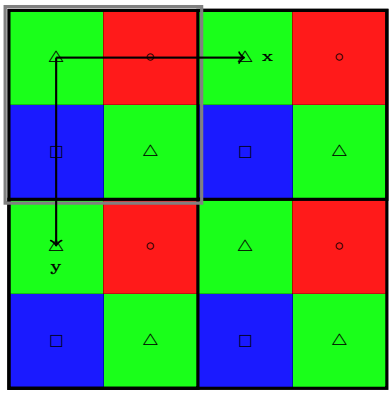

Figure 2.1: Bayer CFA sampling structure shows the constituent sampling structures Ψ_R ($\circ$), Ψ_G ($\triangle$) and Ψ_B ($\square$).

reciprocal lattice Γ^* represent the periodicity of the CFA pattern for Bayer. $\vee_\Gamma$ is the sampling matrix of Γ lattice. Figure 2.1 shows the periodicity of the Bayer CFA pattern, where

$$\vee_\Gamma = \begin{bmatrix} 2 & 0 \\ 0 & 2 \end{bmatrix}, \quad \vee_{\Gamma^*} = \begin{bmatrix} \frac{1}{2} & 0 \\ 0 & \frac{1}{2} \end{bmatrix}. \tag{2.1}$$

There are K elements in one period of the CFA pattern, where $K = |\det \vee_\Gamma|$. For example $K = 4$ for the Bayer pattern. We arrange the K elements of one period as the columns of a matrix $\boldsymbol{B}$. The order is arbitrary, but we usually put $[0, 0]^T$ as the first column. These points $\boldsymbol{b}_i$ are in fact coset representatives of sublattice Γ in Λ. The cosets themselves are $\boldsymbol{b}_i + \Gamma$, $i = 1, ..., K$. A possible matrix $\boldsymbol{B}$ for the Bayer pattern is

$$\boldsymbol{B} = \begin{bmatrix} 0 & 0 & 1 & 1 \\ 0 & 1 & 0 & 1 \end{bmatrix}. \tag{2.2}$$

The assignment of color channels to the cosets will be represented by matrix $\boldsymbol{J}$. This is a $K \times C$ matrix, where C is the number of channels in the pattern, i.e., the number of different color filters. An entry is equal to 1 for the sensor class assigned to this point, and

it is zero for other missing sensor classes at the same point. For Bayer pattern we have

$$\boldsymbol{J} = \begin{bmatrix} 0 & 1 & 0 \\ 1 & 0 & 0 \\ 0 & 0 & 1 \\ 0 & 1 & 0 \end{bmatrix} \tag{2.3}$$

where the columns correspond to R,G and B filters respectively. For each class of R, G and B, there will be a sampling structure Ψ_R, Ψ_G and Ψ_B as shown in Figure 2.1. The union of these three sampling structures forms the lattice Λ. Also, the CFA signal will be defined as follows in the space domain, using space domain multiplexing,

$$f_{CFA}[\mathbf{x}] = \sum_{i=1}^{K} f_i[\mathbf{x}] m_i[\mathbf{x}] \tag{2.4}$$

where $m_i[\mathbf{x}]$ is the indicator function for Ψ_i

$$m_i[\mathbf{x}] = \begin{cases} 1, \text{ x} \in \Psi_i \\ 0, \text{ x} \in \Lambda \backslash \Psi_i \end{cases}$$

.

and $f_i[\mathbf{x}]$ is the signal for the i^{th} sensor class defined over the entire latice Λ. m_i is periodic and represented by a discrete domain Fourier series

$$m_i[\mathbf{x}] = \sum_{k=1}^{K} \mathbf{M}_{ki} \exp(j2\pi \mathbf{x} \cdot \mathbf{d}_k) \tag{2.6}$$

$$\mathbf{M}_{ki} = \sum_{j=1}^{K} m_i[\mathbf{b}_j] \exp(-j2\pi \mathbf{b}_j \cdot \mathbf{d}_k). \tag{2.7}$$

The $\boldsymbol{d}_i$ are representatives of cosets of Λ^* in Γ^*. They are specified by the columns of a $2 \times K$ matrix $\boldsymbol{D}$. We can choose $\boldsymbol{d}_1 = [0 \quad 0]^T$. We have $\boldsymbol{D} = [\boldsymbol{d}_1, \boldsymbol{d}_2, \boldsymbol{d}_3, \boldsymbol{d}_4]$ for Bayer. The following matrix represents $\boldsymbol{D}$ for Bayer

$$\boldsymbol{D} = \frac{1}{2} \begin{bmatrix} 0 & 0 & 1 & 1 \\ 0 & 1 & 0 & 1 \end{bmatrix}. \tag{2.8}$$

The CFA value at each point can be represented as a sum of modulated chroma components plus a baseband luma component. The CFA signal is given by the following equation; it is derived by substituting 2.6 into 2.4 and rearranging it as follows:

$$f_{CFA}[\mathbf{x}] = \sum_{i=1}^{K} q_i[\mathbf{x}] \exp(j2\pi(\mathbf{x} \cdot \mathbf{d}_i)). \tag{2.9}$$

The luma and chroma components are obtained from the original RGB components by

$$\mathbf{q}[\mathbf{x}] = \boldsymbol{M}\mathbf{f}[\mathbf{x}] \tag{2.10}$$

$$\mathbf{f} = [f_1, f_2, f_3]^T = [R, G, B]^T \quad \text{and} \quad \mathbf{q} = [q_1, q_2, \cdots, q_K]^T, \tag{2.11}$$

where q_1 is called the luma component, and the q_2 to q_K are called chromas for each pattern. We can find matrix $\boldsymbol{M}$ coefficients based on the following equations

$$\boldsymbol{N} = 2\pi \boldsymbol{D}^T \times \boldsymbol{B} \tag{2.12}$$

$$\boldsymbol{M} = \frac{1}{K}(e^{-j \times \mathbf{N}})\boldsymbol{J} \tag{2.13}$$

where the exponential of the matrix is carried out term by term, and post multiplication by $\boldsymbol{J}$ is matrix multiplication.

The following matrix shows the calculated matrix $\boldsymbol{M}$ for Bayer,

$$\boldsymbol{M} = \frac{1}{4}\begin{bmatrix} 1 & 2 & 1 \\ -1 & 0 & 1 \\ 1 & 0 & -1 \\ -1 & 2 & -1 \end{bmatrix} \tag{2.14}$$

and the following equations show the luma and chroma components for the Bayer pattern using the matrix $\boldsymbol{M}$ coefficients

$$q_1[x] = \frac{1}{4}f_1[x] + \frac{1}{2}f_2[x] + \frac{1}{4}f_3[x]$$

$$q_2[x] = -\frac{1}{4}f_1[x] + \frac{1}{4}f_3[x]$$

$$q_3[x] = \frac{1}{4}f_1[x] - \frac{1}{4}f_3[x]$$

$$q_4[x] = -\frac{1}{4}f_1[x] + \frac{1}{2}f_2[x] - \frac{1}{4}f_3[x]$$

. In the frequency domain, using the standard modulation property of the Fourier transform, we find

$$F_{CFA}(\mathbf{u}) = \sum_{i=1}^{K} Q_i(\mathbf{u} - \mathbf{d}_i) \quad \text{where} \quad Q_i(\mathbf{u}) \triangleq \mathcal{F}\{q_i[\mathbf{x}]\}. \tag{2.15}$$

Basic frequency-domain demosaicking involves extracting the chroma components with bandpass filters separately, demodulating them to baseband and reconstructing the estimated RGB signal based on these signals with

$$\hat{\mathbf{f}}[\mathbf{x}] = \boldsymbol{M}^{\dagger}\hat{\mathbf{q}}[\mathbf{x}] \tag{2.16}$$

where $\boldsymbol{M}^{\dagger}$ is the pseudo inverse matrix of $\boldsymbol{M}$.

2.2 General methods for demosaicking

The earliest demosaicking techniques employ some well-known interpolation methods like bilinear interpolation, cubic spline interpolation and nearest neighbor replication. Later on, inter channel correlation has been used to reconstruct the red and blue colors using red-to-green and blue-to-green ratio. In fact, these algorithm are based on the assumption that the hue changes smoothly along neighboring pixels. In these methods [8], the green component will be reconstructed using bilinear interpolation. Using the estimated green component, the red and blue color components will be reconstructed using red-to-green and blue-to-green ratios. To be more precise, the interpolated red hue/ blue hue value will be multiplied by the green value to determine the missing red/ blue value at each pixel location. In some other works, the color difference is used instead of color ratio [32]. These methods are not working well for high resolution data sets [30]. There are some methods using wavelet transform, and some method applied frequency domain based demosaicking algorithm.

2.2.1 Interpolation techniques

One of the simplest demosaicking methods is bilinear or bicubic interpolation. In this method, the values of missing color components are estimated by interpolation of neighboring pixel information. Figure 2.2 and 2.3 show a linear interpolation in Bayer pattern.

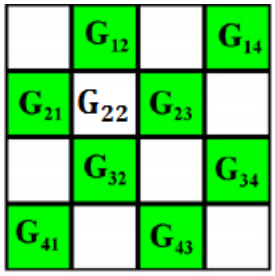

Figure 2.2: Bilinear interpolation for green components for the Bayer pattern

$$G_{22} = \frac{1}{4}(G_{12} + G_{21} + G_{23} + G_{32}) \tag{2.17}$$

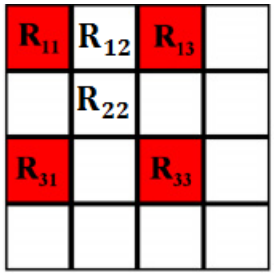

Figure 2.3: Bilinear interpolation for red/ blue components for the Bayer pattern

$$R_{22} = \frac{1}{4}(R_{11} + R_{13} + R_{31} + R_{33}) \tag{2.18}$$

$$R_{12} = \frac{1}{2}(R_{11} + R_{13}) \tag{2.19}$$

An interpolation based technique called Bayer reconstruction transforms RGB color space to YC_rC_b. The luminance image, Y, is reconstructed from green component after

applying bilinear interpolation on the green channel. The chroma values, C_r/C_b, for the given red/blue components will be calculated by $C_r = R - Y$, and $C_b = B - Y$ [14]. The missing chroma will be estimated using bilinear interpolation. The results transform to the RGB color space at the end.

2.2.2 Edge-directed interpolation

Some demosaicking techniques perform adaptive interpolation along the edges to create better results. These methods use different edge classifiers like horizontal or vertical edge classifiers, the gradients, the Laplacian operator and the Jacobian before green channel interpolation. The interpolation applies to the selected direction afterward [1]. Some other methods use a weighting scheme, and estimate the missing information using neighboring pixels, and the calculated weights on the basis of the edge direction. Gunturk et al. [20] also used the edge directed interpolation in their alternating projections algorithm. The local homogeneity for each pixel has been measured in Hirakawa et al. [23]. They select the interpolation direction using the homogeneity function in each pixel's neighborhood. The reconstructed images using edge-directed interpolation are usually sharper, and it contains less blurring artifacts. Thus the results of demosaicked images using this method are good in sharp regions, but they have poor results in problematic areas of the image [36].

2.2.3 Demosaicking methods using wavelet

In a typical wavelet-based demosaicking, first, the luminance image is formed using an interpolation method. The red, green and blue components are also interpolated in the same way. The wavelet transform will be applied on those interpolated images as well as the luminance image separately, and four different wavelet coefficients will result. Some merging scheme will be applied afterward, and the wavelet coefficient of each band of color image will be modified by the wavelet coefficient of the luminance image.

Gunturk et al. [20] used a wavelet-based technique for demosaicking. They combine the optimal edge directed interpolated image with the luminance image using wavelet

transform. Another wavelet based method presented in [14] improved the results visually and quantitatively comparing to the bilinear and gradient-based interpolation methods. A low complexity demosaicking algorithm using wavelet has been presented in [11].

Hirakawa et al. [24] presented a framework for demosaicking using the properties of Smith-Barnwell filterbanks for demosaicking and denoising aspects. They present a general framework for applying wavelet domain denoising algorithm as well as some existing denoising algorithm prior to the demosaicking.

A hybrid demosaicking algorithm also has been presented in [27]. In this method, they used the demosaicking algorithm presented in [29], and proposed an iterative post-processing algorithm using wavelet decomposition to reduce the color artifacts around the edges.

2.2.4 Demosaicking based on the frequency domain representation

The spatial multiplexing of red, green and blue color components can be represented in the frequency domain with one luma component and several chroma components [3]. The number of chromas usually depends on the number of samples in the pattern.

Demosaicking algorithms in the frequency domain usually involve extracting of luma and modulated chromas using two dimensional filters. In the Bayer pattern, one luma and three chromas will be extracted using passband filters, and the RGB values will be estimated in each spatial location using luma and chroma components, as we explained in section 2.1.

Since the components in the frequency domain representation are usually more isolated, the image quality will improve compared to the spatial domain methods. Moreover, some chromas with less interference with the luma can be used to reconstruct an image with less aliasing effect. A method proposed in [21] used the high frequency information of the green image to reconstruct and enhance the red and blue color information. Another method presented in [16] designed an adaptive filter to extract the chromas with less overlap, and it

reduce the aliasing effect. LSLCD method [29] is one of the state of art algorithm that has been described in frequency domain. This method optimized the filters and reduced the overlap between luma and chroma components using least-square optimization method.

2.3 Image quality measurement

There are different metrics for image quality measurement. In this work, two metrics will be calculated: peak signal-to-noise ratio (PSNR) and S-CIELAB. These two metrics provide numerical comparison between the original image and the demosaicked image, and help to compare different demosaicking algorithms.

2.3.1 Peak Signal-to-Noise Ratio

Mean-squared error and peak signal-to-noise ratio are two commonly used measures to compare the reconstructed image with the original image. For an $N_1 \times N_2$ image $RGB(i,j)$, the MSE value for R, G and B will be calculated as follows:

$$MSE(R) = \sum_{i=1}^{N1}\sum_{j=1}^{N2} \frac{(R(i,j) - R(i,j)_{Reconstructed})^2}{N_1 \times N_2} \tag{2.20}$$

$$MSE(G) = \sum_{i=1}^{N1}\sum_{j=1}^{N2} \frac{(G(i,j) - G(i,j)_{Reconstructed})^2}{N_1 \times N_2} \tag{2.21}$$

$$MSE(B) = \sum_{i=1}^{N1}\sum_{j=1}^{N2} \frac{(B(i,j) - B(i,j)_{Reconstructed})^2}{N_1 \times N_2} \tag{2.22}$$

$$CMSE = \frac{MSE(R) + MSE(G) + MSE(B)}{3}. \tag{2.23}$$

The value of MSE, usually depends on the image intensity scaling. To solve this problem, PSNR has been introduced, which measure the estimated error in decibels (db). Larger values of PSNR shows better quality of reconstructed image. Since the values of pixels in one image is scaled between [0 1], the following equation calculates the PSNR of an image and its demosaicked image

$$CPSNR = 10\log_{10}(\frac{1}{CMSE}) \tag{2.24}$$

2.3.2 S-CIELAB

S-CIELAB is a metric based on L*a*b* color space, and it better measures perceptual color difference. S-CIELAB gives us more accurate information about the image quality viewed by human observer. The CIELAB metric is suitable for measuring color difference of large uniform color targets. The S-CIELAB metric extends the CIELAB metric to color images.

To measure perceptual difference between two lights using the CIELAB, the spectral power distribution of the two lights are first converted to XYZ representations, which reflect (within a linear transformation) the spectral power sensitivities of the three cones on the human retina. The spatial filtering pre-processing step will be applied in an opponent color space. The opponent color space contains one luminance and two chrominance channels [26]. The following equation shows the linear transform between the XYZ color space to opponent channel, AC_1C_2.

$$\begin{bmatrix} A \\ C_1 \\ C_2 \end{bmatrix} = \begin{bmatrix} 0.297 & 0.72 & -0.107 \\ -0.449 & 0.29 & -0.077 \\ 0.086 & -0.59 & 0.501 \end{bmatrix} \begin{bmatrix} X \\ Y \\ Z \end{bmatrix} \tag{2.25}$$

The filtering step contains the two-dimensional separable convolution kernels. These kernels are in the form of a series of Gaussian functions that can be found in [26]. Then, the filtered opponent channels will be transformed back into XYZ space using the inverse transform function. The XYZ values are transformed into an L*a*b* space, in which equal distance is supposed to correspond to equal perceptual difference (perceptually uniform space). Then, the perceptual difference between the two targets can be calculated by taking the Euclidean distance of the two in this L*a*b* space. The S-CIELAB software presented in [26] has been used in this research.

Color discrimination and appearance is a function of spatial pattern. In general, as the spatial frequency of the target goes up (finer variations in space), color differences become harder to see, especially differences along the blue-yellow color direction.

So, if we want to apply the CIE L*a*b* metric to color images, the spatial patterns of the image have to be taken into account. The goal of the S-CIELAB metric is to add a

spatial pre-processing step to the standard CIELAB metric to account for the spatial-color sensitivity of the human eye.

2.4 Review of different CFA patterns

Color Filter Arrays (CFAs) vary due to the type and placement of their color filters. Each filter in a CFA is sensitive to a specific range of wavelengths to detect a certain color. Most CFAs contain three primary color components: red, green and blue. Some of them have an additional panchromatic/white filter as well. There are also some CFAs with complementary color components: cyan, magenta and yellow. The basic CFA structure containing four pixels is called Bayer, with two green, one blue and one red filter.

Due to the human eye sensitivity to the green light, usually the number of green filters is twice as large as for the rest of the color components in RGB CFAs.

2.4.1 Three channel CFAs

The type of color filters in three channel CFAs can be either red, green and blue or cyan, magenta and yellow. There are different types of structures with red, green and blue filters like Bayer, Fujifilm [19] and Diagonal stripe pattern.

Bayer CFA pattern

Bayer is the three channel CFA, containing two green, one blue and one red in each 2×2 pattern. It is used in many cameras like Canon, Olympus, Lumix and Sony. Due to the popularity of Bayer pattern, many demosaicking methods have been designed for it. Figure 2.4 shows one period of the Bayer pattern.

Fujifilm X-Trans pattern

The Fujifilm X-Trans pattern, as we can see in Figure 2.5 is a three channel 6×6 pattern. It can be considered as a 3×6 pattern where half of the pattern is the shifted version of

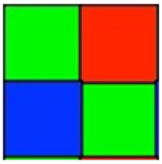

Figure 2.4: Bayer CFA pattern

the other part. This pattern has been developed by Fujifilm company [19]. According to the manufacturer, this pattern eliminates false colors while realizing high resolution [19].

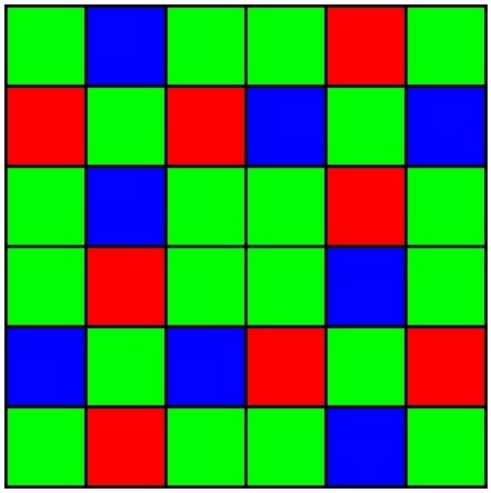

Figure 2.5: Fujifilm X-Trans CFA pattern

Diagonal stripe pattern

This pattern is a 1×3 pattern and contains three basic color component in one period. Since the defects are usually observed along rows or columns of the sensor cells, this pattern is robust against image sensor imperfections [31]. Figure 2.6 shows diagonal stripe pattern. Based on the previous work, the result of demosaicking using this pattern is not as good as RGB-Bayer [15].

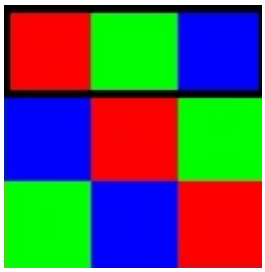

Figure 2.6: Diagonal Stripe CFA pattern

CYYM pattern

This pattern contains one cyan, two yellow and one magenta, and is used in a few cameras of Kodak. It has the same structure that has been discussed in Bayer with different color components. The advantage of using subtractive primaries is being more sensitive to light. This pattern did not become very popular compared to the other RGB patterns.

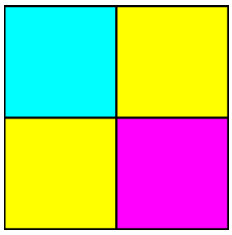

Figure 2.7: CYYM CFA pattern

2.4.2 Four channel CFAs

Four channel CFAs receive the color information through four different color filters. The four color filters usually take a combination of the first three primaries, which gives better estimation of the missing color information.

RGBE pattern

This is a Bayer-like pattern, where one of the green filters is modified to emerald, and is used in a few Sony cameras. According to the manufacturer [42], using the emerald filter reduces the color reproduction errors, and also records images closer to the human eye perception.

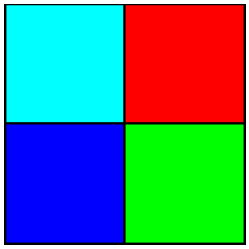

Figure 2.8: RGBE CFA pattern

RGBW pattern

There are different kinds of RGBW patterns. The most simple pattern is RGBW-Bayer which is a Bayer-like pattern. One of the green filters has been replaced with panchromatic/ white filter in this pattern. Another popular pattern is RGBW-Kodak CFA, and it has been used in many cameras. This pattern is a 4×4 and half of the filters in the pattern are white. There is also a 5×5 pattern, that has been introduced in [45]. These patterns will be studied in detail in Chapter 3 and 4.

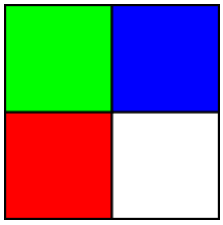

Figure 2.9: RGBW-Bayer CFA pattern

CYGM pattern

Due to the human eye sensitivity to green color, a yellow color filter has been replaced by a green filter in CYYM three channel pattern. Therefore, the pattern has one cyan, one yellow, one green and one magenta to provide a compromise between maximum light sensitivity and high color quality. It has been used in Nikon and Canon cameras such as Powershot S10, Canon digital IXUS S100 for a period of time, but it has been replaced with other patterns like Bayer very soon there after.

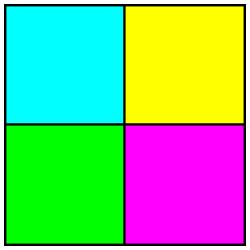

Figure 2.10: CYGM CFA pattern

2.5 Noise effect on CFA image

CFA sensors capture an image through the photo-electric conversion mechanism of a silicon semiconductor. Incoming photons produce free electrons within the semiconductor in proportion to the amount of incoming photons and those electrons are gathered within the imaging chip. Image capture is therefore essentially a photon-counting process.

As such, image capture is governed by the Poisson distribution, which is defined with a photon arrival rate variance equal to the mean photon arrival rate. The arrival rate variance is a source of image noise because if a uniformly illuminated, uniform color patch is captured with a perfect optical system and sensor, the resulting image will not be uniform but rather have a dispersion about a mean value. The dispersion is called image noise because it reduces the quality of an image when a human is observing it. Image noise can also be structured, as is the case with dead pixels or optical pixel crosstalk. We focus

on the Poisson-distributed noise (also called shot noise) with the addition of electronic amplifier read noise, which is modeled with a Gaussian distribution [2].

2.5.1 Demosaicking methods with a noise reduction stage

Many demosaicking algorithms have been designed for noise-free CFAs. Recently, the effect of noise on the captured image has been addressed in some other works, and they present demosaicking algorithms for noisy images. These methods mainly focus on restoring more details and reducing the amount of noise in the reconstructed image. In demosaicking methods with a noise reduction stage, usually, the noise will be modeled and added to the input image for simulation. Jeon and Dubois modeled the noise in the white-balanced, gamma corrected signal as signal independent white Gaussian noise. They used three different variances for different color channels of RGB Bayer CFAs [18].

In some previous works, the noise reduction step is applied to the demosaicked image, while some other methods implement the demosaicking stage after noise reduction. The effect of noise in low-light images has been addressed in [7]. They applied denoising step on the noisy image prior to the demosaicking step to prevent further corruption in the demosaicking process. Their method results in sharper low-light images, and reduces noise artifacts in the demosaicking step.

Most of the recent works in this area apply joint denoising and demosaicking schemes to the noisy image. Nawrath et al.[35] present a non-local filtering for the denoising step and produce demosaicked image with less color artifacts and less blurry effect. They stated that the difference between two color channels is locally nearly constant. According to this rule, they applied a non-local means filter to the joined difference channels and interpolated color image. The state of the art joint demosaicking and denoising method for RGB-Bayer CFA has been proposed in [25]. As we discussed before, the panchromatic/white filter receives more light comparing to the other color filters. Due to the lack of literature on joint demosaicking and denoising algorithm using RGBW CFAs, we propose both demosaicking algorithm and noise reduction method for RGBW patterns.

There are several methods to reduce noise in gray scale or color images, but they are not

working well for CFA images. Sung Hee et al. [43] proposed a noise reduction method for CFA images. In this method, the denoising step will be applied before demosaicking to the input CFA image. They also presented a comparison between two adaptive demosaicking algorithm (Hirakawa and Dubois) and a bilinear demosaicking method. They compare the demosaicking error as a function of noise-level for the mentioned methods. They stated that the adaptive algorithm performs extremely well under low sensor noise conditions, their performance decreases as noise increases compared to the bilinear method. Consequently, there is an interaction between input noise and the demosaicking algorithm that is used.

In some joint denoising-demosaicking algorithm, we need to estimate the noise value on a specific image before applying the noise reduction step. An accurate noise estimator would significantly benefit many image denoising methods. There are some noise estimation method designed for images. A recent work presented a method to estimate additive noise by utilizing the mean deviation of a smooth region selected from a noisy image. The noise distribution is estimated by computing the average mean deviation of all non-overlapping blocks in the smooth region [41].

Tomasi et al.[44] presented the bilateral filter. This method is based on matching distance (spatial), and similarity (intensity) criteria, and preserve sharp edges in noise reduction process.

Non-local filter method presented by Buades et al. [5], finds the similar patches to the area around each pixel, in entire image, and weights the similar patches by their similarity. Each pixel will be replaced by the weighted average of the center pixels of the matching patch. This method is slow in practice, and it usually searches for similar patches in a small area around each pixel.

Later on, Dabov et al. [12] presented BM3D method similar to Buades's method. In this method similar patches will be collaboratively filtered to provide an estimate for each pixel in the blocks. So, there will be several estimates for each pixel, and this method combined them to generate basic estimate of the true image. Then, another block matching step will be performed on the basic estimate, as a final denoising step.

The $BM3D$ method, is based on an enhanced sparse representation in the transform

domain, and it consist of two main steps: grouping and aggregation. The enhancement of the sparsity is achieved by grouping similar $2D$ image blocks into $3D$ data arrays which is known as grouping step. The collaborative filtering is applied on these $3D$ blocks afterward. This step contains three parts: $3D$ transformation of a group, shrinkage of the transform spectrum, and inverse $3D$ transform. The filtered blocks will returned to their original positions. Because of the overlapping of the blocks, there will be different estimates for each pixel. During aggregation step, those redundant information will be combined using averaging procedure.

Another method called clustering-based sparse representation (CSR) have been proposed in 2011. In this method, a dictionary of reference patches will be created, and the patches will be built as weighted combination of these dictionary patches. The average value of all patches in the same location will be assigned as pixel value[13].

According to a comparison has been presented in [6] a different denoising method, BM3D is working well among the listed method, and it preserve details of the image as well as sharp edges.

2.5.2 State of art joint demosaicking-denoising method for noisy RGB-Bayer patterns

Jeon and Dubois proposed a state of art demosaicking-denoising method for RGB-Bayer pattern. They used the least-square demosaicking method that has been proposed in [18]. For the design, they artificially add noise with different noise levels to the input images, and use the noisy images for training a set of the least-square filters. Several least-square filters adapted to different noise level have been designed in this method. They estimate the noise level of the input using Amer et al. noise estimation method [4], and an appropriate set of filters will be chosen using the estimated parameters.

Since the reconstruction of luma components is crucial in the demosaicking systems, and results in better quality of the reconstructed image, they utilize a separate noise reduction stage for luma components. They used the Block Matching $3D$ ($BM3D$) denoising

algorithm [12] , which is one of the state of art denoising methods. The luma denoising step improves the quality of output RGB image.

2.6 Summary

In this chapter, we reviewed different demosaicking algorithms in the space domain and the frequency domain. Also, different CFA patterns have been studied in this chapter. There is not enough literature on some of the discussed CFAs, and they need to be studied in detail. Some commercially well-known CFAs will be studied in this work, and the demosaicking algorithm will be provided for these CFAs. Four-channel CFAs are widely used in cameras recently. The effect of noise on four-channel CFAs with panchromatic filters has not been fully studied. The frequency domain analysis containing noise reduction algorithm using RGBW CFAs will be discussed in this research.

Chapter 3

Demosaicking algorithms in the noise-free case

As discussed in the previous chapter, there are many popular CFAs, and some related demosaicking algorithms have been provided in the literature in each case. In this thesis we narrow down our research to two main categories: three-channel CFAs, and four channel CFAs, since these cover most cases in actual use. We start by considering the noise-free (or low-noise) case. Due to the lack of published research on the Fujifilm X-Trans pattern and given its claimed advantages, we focused on this pattern as a sample of three-channel CFAs.

The RGBW CFAs have been chosen as four-channel CFAs, due to their anticipated benefits in the noisy case, and three different RGBW patterns have been analyzed in our work. The results of the reconstructed images have been compared, and the best RGBW pattern has been chosen for the noise reduction step. The following sections explain the details of the demosaicking algorithms for different identified patterns.

3.1 Demosaicking algorithm structure

Different CFA patterns may have different sizes. Using the smallest repeated pattern, the CFA signal is sampled on lattice $\Lambda = Z^2$ with reciprocal lattice $\Lambda^* = Z^2$.

Using these lattices, we can model the CFA signal as a sum of luma and chroma components.

$$f_{CFA}[\mathbf{x}] = \sum_{i=1}^{K} q_i[\mathbf{x}] \exp(j2\pi(\mathbf{x} \cdot \mathbf{d}_i)), \quad \text{where}$$

We also calculate matrix $\boldsymbol{B}$ and matrix $\boldsymbol{D}$ for this CFA pattern, as described in chapter 2. Matrix $\boldsymbol{M}$ also will be calculated afterward.

Since we have three individual color components for three-channel CFAs in the space domain related to R, G and B, there should be at least three individual components in the frequency domain (chromas) as well. Generally, there are C filter types, where $C = 3$ for three-channel CFAs, and $C = 4$ for four-channel CFAs, and there should be at least $K = C$ components for a sample CFA.

Using Fourier analysis (discrete-domain Fourier series), we find that the spatial multiplexing of C components is equivalent to the frequency domain multiplexing of K components. The basic demosaicking algorithm involves extracting the K components using bandpass filters, demodulating them to baseband and reconstructing the C original components. This has no advantage over spatial interpolation. However, we can reduce the number of K components, and design an adaptive algorithm.

Although the number of chromas vary depending on the CFA pattern in different cameras, there should be some relation between chromas. It is always beneficial to decrease redundancy between chromas to three basic components, since it reduces the computational complexity. The smaller number of chromas also results in less overlap between chromas. It will also lead us to more accurate chroma extraction.

Using matrix $\boldsymbol{M}$, we can find the dependency of chromas. We can divide chromas into several groups of dependent chromas. We have to choose one chroma per group as a basic chroma, and fully extract it. Then we will be able to fully reconstruct the rest of chromas in the same group. The group assignment of chromas are not necessarily unique, and there should be a minimum of three basic chromas for each three-channel pattern and four for four-channel CFAs.

In this section, we present our applied demosaicking algorithm as a general model, so it can be applied on any other CFA pattern. As we discussed in the previous section, the following equation shows the relation between chroma components in frequency domain and the RGB image.

$$\boldsymbol{q}[\mathbf{x}] = \boldsymbol{M}\boldsymbol{f}[\mathbf{x}] \tag{3.1}$$

$$\boldsymbol{f} = \begin{bmatrix} f_1, & f_2, & f_3, & f_4 \end{bmatrix}^T \tag{3.2}$$

$$\boldsymbol{q} = \begin{bmatrix} q_1, & q_2, & \dots & , & q_K \end{bmatrix}^T \tag{3.3}$$

Assuming $\boldsymbol{M}$ is a $K \times C$ matrix, we are concerned with the case where $K > C$, and we would like to simplify matrix $\boldsymbol{M}$.

We can minimize the number of rows in $\boldsymbol{M}$ and decrease the number of color components in the frequency domain as follows in two steps. First, we delete zero rows of $\boldsymbol{M}$ as not relevant. Second, as experience shows that in most cases of interest, the rows of $\boldsymbol{M}$ each belong to one of C one-dimensional sub-spaces of R^C, we need to find those rows in matrix $\boldsymbol{M}$.

Since we simplify the matrix $\boldsymbol{M}$, we will be able to design the adaptive demosaicking algorithm. In the adaptive algorithm, only one color component in each group will be estimated, and it will be used to determine all the others belonging to the same group. The specific component in each group can be chosen locally based on an estimate of which component in its group is least affected locally by crosstalk. Once all chromas are adaptively estimated, they can be remodulated and subtracted from the CFA signal to estimate the luma.

The following examples show the process of matrix $\boldsymbol{M}$ simplification more clearly for different CFAs. In the case of Bayer, as we discussed in Section 2.1, equation 2.13 we have

$$\boldsymbol{M} = \frac{1}{4} \times \begin{bmatrix} 1 & 2 & 1 \\ -1 & 0 & 1 \\ 1 & 0 & -1 \\ -1 & 2 & -1 \end{bmatrix}. \tag{3.4}$$

In this CFA $m_{3i} = -m_{2i}$, and thus $q_3 = -q_2$. Thus, only one of q_2 and q_3 is needed to reconstruct $\boldsymbol{F}$, and the best one can be chosen locally using an adaptive algorithm.

A more complex case is the Fujifilm X-Trans CFA, where K is 18. This will be studied in detail in Section 3.2. Five rows of $\boldsymbol{M}$ are zero, so they can be ignored. There are thirteen remaining rows, and we call the downsized matrix $\boldsymbol{M'}$.

$$\boldsymbol{M'} = \frac{1}{9} \times \begin{bmatrix} 2 & 5 & 2 \\ -0.25 - 0.43j & 0.5 + 0.86j & -0.25 - 0.43j \\ -0.25 + 0.43j & 0.5 - 0.86j & -0.25 + 0.43j \\ 0.5 - 0.86j & -1 + 1.73j & 0.5 - 0.86j \\ 0.5 + 0.86j & -1 - 1.73j & 0.5 + 0.86j \\ -0.25 + 0.43j & 0.5 - 0.86j & -0.25 + 0.43j \\ -0.25 - 0.43j & 0.5 + 0.86j & -0.25 - 0.43j \\ -1 & 2 & -1 \\ -1 & 2 & -1 \\ 0.75 + 1.3j & 0 & -0.75 - 1.3j \\ -0.75 - 1.3j & 0 & 0.75 + 1.3j \\ 0.75 - 1.3j & 0 & -0.75 + 1.3j \\ -0.75 + 1.3j & 0 & 0.75 - 1.3j \end{bmatrix} \tag{3.5}$$

These rows lie in three $1D$ subspaces spanned by $a_1[2, 5, 2]$, $a_2[-1, 2, 1]$ and $a_3[1, 0, -1]$ where a_1, a_2 and a_3 are arbitrary complex constants which we can choose according to our convenience.

Next consider Kodak RGBW. In this CFA $C = 4$ and $K = 16$, but four rows are zero,

and can be ignored. The remaining rows are:

$$\boldsymbol{M'} = \frac{1}{16} \times \begin{bmatrix} 2 & 4 & 2 & 8 \\ -1+j & 0 & 1-j & 0 \\ -1-j & 0 & 1+j & 0 \\ 1-j & 0 & -1+j & 0 \\ 1+j & 0 & -1-j & 0 \\ 2 & -4 & 2 & 0 \\ -2 & 4 & -2 & 0 \\ -1+j & 0 & 1-j & 0 \\ 1-j & 0 & -1+j & 0 \\ -1-j & 0 & 1+j & 0 \\ 1+j & 0 & -1-j & 0 \\ -2 & -4 & -2 & 8 \end{bmatrix} \tag{3.6}$$

By looking at matrix $\boldsymbol{M'}$, there are some obvious similarities between rows. They lie in four $1D$ subspaces spanned by $a_1[1, 2, 1, 4]$ as group one, $a_2[1, 0, -1, 0]$ as group two, $a_3[1, -2, 1, 0]$ as group three and $a_4[1, 2, 1, -4]$ as group four. These subspaces can be easily found by inspection.

If we can reconstruct one chroma based on the other, we assume those chromas belong to the same class. Here we assume Luma (first row) as a separate class, rows $2-5$ and $8-11$ as second class, rows 6 and 7 as our third class, and the last row as the fourth class of chromas.

The matrix $\boldsymbol{J}$ is defining the four input channels: R, G, B and W, while each column of the matrix represents one of the colors in this pattern. Panchromatic pixels in the CFA will be calculated using equation 3.7.

$$W = a_R(R) + a_B(B) + a_G(G) \tag{3.7}$$

In the frequency domain, the Fourier transform of the CFA signal is

$$F_{\text{CFA}}(\mathbf{u}) = \sum_{i=1}^{N} Q_i(\mathbf{u} - \mathbf{d}_i) \quad \text{where} \quad Q_i(\mathbf{u}) \triangleq \mathcal{F}\{q_i[\mathbf{x}]\}. \tag{3.8}$$

The chroma components are extracted with bandpass filters centered at the frequencies $\mathbf{d}_i$. The next step in the demosaicking algorithm is reconstructing the full RGB color image using the pseudo inverse matrix $\boldsymbol{M}^{\dagger}$.

There are two main issues in adaptive algorithm: how to design appropriate filters to extract the modulated chroma components, and how to adaptively estimate the basic chroma in each group to minimize the effect of crosstalk. These issues will be addressed for each of the CFA patterns to be presented in the subsequent section.

3.2 Three channel color filter array

The three-channel color filter arrays usually contain three primary color filters: red, green and blue. Due to the different CFA structures, the number of each color filter type in one period of the pattern varies. The most widely used three-channel CFA is Bayer, containing two green, one blue and one red filter in one period of the pattern. Because of the human eye's sensitivity to the green color, the number of green pixels in most of the three channel CFAs is usually twice or almost twice the number of blue or red pixels. The quality of the output images depends on the number of different color filters in each pattern as well as the arrangement of the color filters in the template.

3.3 Demosaicking for the Fujifilm X-Trans pattern

In this work, we implement demosaicking algorithms related to the Fujifilm X-Trans CFA pattern. The Fujifilm CFA pattern is a 6×6 template containing 20 green pixels, 8 blue and 8 red as we can see in Figure 3.1. The number of green pixels is more than the total number of blue and red pixels. This template provides a higher degree of randomness with an array of 6×6 pixel units. According to the manufacturer, without using an optical low-pass filter, moiré and false colors are eliminated while realizing high resolution [19]. Analysis of this pattern is more complicated than for the Bayer pattern due to the large number of sensors in one period of the CFA. In the following sections, two different analysis

approaches will be presented for Fujifilm X-Trans pattern.

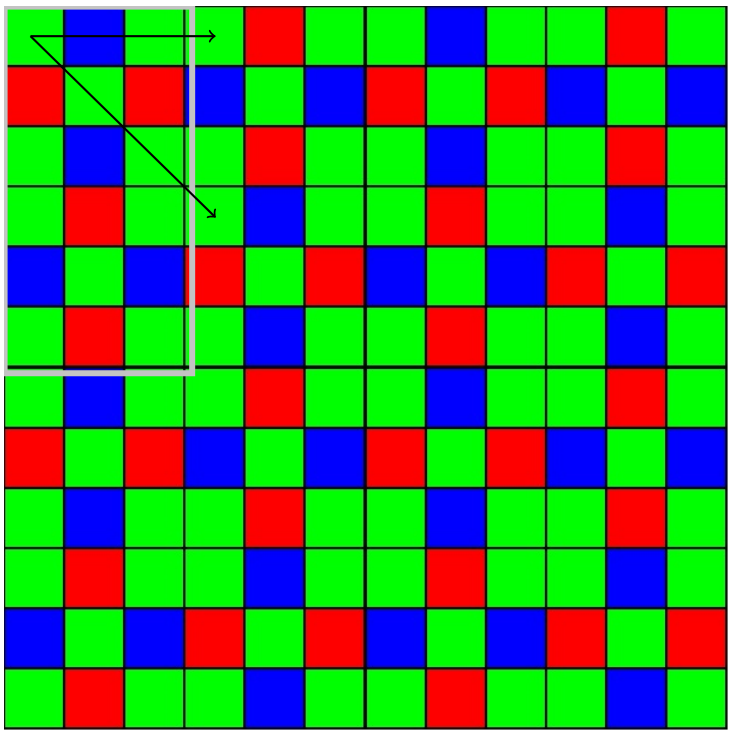

Figure 3.1: Fujifilm X-Trans CFA pattern

Demosaicking algorithm

Although the pattern is generally viewed as 6×6, it is in fact 3×6 with periodicity given by a hexagonal lattice. The second 3×6 part can be assumed as a shifted version of the first half. The CFA signal is sampled on lattice $\Lambda = \mathbb{Z}^2$ with reciprocal lattice $\Lambda^* = \mathbb{Z}^2$. A lattice and it's corresponding reciprocal lattice to represent the periodicity of the CFA pattern can be given by

$$\vee_\Gamma = \begin{bmatrix} 6 & 3 \\ 0 & 3 \end{bmatrix}, \quad \vee_{\Gamma^*} = \begin{bmatrix} \frac{1}{6} & 0 \\ -\frac{1}{3} & \frac{1}{3} \end{bmatrix}. \tag{3.9}$$

The analysis of this CFA can be carried out using the general theory described in [18], and summarized in Chapter 2. According to the analysis, the CFA signal can be represented as a sum of modulated chroma components plus a baseband luma component.

The CFA signal is given by

$$f_{\text{CFA}}[\mathbf{x}] = \sum_{i=1}^{K} q_i[\mathbf{x}] \exp(j2\pi(\mathbf{x} \cdot \boldsymbol{d}_i)) \quad \text{where} \quad K = 18. \tag{3.10}$$

According to [18], $\boldsymbol{d}_i$ refers to the columns of matrix $\boldsymbol{D}$ and they are coset representatives of Λ^* in Γ^*. The matrix $\boldsymbol{D}$ is a $2 \times K$ matrix where K is the number of samples in one period of the lattice, which is equal to 18 for the Fujifilm pattern. The following matrix is used here

$$\boldsymbol{D} = \frac{1}{6} \times \begin{bmatrix} 0 & 2 & -2 & 1 & -1 & 2 & -2 & 1 & -1 & 0 & 0 & 2 & -2 & 3 & -1 & 3 & 1 & 3 \\ 0 & 0 & 0 & 1 & -1 & 2 & -2 & -1 & 1 & -2 & 2 & -2 & 2 & -1 & 3 & 1 & 3 & 3 \end{bmatrix}. \tag{3.11}$$

The luma and chroma components are obtained from the original RGB components by

$$\boldsymbol{q}[x] = \boldsymbol{M}\mathbf{f}[\mathbf{x}] \tag{3.12}$$

$$\boldsymbol{f} = [f_1, f_2, f_3]^T = [R, G, B]^T \quad \text{and} \quad \boldsymbol{q} = [q_1, q_2, \cdots, q_{18}]^T. \tag{3.13}$$

For finding matrix $\boldsymbol{M}$ we need to calculate matrices $\boldsymbol{B}$ and $\boldsymbol{J}$. Also, $\boldsymbol{b}_i$ refers to the columns of matrix $\boldsymbol{B}$ which gives the coset representatives of Γ in Λ. We use

$$\boldsymbol{B} = \begin{bmatrix} 0 & 1 & 2 & 0 & 1 & 2 & 0 & 1 & 2 & 0 & 1 & 2 & 0 & 1 & 2 & 0 & 1 & 2 \\ 0 & 0 & 0 & 1 & 1 & 1 & 2 & 2 & 2 & 3 & 3 & 3 & 4 & 4 & 4 & 5 & 5 & 5 \end{bmatrix}. \tag{3.14}$$

Color channels will be represented by

$$\boldsymbol{J} = \begin{bmatrix} 0 & 0 & 0 & 1 & 0 & 1 & 0 & 0 & 0 & 0 & 1 & 0 & 0 & 0 & 0 & 0 & 1 & 0 \\ 1 & 0 & 1 & 0 & 1 & 0 & 1 & 0 & 1 & 1 & 0 & 1 & 0 & 1 & 0 & 1 & 0 & 1 \\ 0 & 1 & 0 & 0 & 0 & 0 & 0 & 1 & 0 & 0 & 0 & 0 & 1 & 0 & 1 & 0 & 0 & 0 \end{bmatrix}^T. \tag{3.15}$$

The following matrix shows the calculated matrix M for 18 components using 2.13 in

Section 2.1. Note that only 13 components are nonzero.

$$\boldsymbol{M} = \begin{bmatrix} 0.2222 & 0.5556 & 0.2222 \\ -0.0278 - 0.0481j & 0.0556 + 0.0962j & -0.0278 - 0.0481j \\ -0.0278 + 0.0481j & 0.0556 - 0.0962j & -0.0278 + 0.0481j \\ 0 & 0 & 0 \\ 0 & 0 & 0 \\ 0.0556 - 0.0962j & -0.1111 + 0.1925j & 0.0556 - 0.0962j \\ 0.0556 + 0.0962j & -0.1111 - 0.1925j & 0.0556 + 0.0962j \\ 0 & 0 & 0 \\ 0 & 0 & 0 \\ -0.0278 + 0.0481j & 0.0556 - 0.0962j & -0.0278 + 0.0481j \\ -0.0278 - 0.0481j & 0.0556 + 0.0962j & -0.0278 - 0.0481j \\ -0.1111 & 0.2222 & -0.1111 \\ -0.1111 & 0.2222 & -0.1111 \\ 0.0833 + 0.1443j & 0 & -0.0833 - 0.1443j \\ -0.0833 - 0.1443j & 0 & 0.0833 + 0.1443j \\ 0.0833 - 0.1443j & 0 & -0.0833 + 0.1443j \\ -0.0833 + 0.1443j & 0 & 0.0833 - 0.1443j \\ 0 & 0 & 0 \end{bmatrix} \tag{3.16}$$

In the frequency domain, using the standard modulation property of the Fourier transform, we find

$$F_{\text{CFA}}(\mathbf{u}) = \sum_{i=1}^{18} Q_i(\mathbf{u} - \boldsymbol{d}_i) \quad \text{where} \quad Q_i(\mathbf{u}) \triangleq \mathcal{F}\{q_i[\mathbf{x}]\} \tag{3.17}$$

Figure 3.2 shows the power spectral density of a sample X-Trans CFA image, illustrating the position of luma and chroma components in one unit cell of Λ^*.

Basic frequency-domain demosaicking involves extracting the luma and the twelve nonzero chroma components with bandpass filters separately, demodulating them to baseband and reconstructing the estimated RGB signal based on these signals with

$$\hat{\boldsymbol{f}}[\mathbf{x}] = \boldsymbol{M}^{\dagger}\hat{\mathbf{q}}[\mathbf{x}] \tag{3.18}$$

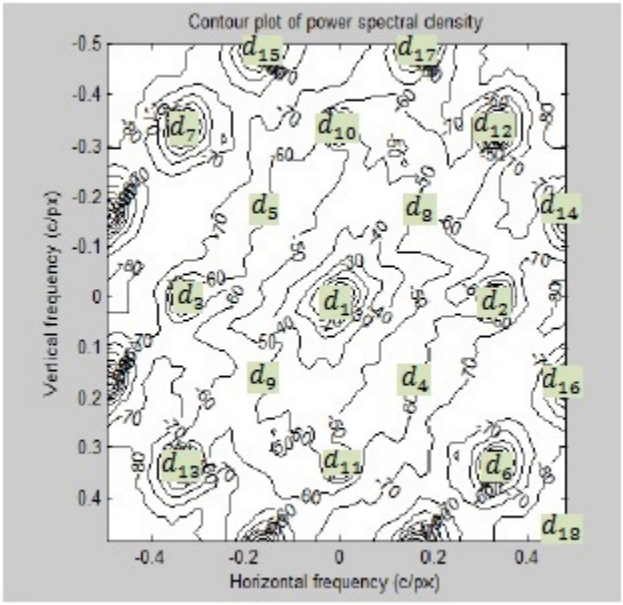

Figure 3.2: Luma- Chroma position for Fujifilm X-Trans pattern

where $\boldsymbol{M}^{\dagger}$ is the pseudo inverse matrix of $\boldsymbol{M}$.

Due to the similarity of different chromas and their distance from luma in this pattern, three baseband Gaussian filters have been designed in our basic implementation. The Gaussian filters are $2D$ filter with $\sigma = 2.32$ for both dimension. The filter sizes have been set experimentally. Different chromas have been filtered by modulating these Gaussian filters to the different band center frequencies. The first filter extracted q_2, q_3, q_{10} and q_{11}. The second one has been used for q_6, q_7, q_{12} and q_{13} and the last one extracts q_{14}, q_{15}, q_{16} and q_{17}.

The Luma component will be extracted as follows:

$$\hat{\boldsymbol{q}}_1[\mathbf{x}] = f_{\mathrm{CFA}}[\mathbf{x}] - \sum_{i=2}^{18} \hat{\mathbf{q}}_i \exp(j2\pi(\mathbf{x} \cdot \boldsymbol{d}_i)). \tag{3.19}$$

Although we model the whole system for 18 components, there are 5 components with $q_i[x]$ equal to zero. These are correspond to d_4, d_5, d_8, d_9 and d_{18}.

Based on the dependence of different chroma components we can categorize all 18 component into 5 groups and estimate the rest of the components based on them. The

following equations show the relations between the 13 nonzero components.

$$p_1(\mathbf{x}) \triangleq q_1(\mathbf{x}) \quad Luma \tag{3.20}$$

$$p_2(\mathbf{x}) \triangleq q_{12}(\mathbf{x}) = q_{13}(\mathbf{x}) \tag{3.21}$$

$$p_3(\mathbf{x}) \triangleq q_2(\mathbf{x}) = q_3^*(\mathbf{x}) = q_{10}^*(\mathbf{x}) = q_{11}(\mathbf{x}) \tag{3.22}$$

$$p_4(\mathbf{x}) \triangleq q_6(\mathbf{x}) = q_7^*(\mathbf{x}) \tag{3.23}$$

$$p_5(\mathbf{x}) \triangleq q_{14}(\mathbf{x}) = q_{16}^*(\mathbf{x}) = -q_{15}(\mathbf{x}) = -q_{17}^*(\mathbf{x}) \tag{3.24}$$

By inspecting the values of matrix M, the values of some components can be retrieved based on the others. The following equations show further relations between different components:

$$q_{12}(\mathbf{x}) = q_{13}(\mathbf{x}) = -(q_6(\mathbf{x}) + q_7(\mathbf{x})) \tag{3.25}$$

$$q_6(\mathbf{x}) = -(q_2(\mathbf{x}) + q_3(\mathbf{x})) + j(q_2(\mathbf{x}) - q_3(\mathbf{x})) \tag{3.26}$$

Thus we can calculate p_2, p_3 and p_4 using the real and imaginary part of one of them. Since the value of p_2 is real, we need to have either p_3 or p_4 to find the rest.

$$p_2(\mathbf{x}) = -2\mathrm{Re}\{p_4(\mathbf{x})\} \tag{3.27}$$

$$p_4(\mathbf{x}) = -2Re\{p_3(\mathbf{x})\} + j2\mathrm{Im}\{p_3(\mathbf{x})\} \equiv 2p_3^*(\mathbf{x}) \tag{3.28}$$

We can conclude that all the first 8 chroma components can be calculated based on any one of these components. Thus we are able to estimate some of the chromas which have more interference with Luma based on the other components that are further from Luma. This is the key idea behind the extension of adaptive luma-chroma demultiplexing for Bayer pattern to the X-Trans pattern.

In summary we have p_1 as luma, p_5 as the first chroma and one of p_2, p_3 and p_4 as the second chroma. In the adaptive method, weights will be assigned to the chromas selectively. The more accurately reconstructed chroma in each group receives a higher weight and the other chroma component will be updated sequentially. The new estimated

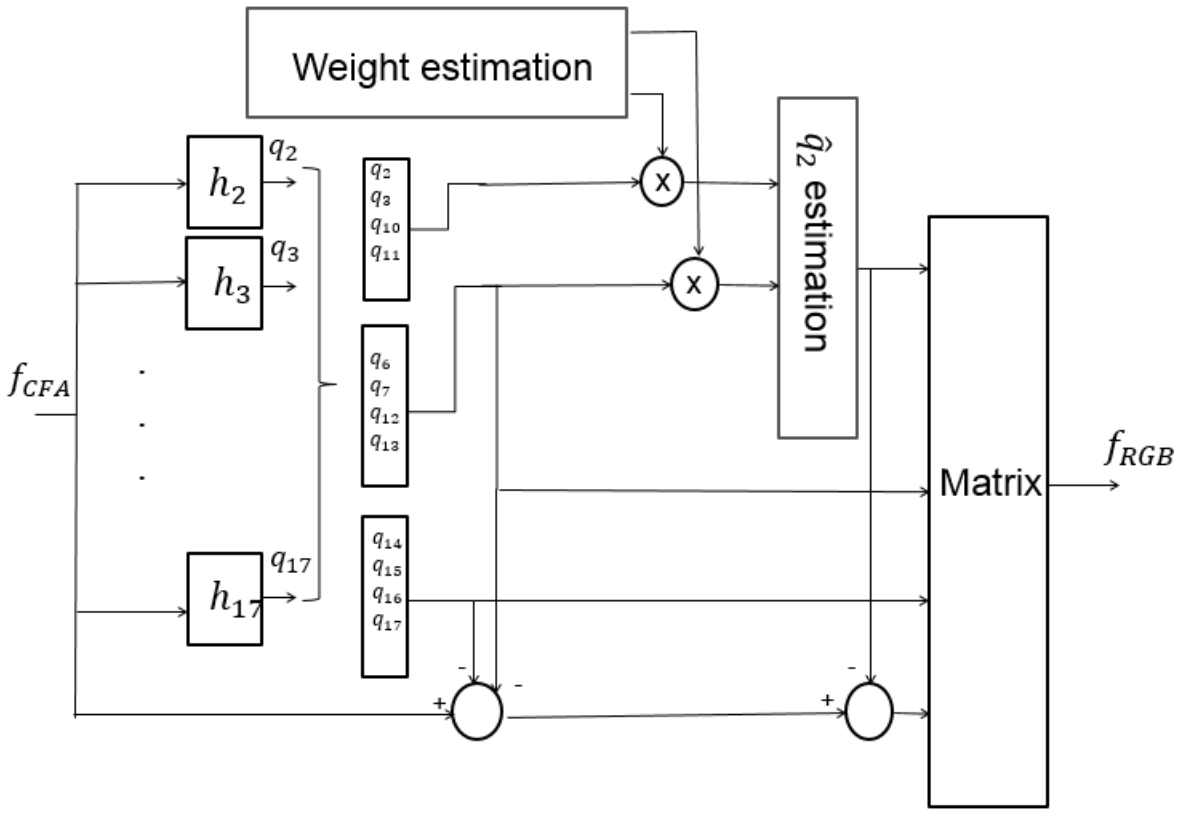

Figure 3.3: Fujifilm adaptive demosaicking system

chromas improve the luma estimation when using equation 3.19. Figure 3.3 shows the structure of the adaptive demosaicking algorithm.

There are four chroma components which are very close to the luma: q_2, q_3, q_{10} and q_{11}. We are trying to find a more accurate value for q_2, and calculate the other three components using the updated q_2. Since q_2, q_3, q_6, q_7, q_{10}, q_{11}, q_{12} and q_{13} are closer to the luma, we used a weighted form of each one adaptively to reconstruct the q_2 component with least overlap with luma. In this method, the energy function has been calculated between luma and one of each pairs of chromas. Every two symmetrically located chromas have been assumed as a pair: q_2 and q_3, q_6 and q_7, q_{10} and q_{11}, q_{12} and q_{13}.

To optimize the weight assignment process, we create a filter to extract the overlapped information in the middle of the Euclidean distance of luma and the given chroma. The filtered information shows the average local energy as an overlapping index at that location.

Specifically, a baseband Gaussian filter h_G, with a certain standard deviation r_G has been designed for this process. The r_G has been set experimentally to give the best filtering performance. The Gaussian filter has been modulated to the certain frequency between luma and chroma, to filter the local energy. The modulated filter is shown as h_{Gx}. The filtered signal will be squared and will be filtered using a 5×5 moving average filter afterward.

This value has an inverse relation with the accuracy of the filtered chroma. So, we assign the inverse form of energy index to the mentioned chroma as weight (w). Four different weights have been calculated in this way, and each weight has been assigned to a pair of above chromas. Therefore, the chroma having less overlap with the luma receives more weight, and the least accurate one receives less weight in each pixel of the image. Each of those four weights has been divided by the sum of w_1 to w_4 to make sure that the total value of the assigned weights is equal to one. The following equations show the weighting process.

$$energy = (f_{CFA} * h_{Gx})^2 * h_{5\times5} \tag{3.29}$$

$$w = \frac{1}{energy} \tag{3.30}$$

$$\hat{q_2}(\mathbf{x}) = \frac{(w_2)q_2(\mathbf{x}) + (w_6)q_6(\mathbf{x}) + (w_{10})q_{10}(\mathbf{x}) + (w_{12})q_{12}(\mathbf{x})}{w_2 + w_6 + w_{10} + w_{12}} \tag{3.31}$$

$$\hat{q}_3(\mathbf{x}) = \hat{q}_2^*(\mathbf{x}) \tag{3.32}$$

$$\hat{q}_{10}(\mathbf{x}) = \hat{q}_2^*(\mathbf{x}) \tag{3.33}$$

$$\hat{q}_{11}(\mathbf{x}) = \hat{q}_2(\mathbf{x}) \tag{3.34}$$

The updated q_2 will be used to reconstruct the enhanced q_3, q_{10}, q_{11} and luma in adaptive demosaicking algorithm. The luma component will also be updated afterward. The non-adaptive algorithm extracts the chromas using the Gaussian filters and simply reconstructs the RGB image using the extracted chromas.

In comparing demosaicking algorithms using Fujifilm and Bayer patterns, we note that there were also three selected independent components in Bayer. Since the updated q_2 in

the presented algorithm depend on q_6, q_{10}, q_{12} chromas, we will not be able to optimize the weighting scheme that has been described above. Thus, we need to minimize the dependency between chromas. The following method expresses the Bayer-like analysis for the X-Trans Fujifilm pattern. In this method q_2 will be reconstructed using two chromas, and the assigned weights will be optimized.

Bayer-like analysis for Fujifilm CFA pattern

In this method we are trying to reconstruct the remaining thirteen components using one luma and two chromas as we have before for Bayer. Since we are reconstructing an RGB image, we need in fact three degrees of freedom. The signal q_1 is a luma signal, given by

$$q_1[\mathbf{x}] = \frac{1}{9}(2f_R[\mathbf{x}] + 5f_G[\mathbf{x}] + 2f_B[\mathbf{x}]) \triangleq f_L[\mathbf{x}] \tag{3.35}$$

Note that this is different than the luma component in the Bayer CFA. There are essentially two distinct chroma signals, which can be taken to be the same ones as in the Bayer CFA:

$$f_{C1}[\mathbf{x}] = \frac{1}{4}(-f_R[\mathbf{x}] + 2f_G[\mathbf{x}] - f_B[\mathbf{x}]) \tag{3.36}$$

$$f_{C2}[\mathbf{x}] = \frac{1}{4}(-f_R[\mathbf{x}] + f_B[\mathbf{x}]) \tag{3.37}$$

We can relate the remaining twelve q signals to f_{C1} and f_{C2} as follows:

$$
\begin{aligned}
q_2[\mathbf{x}] &= (0.1111 + 0.1925j) f_{C1}[\mathbf{x}] \\
q_3[\mathbf{x}] &= (0.1111 - 0.1925j) f_{C1}[\mathbf{x}] = q_2^*[\mathbf{x}] \\
q_6[\mathbf{x}] &= (-0.2222 + 0.3850j) f_{C1}[\mathbf{x}] = -2q_2^*[\mathbf{x}] \\
q_7[\mathbf{x}] &= (-0.2222 - 0.3850j) f_{C1}[\mathbf{x}] = -2q_2[\mathbf{x}] \\
q_{10}[\mathbf{x}] &= (0.1111 - 0.1925j) f_{C1}[\mathbf{x}] = q_2^*[\mathbf{x}] \\
q_{11}[\mathbf{x}] &= (0.1111 + 0.1925j) f_{C1}[\mathbf{x}] = q_2[\mathbf{x}] \\
q_{12}[\mathbf{x}] &= 0.4444 f_{C1}[\mathbf{x}] = 2(q_2[\mathbf{x}] + q_2^*[\mathbf{x}]) \\
q_{13}[\mathbf{x}] &= 0.4444 f_{C1}[\mathbf{x}] = 2(q_2[\mathbf{x}] + q_2^*[\mathbf{x}]) \\
q_{14}[\mathbf{x}] &= (-0.3333 - 0.5772j) f_{C2}[\mathbf{x}] \\
q_{15}[\mathbf{x}] &= (0.3333 + 0.5772j) f_{C2}[\mathbf{x}] = -q_{14}[\mathbf{x}] \\
q_{16}[\mathbf{x}] &= (-0.3333 + 0.5772j) f_{C2}[\mathbf{x}] = q_{14}^*[\mathbf{x}] \\
q_{17}[\mathbf{x}] &= (0.3333 - 0.5772j) f_{C2}[\mathbf{x}] = -q_{14}^*[\mathbf{x}]
\end{aligned}
$$

The first eight of these can be used to estimate f_{C1} and the last four can be used to estimate f_{C2}.

Although the above relationships between different q components hold for the actual q components, they will not in general hold exactly for estimates of the q signals from the CFA signal, mainly because of crosstalk between the different components. However, assuming symmetric bandpass filters are used to extract the modulated components from the CFA signal, pairs at mirror frequencies (i.e., $\mathbf{d}$ and $-\mathbf{d}$) will be conjugates of each other. These mirror pairs are (q_2, q_3), (q_6, q_7), (q_{10}, q_{11}), (q_{12}, q_{13}) (these are real), (q_{14}, q_{16}) and (q_{15}, q_{17}). These pairs should be estimated as a unit, with their sum being real. Thus, there are four pairs used to estimate f_{C1} and two pairs used to estimate f_{C2}. Consider for example the case of q_2 and q_3. We have defined

$$r_2[\mathbf{x}] = q_2[\mathbf{x}] \exp(j2\pi \mathbf{d}_2 \cdot \mathbf{x}) \tag{3.38}$$

$$r_3[\mathbf{x}] = q_3[\mathbf{x}] \exp(j2\pi \mathbf{d}_3 \cdot \mathbf{x}) \tag{3.39}$$

$$= q_2^*[\mathbf{x}] \exp(-j2\pi \mathbf{d}_2 \cdot \mathbf{x}) = r_2^*[\mathbf{x}] \tag{3.40}$$

Assuming we use mirror symmetric bandpass filters to estimate r_2 and r_3, we will necessarily find

$$\hat{r}_3[\mathbf{x}] = \hat{r}_2^*[\mathbf{x}].$$

After demodulating these two signals to baseband, we find

$$\hat{q}_2[\mathbf{x}] = \hat{r}_2[\mathbf{x}] \exp(-j2\pi \mathbf{d}_2 \cdot \mathbf{x}) \tag{3.41}$$

$$\hat{q}_3[\mathbf{x}] = \hat{r}_3[\mathbf{x}] \exp(-j2\pi \mathbf{d}_3 \cdot \mathbf{x}) \tag{3.42}$$

$$= \hat{r}_2^*[\mathbf{x}] \exp(j2\pi \mathbf{d}_2 \cdot \mathbf{x}) = \hat{q}_2^*[\mathbf{x}] \tag{3.43}$$

Then, $\hat{s}_{2,3}[\mathbf{x}] \triangleq \hat{q}_2[\mathbf{x}] + \hat{q}_3[\mathbf{x}]$ is real, and can be used as an estimate of $q_2[\mathbf{x}] + q_3[\mathbf{x}] = 0.2222 f_{C1}[\mathbf{x}]$. In a similar fashion: $\hat{s}_{10,11}[\mathbf{x}] \triangleq \hat{q}_{10}[\mathbf{x}] + \hat{q}_{11}[\mathbf{x}]$ is real, and can be used as an estimate of $q_{10}[\mathbf{x}] + q_{11}[\mathbf{x}] = 0.2222 f_{C1}[\mathbf{x}]$; $\hat{s}_{6,7}[\mathbf{x}] \triangleq \hat{q}_6[\mathbf{x}] + \hat{q}_7[\mathbf{x}]$ is real, and can be used as an estimate of $q_6[\mathbf{x}] + q_7[\mathbf{x}] = -0.4444 f_{C1}[\mathbf{x}]$; and finally, $\hat{s}_{12,13}[\mathbf{x}] \triangleq \hat{q}_{12}[\mathbf{x}] + \hat{q}_{13}[\mathbf{x}]$ is real, and can be used as an estimate of $q_{12}[\mathbf{x}] + q_{13}[\mathbf{x}] = 0.8888 f_{C1}[\mathbf{x}]$.

We could combine these to form a non-adaptive estimate of f_{C1} by giving them equal weighting:

$$\hat{f}_{C1}[\mathbf{x}] = \tfrac{0.25}{0.2222}\hat{s}_{2,3}[\mathbf{x}] + \tfrac{0.25}{0.2222}\hat{s}_{10,11}[\mathbf{x}] - \tfrac{0.25}{0.4444}\hat{s}_{6,7}[\mathbf{x}] + \tfrac{0.25}{0.8888}\hat{s}_{12,13}[\mathbf{x}] \tag{3.44}$$

$$= \tfrac{9}{8}\hat{s}_{2,3}[\mathbf{x}] + \tfrac{9}{8}\hat{s}_{10,11}[\mathbf{x}] - \tfrac{9}{16}\hat{s}_{6,7}[\mathbf{x}] + \tfrac{9}{32}\hat{s}_{12,13}[\mathbf{x}] \tag{3.45}$$

or alternatively (and better, since in general $s_{2,3}$ and $s_{10,11}$ suffer more crosstalk than $s_{6,7}$ and $s_{12,13}$)

$$\hat{f}_{C1}[\mathbf{x}] = -\tfrac{9}{8}\hat{s}_{6,7}[\mathbf{x}] + \tfrac{9}{16}\hat{s}_{12,13}[\mathbf{x}]. \tag{3.46}$$

A general formula is

$$\hat{f}_{C1}[\mathbf{x}] = \tfrac{9}{2}w_a\hat{s}_{2,3}[\mathbf{x}] + \tfrac{9}{2}w_b\hat{s}_{10,11}[\mathbf{x}] - \tfrac{9}{4}w_c\hat{s}_{6,7}[\mathbf{x}] + \tfrac{9}{8}w_d\hat{s}_{12,13}[\mathbf{x}] \tag{3.47}$$

where $w_a + w_b + w_c + w_d = 1$.

A similar approach can be used to estimate f_{C2}. We define $\hat{s}_{14,16}[\mathbf{x}] = \hat{q}_{14}[\mathbf{x}] + \hat{q}_{16}[\mathbf{x}]$ to estimate $q_{14}[\mathbf{x}] + q_{16}[\mathbf{x}] = -0.6666 f_{C2}[\mathbf{x}] =$, and $\hat{s}_{15,17}[\mathbf{x}] = \hat{q}_{15}[\mathbf{x}] + \hat{q}_{17}[\mathbf{x}]$ to estimate $q_{15}[\mathbf{x}] + q_{17}[\mathbf{x}] = 0.6666 f_{C2}[\mathbf{x}] =$ Averaging these two,

$$\hat{f}_{C2}[\mathbf{x}] = -\tfrac{3}{4}\hat{s}_{14,16}[\mathbf{x}] + \tfrac{3}{4}\hat{s}_{15,17}[\mathbf{x}]. \tag{3.48}$$

Again, a general formula is

$$\hat{f}_{C2}[\mathbf{x}] = -\tfrac{3}{2} v_a \hat{s}_{14,16}[\mathbf{x}] + \tfrac{3}{2} v_b \hat{s}_{15,17}[\mathbf{x}] \tag{3.49}$$

where $v_a + v_b = 1$. Given our best estimate of $f_{C1}[\mathbf{x}]$ and $f_{C2}[\mathbf{x}]$, we can estimate f_L by subtracting the modulated components

$$\hat{f}[\mathbf{x}] = f_{\mathrm{CFA}}[\mathbf{x}] - \sum_{i=1}^{17} \hat{q}_i[\mathbf{x}] \exp(j2\pi(\mathbf{x} \cdot \mathbf{d}_i)) \tag{3.50}$$

Finally, we can recover the RGB components by the inverse transform

$$\begin{bmatrix} \hat{f}_R[\mathbf{x}] \\ \hat{f}_G[\mathbf{x}] \\ \hat{f}_B[\mathbf{x}] \end{bmatrix} = \begin{bmatrix} 1 & -\frac{10}{9} & -2 \\ 1 & \frac{8}{9} & 0 \\ 1 & -\frac{10}{9} & 2 \end{bmatrix} \begin{bmatrix} \hat{f}_L[\mathbf{x}] \\ \hat{f}_{C1}[\mathbf{x}] \\ \hat{f}_{C2}[\mathbf{x}] \end{bmatrix} \tag{3.51}$$

Testing on the 24 Kodak images, with $v_a = v_b = 0.5$ in all cases, we find that $w_a = w_b = 0$, $w_c = w_d = 0.5$ gives good overall performance found among choices for the weights (CPSNR ranges from 31.2 dB to 40.1 dB with a mean value of 36.0 dB). In comparison, equal weights $w_a = w_b = w_c = w_d = 0.25$ is much poorer (CPSNR ranges from 25.4 dB to 36.5 dB with a mean value of 32.3 dB). Interestingly, slightly better results are obtained with an asymmetric choice $w_a = w_b = w_c = 0$, $w_d = 1$ (CPSNR ranges from 31.3 dB to 40.2 dB with a mean value of 36.1 dB). On the other hand, the alternate choice $w_a = w_b = w_d = 0$, $w_c = 1$ is worse (CPSNR ranges from 30.2 dB to 38.9 dB with a mean value of 35.0 dB).

An adaptive estimate would be formed by determining which of the terms are least affected by crosstalk and giving them a higher weighting, while giving the remaining terms more affected by crosstalk a lower weighting. In other words, we seek an adaptive choice of the weights $w_a[\mathbf{x}]$, $w_b[\mathbf{x}]$, $w_c[\mathbf{x}]$, $w_d[\mathbf{x}]$, $v_a[\mathbf{x}]$, $v_b[\mathbf{x}]$ based on local properties of the image.

In the Bayer-like adaptive method we assumed $w_a = w_b = w_c = 0$, $w_d = 1$. The w_d is the assigned weight to $\hat{s}_{12,13}[\mathbf{x}]$, and the other weights do not effect the $\hat{f_{C1}}[\mathbf{x}]$. Thus, we need to extract q_{12} and q_{13} correctly. In the following section we will discuss about designing a Least-Squares filter to extract q_{12} and q_{13}.

Designing filter using Least-Square method

In the previous sections, we designed Gaussian filters for q_2 and q_{10} which are close to the luma. In this section, the least-squares method will be explained. We want to design a filter to extract q_{12} and q_{13}, or $s_{12,13} = q_{12} + q_{13}$, which are all real. Let us first design the complex filter to estimate q_{12}, and it will be the same procedure for any other chroma. We can call the design filter h_{12} for q_{12}. We have:

$$\hat{r}_{12}[\mathbf{x}] = (f_{CFA} * h_{12})[\mathbf{x}] \tag{3.52}$$

$$\hat{q}_{12}[\mathbf{x}] = \hat{r}_{12}[\mathbf{x}] \exp(-j2\pi \mathbf{d}_{12} \cdot \mathbf{x}) \tag{3.53}$$

On the training image $q_{12}[\mathbf{x}] = 0.4444 f_{C1}[\mathbf{x}]$, $r_{12}[\mathbf{x}] = q_{12}[\mathbf{x}] \exp(j2\pi \mathbf{d}_{12} \cdot \mathbf{x})$. Let $W^{(i)}$ be the support of the i^{th} training image, $i = 1, ..., P$. Then the least-square filter is

$$h_{12} = \arg\min_{h} \sum_{i=1}^{P} \sum_{\mathbf{x} \in W^{(i)}} \left| (r_{12}^{(i)} - h * f_{CFA}^{(i)})[\mathbf{x}] \right|^2 \tag{3.54}$$

Let S be the region of support of h_{12}, $|S| = N_B$, then

$$(h * f_{CFA}^{(i)})[n_1, n_2] = \sum_{(k_1,k_2) \in S} h[k_1, k_2] f_{CFA}^{(i)}[n_1 - k_1, n_2 - k_2] \tag{3.55}$$

We prefer to express it in matrix form as follows. First, arrange the filter coefficients into an $N_B \times 1$ column matrix, taking the coefficients of $\mathbf{h}$ column by column from left to right.

$$\mathbf{h}_{1D} = \begin{bmatrix} \mathbf{h}(:,1) \\ \mathbf{h}(:,2) \\ \vdots \\ \mathbf{h}(:,N_{filt}) \end{bmatrix} \tag{3.56}$$

where $N_B = N_{filt}^2$ Let $N_w = \left|W^{(i)}\right|$, assumed the same for all i. Arrange $r_{12}^{(i)}$ into an $N_B \times 1$ column matrix in the same way.

$$\mathbf{r}_{1D,12}^{(i)} = \begin{bmatrix} \mathbf{r}_{12}^{(i)}(:,1) \\ \mathbf{r}_{12}^{(i)}(:,2) \\ \vdots \\ \mathbf{r}_{12}^{(i)}(:,N_W) \end{bmatrix} \tag{3.57}$$

Then

$$\hat{\mathbf{r}}_{1D,12} = \mathbf{Z}^{(i)}\mathbf{h}_{1D} \tag{3.58}$$

where $\mathbf{Z}^{(i)}$ is an $N_W \times N_B$ matrix. Each column of $\mathbf{Z}^{(i)}$ is a reshaped version of $f_{CFA}^{(i)}[n_1 - k_1, n_2 - k_2]$ for some k_1 and k_2, rearranged in the order of $\mathbf{h}_{1D}$.

$$\mathbf{Z}^{(i)}(:, m[k_1, k_2]) = \begin{bmatrix} f_{CFA}^{(i)}[n_1 - k_1, n_2 - k_2](:, 1) \\ f_{CFA}^{(i)}[n_1 - k_1, n_2 - k_2](:, 2) \\ \vdots \\ f_{CFA}^{(i)}[n_1 - k_1, n_2 - k_2](:, N_W) \end{bmatrix} \tag{3.59}$$

where $h_{1D}[m[k_1, k_2]] = h[k_1, k_2]$.

$\mathbf{Z}$ is real value and $\mathbf{r}$ is complex. Equation 3.54 can be written in matrix form as

$$h_{12} = \arg\min_{h} \sum_{i=1}^{P} \left|\left|\mathbf{Z}^{(i)}\mathbf{h} - {\mathbf{r}_{12}}^{(i)}\right|\right|^2 \tag{3.60}$$

This is a standard least-squares problem with solution [34]

$$\mathbf{h}_{1D,12} = [\sum_{i=1}^{p} \mathbf{Z}^{(i)T}\mathbf{Z}^{(i)}]^{-1}[\sum_{i=1}^{p} \mathbf{Z}^{(i)T}\mathbf{r}_{1D,12}^{(i)}] \tag{3.61}$$

$$\mathbf{h}_{12} = \begin{bmatrix} h_{12}(1,1) & \cdots & h_{12}(N_{filt}, 1) \\ \vdots & \ddots & \vdots \\ h_{12}(1, N_{filt}) & \cdots & h_{12}(N_{filt}, N_{filt}) \end{bmatrix} \tag{3.62}$$

Results and discussion

The proposed demosaicking algorithms for the Fujifilm X-Trans pattern have been implemented in the Matlab environment. We reconstruct 24 Kodak images using Fujifilm pattern to compare them with the previous works using Bayer patterns. In fact, we simulated the digital camera processing system. The first step is applying white balancing and gamma correction method on the captured image. Then the CFA images will be reconstructed using the white balanced gamma corrected image. The output images will be reconstructed using the proposed demosaicking process, and the reconstructed images

will be compared with the input (Captured) images. Since the Kodak dataset is a white balanced and gamma corrected dataset, we skip the first step in the camera process. We only apply the demosaicking algorithm on the input Kodak images, and the PSNR and S-CIELAB results calculate the differences between the reconstructed images and the input images as ground truth images.

Table 3.1 and 3.2 show the PSNR and S-CIELAB comparison between the least-squares luma-chroma demultiplexing (LSLCD) method using Bayer and Fujifilm patterns, adaptive and nonadaptive demosaicking schemes using X-Trans pattern for each image as well as the average over 24 Kodak images. The proposed least-square method for Fujifilm pattern is applied based on the Bayer-like adaptive demosaicking. The least-square filters have been designed for two components to optimize the filtering stage. The results show slight changes in terms of PSNR using optimized filter set. Columns of Table 3.1 and 3.2 will be described as follows:

- a) PSNR and S-CIELAB of least-square method using RGB-Bayer pattern over Kodak dataset [29]. The software and results are available at [28]
- b) PSNR and S-CIELAB of non-adaptive demosaicking method using Fujifilm X-Trans pattern over Kodak dataset
- c) PSNR and S-CIELAB of adaptive demosaicking method using Fujifilm X-Trans pattern over Kodak dataset (First adaptive approach)
- d) PSNR and S-CIELAB of Bayer-like adaptive demosaicking method using Fujifilm X-Trans pattern over Kodak dataset (Second adaptive approach)
- e) PSNR and S-CIELAB of least-square method using Fujifilm X-Trans pattern over Kodak dataset. It has been presented using Bayer-like adaptive demosaicking algorithm in this chapter.

Both tables show that the proposed adaptive and least-square demosaicking schemes using the Fujifilm pattern give us lower PSNR than the LSLCD demosaicking scheme using Bayer pattern, but the visual results show improvement in the reconstructed details and

its colors. The result of PSNR and S-CIELAB lead to the same conclusions according to Table 3.1 and 3.2.

Figure 3.4 shows the horizontal, vertical and diagonal details in the reconstructed images using Bayer and Fujifilm pattern. The visual results show that the X-trans pattern gives less false colors than Bayer pattern on these details.

Comparing Fujifilm X-Trans and RGB-Bayer patterns based on the provided PSNR, S-CIELAB and the reconstructed images, we can conclude that the quality of the reconstructed image with least-square method using Bayer pattern is better than reconstructed images with least-square method using Fujifilm X-Trans pattern across the edges while the number of false color in reconstructed image using Fujifilm X-Trans pattern is less than RGB-Bayer. Since there are more color components in Fujifilm X-Trans pattern, the overlapping effect between color components will increase, and extracting accurate color components will be more complicated. Thus it will result in lower quality in the sharp area and edges. There is a trade off between the amount of correct estimated colors and the quality of the images in the edges. Thus, less color components in the pattern results in more false color and better reconstructed edges.

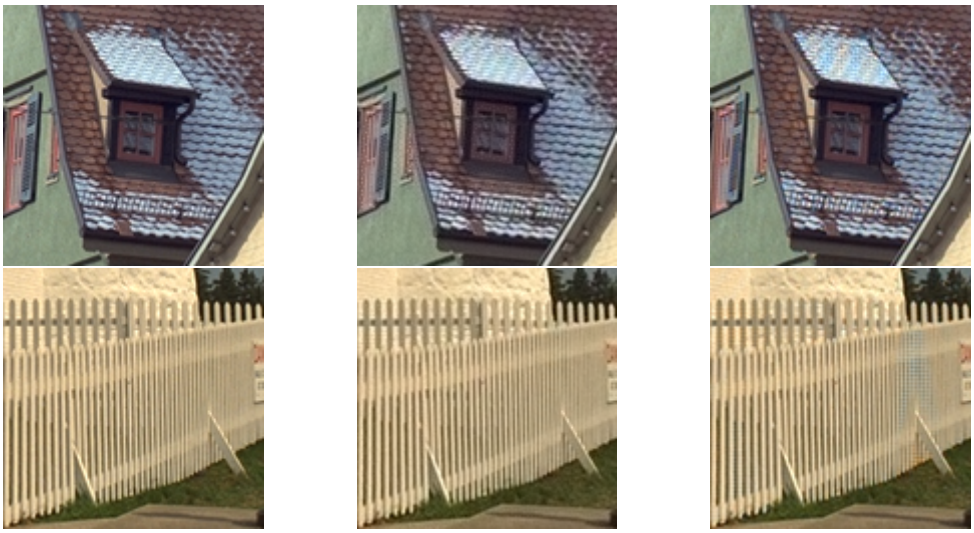

(a) Original image (b) Reconstructed using X-Trans (c) Reconstructed using Bayer

Figure 3.4: Comparison between The new method using X-Trans and LSLCD method using Bayer

Image number	(a)	(b)	(c)	(d)	(e)
01	37.92	32.09	36.21	35.64	35.82
02	40.65	35.75	36.52	36.54	36.64
03	42.22	37.14	36.76	36.68	36.77
04	41.09	36.16	36.22	36.01	36.08
05	37.92	32.15	32.72	32.62	32.73
06	39.95	35.72	38.82	38.45	38.55
07	42.52	36.80	36.84	36.70	36.73
08	35.32	26.90	33.95	33.61	33.68
09	42.57	36.37	38.15	37.96	38.08
10	42.63	37.22	38.95	38.54	38.63
11	39.81	34.37	36.49	36.25	36.32
12	43.14	37.93	39.19	38.89	39.01
13	34.20	30.91	32.91	32.38	32.46
14	36.77	31.54	31.13	31.28	31.34
15	39.83	35.50	35.99	35.73	35.79
16	43.63	39.73	41.00	40.22	40.28
17	41.63	37.62	39.28	39.23	39.29
18	37.28	32.92	34.36	34.18	34.23
19	40.53	33.33	38.21	37.90	37.96
20	40.97	36.54	37.66	37.51	37.57
21	38.79	34.84	37.08	36.84	36.90
22	38.57	32.99	34.94	34.92	35.03
23	42.98	37.50	37.06	36.98	37.02
24	35.34	33.11	35.53	35.42	35.55
Average over 24 images	39.8	34.80	36.50	36.27	36.35

Table 3.1: PSNR of Kodak images using Bayer and Fujifilm X-Trans patterns.(a) RGB-Bayer (Least-Square method), (b) Fujifilm (Non Adaptive demosaicking), (c) Fujifilm (Adaptive demosaicking), (d) Fujifilm (Bayer-like Adaptive demosaicking), (e) Fujifilm (Least-Square method)

.

Image number	(a)	(b)	(c)	(d)	(e)
1	1.19	2.37	1.68	2.16	2.11
2	0.66	1.21	1.15	1.21	1.20
3	0.51	0.98	0.98	1.13	1.12
4	0.66	1.26	1.25	1.37	1.37
5	1.07	2.43	2.34	2.58	2.55
6	0.78	1.19	1.03	1.27	1.25
7	0.55	1.26	1.25	1.33	1.33
8	1.47	3.52	1.93	2.34	2.32
9	0.58	1.19	0.99	1.15	1.13
10	0.54	1.05	0.92	1.05	1.04
11	0.75	1.43	1.22	1.43	1.42
12	0.48	0.88	0.79	0.96	0.95
13	1.62	2.57	2.25	2.95	2.91
14	1.00	1.90	1.92	2.14	2.13
15	0.64	1.23	1.12	1.25	1.24
16	0.53	0.83	0.79	1.00	0.99
17	0.51	0.86	0.77	0.90	0.89
18	0.99	1.87	1.70	1.97	1.95
19	0.77	1.44	1.11	1.31	1.29
20	0.57	0.95	0.86	1.03	1.02
21	0.91	1.42	1.28	1.53	1.51
22	0.93	1.94	1.63	1.83	1.81
23	0.49	1.04	1.06	1.13	1.14
24	0.98	1.72	1.34	1.57	1.55
Average over 24 images	0.79	1.52	1.31	1.52	1.51

Table 3.2: S-CIELAB of Kodak images using Bayer and Fujifilm X-Trans patterns.(a) RGB-Bayer (Least-Square method), (b) Fujifilm (Non Adaptive demosaicking), (c) Fujifilm (Adaptive demosaicking), (d) Fujifilm (Bayer-like Adaptive demosaicking), (e) Fujifilm (Least-Square method)

.

3.4 Four channel color filter array

Most of the four channel CFAs contain red, green, blue and white/ panchromatic filters. There are some other four channel CFAs like: RGBE and CYGM. RGBE is an alternative for Bayer and one of the green pixels in Bayer has been modified to emerald. It has been used in some Sony cameras. CYGM is used in a few cameras and it is a 2×2 pattern with one cyan, one yellow, one green, and one magenta. Figure 3.5 shows some sample four channel patterns. White filters in RGBW patterns usually pass all the color spectrum and the measured values through white filters can be estimated as a combination of red, green and blue values.

Since the white filters receive more signal to noise ratio than color filters, we decided to study the noise reduction impact on different RGBW patterns. The following sections present non-adaptive as well as adaptive demosaicking algorithms on RGBW-Bayer, RGBW-Kodak and a proposed RGBW (5×5) in [45]. The optimized method using the least square method is also provided for RGBW-Bayer, and the noise effect on this pattern will be discussed in chapter 4.

Since most of standard datasets like Kodak dataset contain red, green and blue color information, and they do not provide clear/panchromatic color information, we will estimated the value of clear/panchromatic filters in three different ways as follows:

- Initially, the clear/panchromatic pixels value will be assumed as a combination of equal amount of red, green and blue pixels values as $W = \frac{1}{3}R + \frac{1}{3}G + \frac{1}{3}B$. Then the CFA image will be calculated based on Kodak dataset for RGBW-Kodak, RGBW-5×5 and RGBW-Bayer patterns. The demosaicking algorithm will be designed and tested on the CFA images of all three patterns. The results will be compared and the best demosaicking algorithm using one of these CFA patterns will be chosen.

- Secondly, the clear/panchromatic pixels will be assumed as a linear combination of red, green and blue pixel values with different coefficient. Those coefficients are not necessarily equal. The panchromatic pixels will be estimated as $W = \alpha_R R + \alpha_G G + \alpha_B B$, and α_R, α_G and α_B will be estimated using an optimization method over

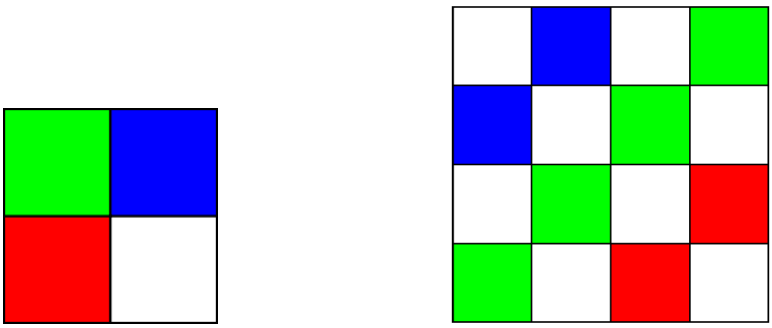

(a) RGBW-Bayer pattern

(c) RGBW-Kodak pattern

(b) RGBE pattern

(d) CYGM pattern

Figure 3.5: Sample four channel CFA patterns

Macbeth color checker [37]. Then, the chosen CFA among three four-channel CFAs will be calculated using the new set of coefficients, and the demosaicking algorithm for the same CFA will be updated.

- Finally, the estimated clear/ panchromatic pixel values will be validated using a hyperspectral image dataset. The red, green, blue and panchromatic pixels for the chosen CFA will be calculated on the hyperspectral images, and the demosaicking algorithm for the same CFA will be tested using hyperspectral image information.

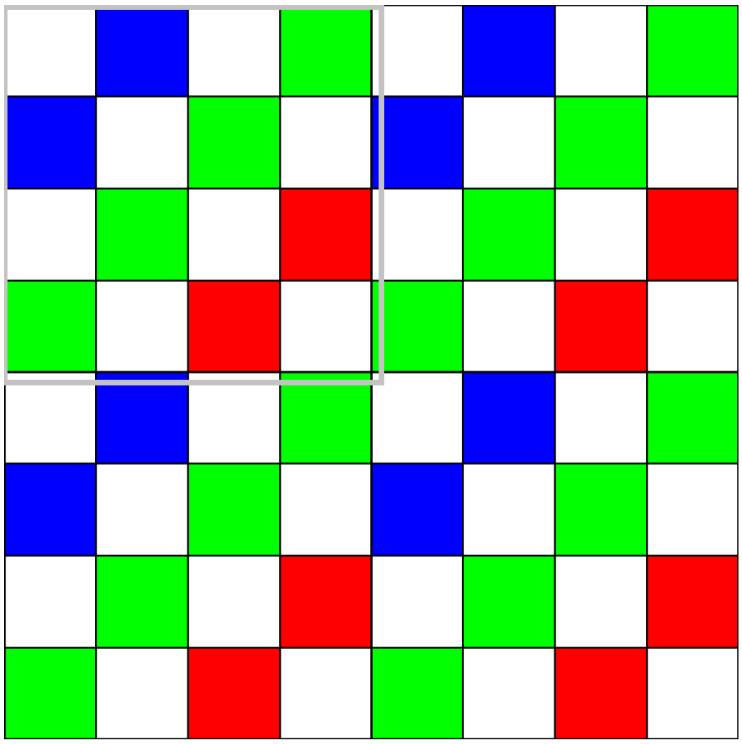

Figure 3.6: An 8×8 section of the Kodak-RGBW pattern showing four periods

3.4.1 RGBW-Kodak pattern

We have studied and optimized the reconstruction technique for a new sampling structure with four color components. The Kodak-RGBW CFA pattern is a 4×4 template containing eight white pixels, four green pixels, two blue and two red as illustrated in Figure 3.6 [22].

This study involves the design of an appropriate demosaicking method which has been tested on the Kodak image dataset. Since four-channel CFAs usually improve signal to noise ratio and reconstruction fidelity, we attempt to model the demosaicking steps using Kodak-RGBW pattern and simulate non-adaptive and adaptive demosaicking algorithms in Matlab software. Due to the success of methods for solving the demosaicking problem in the frequency domain, we also present an algorithm using a frequency domain method. A detailed optimization of filter parameters and the region of support will be addressed.

Demosaicking algorithm

The CFA signal is sampled on lattice $\Lambda = Z^2$ with reciprocal lattice $\Lambda^* = Z^2$. The pattern is 4×4 and one period with respect to the periodicity lattice covers the sixteen different points for each pixel. The periodicity lattice and corresponding reciprocal lattice are given by:

$$V_\Gamma = \begin{bmatrix} 4 & 0 \\ 0 & 4 \end{bmatrix}, V_{\Gamma^*} = \begin{bmatrix} \frac{1}{4} & 0 \\ 0 & \frac{1}{4} \end{bmatrix}. \tag{3.63}$$

The demosaicking model that is used in this study has been described in [18] and we modified it for RGBW-Kodak pattern. According to the analysis, the CFA signal can be described as a sum of chroma and luma components.

$$f_{CFA}[\mathbf{x}] = \sum_{i=1}^{K} q_i[\mathbf{x}] \exp(j2\pi(\mathbf{x} \cdot \mathbf{d}_i)), K = 16 \tag{3.64}$$

As we discussed in chapter 2, $\boldsymbol{b}_i$ refers to the columns of matrix $\boldsymbol{B}$ which gives the coset representatives of Γ in Λ. Also d_i refers to the columns of matrix $\boldsymbol{D}$ and they are coset representatives of Λ^* in Γ^*. The matrix $\boldsymbol{D}$ is a $2 \times K$ matrix where K is the number of components in one period of the lattice, which is equal to 16 for the RGBW-Kodak pattern. We have used

$$\boldsymbol{D} = \frac{1}{4} \times \begin{bmatrix} 0 & 1 & -1 & 0 & 0 & 1 & -1 & 1 & -1 & 2 & 0 & 2 & -1 & 2 & 1 & 2 \\ 0 & 0 & 0 & 1 & -1 & 1 & -1 & -1 & 1 & 0 & 2 & -1 & 2 & 1 & 2 & 2 \end{bmatrix}, \tag{3.65}$$

$$\boldsymbol{B} = \begin{bmatrix} 0 & 1 & 2 & 3 & 0 & 1 & 2 & 3 & 0 & 1 & 2 & 3 & 0 & 1 & 2 & 3 \\ 0 & 0 & 0 & 0 & 1 & 1 & 1 & 1 & 2 & 2 & 2 & 2 & 3 & 3 & 3 & 3 \end{bmatrix}. \tag{3.66}$$

The luma and chroma components can be extracted from the CFA image, so we can calculate them using the following equation:

$$\boldsymbol{q}[\mathbf{x}] = \boldsymbol{M}\boldsymbol{f}[\mathbf{x}] \tag{3.67}$$

$$\boldsymbol{f} = \begin{bmatrix} f_1 & , & f_2 & , & f_3 \end{bmatrix}^T, and \quad \boldsymbol{q} = \begin{bmatrix} q_1 & , & q_2 & , & \dots & , & q_{16} \end{bmatrix}^T \tag{3.68}$$

The calculated matrix $\boldsymbol{M}$ for 16 components is shown below for Kodak-RGBW pattern.

$$\boldsymbol{M} = \begin{bmatrix} 0.125 & 0.25 & 0.125 & 0.5 \\ -0.0625+0.0625j & 0 & 0.0625-0.0625j & 0 \\ -0.0625-0.0625j & 0 & 0.0625+0.0625j & 0 \\ 0.0625-0.0625j & 0 & -0.0625+0.0625j & 0 \\ +0.0625+0.0625j & 0 & -0.0625-0.0625j & 0 \\ 0.125 & -0.25 & 0.125 & 0 \\ -0.125 & 0.25 & -0.125 & 0 \\ 0 & 0 & 0 & 0 \\ 0 & 0 & 0 & 0 \\ 0 & 0 & 0 & 0 \\ 0 & 0 & 0 & 0 \\ -0.0625+0.0625j & 0 & 0.0625-0.0625j & 0 \\ +0.0625-0.0625j & 0 & -0.0625+0.0625j & 0 \\ -0.0625-0.0625j & 0 & +0.0625+0.0625j & 0 \\ +0.0625+0.0625j & 0 & -0.0625-0.0625j & 0 \\ -0.125 & -0.25 & -0.125 & 0.5 \end{bmatrix} \tag{3.69}$$

The matrix $\boldsymbol{J}$ is defining the four input channels: R, G, B and W, while each column of the matrix represents one of the colors in this pattern.

$$\boldsymbol{J} = \begin{bmatrix} 0 & 0 & 0 & 1 & 0 & 0 & 1 & 0 & 0 & 0 & 0 & 0 & 0 & 0 & 0 & 0 \\ 0 & 1 & 0 & 0 & 1 & 0 & 0 & 0 & 0 & 0 & 0 & 1 & 0 & 0 & 1 & 0 \\ 0 & 0 & 0 & 0 & 0 & 0 & 0 & 0 & 0 & 1 & 0 & 0 & 1 & 0 & 0 & 0 \\ 1 & 0 & 1 & 0 & 0 & 1 & 0 & 1 & 1 & 0 & 1 & 0 & 0 & 1 & 0 & 1 \end{bmatrix}^T \tag{3.70}$$

As we discussed before, we assumed to have three-channel CFA camera input and simulate the values of the white filter in the CFA image. Ideally the white filter should pass all three colors and does not absorb any color spectrum. So the value of the white pixels in CFA image can be estimated as $W = \frac{1}{3}R + \frac{1}{3}G + \frac{1}{3}B$. This research is trying to show that the captured panchromatic filter values in digital cameras usually contain less noise compared to the other three color filters. This hypothesis will be discussed in presence of noise in

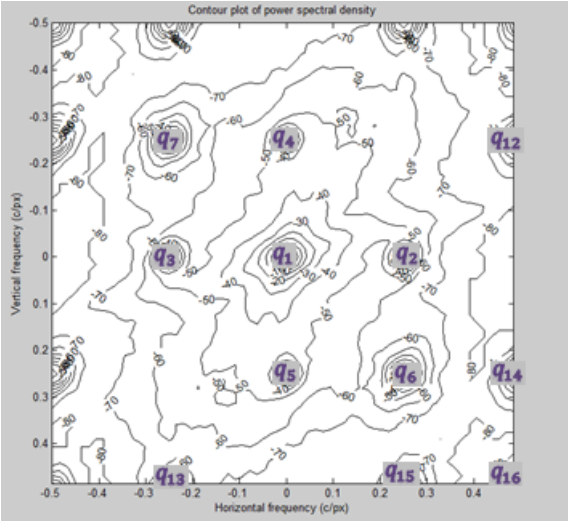

Figure 3.7: Luma- Chroma position in one unit cell for RGBW-Kodak pattern

Chapter 4.

$$W = \frac{1}{3}(R + B + G) \tag{3.71}$$

In the frequency domain, the Fourier transform of the CFA signal is given by:

$$F_{\text{CFA}}(\mathbf{u}) = \sum_{i=1}^{16} Q_i(\mathbf{u} - \mathbf{d}_i) \quad \text{Where} \quad Q_i(\mathbf{u}) \triangleq \mathcal{F}\{q_i[\mathbf{x}]\} \tag{3.72}$$

The chroma components are extracted with bandpass filters centered at the frequencies $\mathbf{d}_i$. The next step in the non-adaptive demosaicking algorithm is reconstructing the full RGB color image using the pseudo inverse matrix $\boldsymbol{M}^\dagger$ and extracted chromas using the following equation. Figure 3.7 shows the position of 16 extracted component in one unit cell of Λ^*. Since we cannot fully extract the luma and chromas close to luma, those chromas can be reconstructed using the rest of the components.

$$\hat{\boldsymbol{f}}[\mathbf{x}] = \boldsymbol{M}^\dagger \hat{\boldsymbol{q}}[\mathbf{x}] \tag{3.73}$$

Based on the matrix $\boldsymbol{M}$, q_2 to q_5 and q_{12} to q_{15} can be reconstructed by using only one of them. Also matrix $\boldsymbol{M}$ shows that the values of components q_8 to q_{11} are zero.

Usually we are able to better extract the components which are further from the luma, and we prefer to use the information of those components to reconstruct the other components which are closer to the luma to avoid overlapping effects between luma and the

components close to luma [18]. In this adaptive algorithm we have four components close to the luma: q_2 to q_5, and we can reconstruct them using one of the components from q_{12} to q_{15} using the following equations.

$$q_2 = {q_3}^* = -q_4 = -{q_5}^* = q_{12} = -q_{13} = q_{14}^* = -q_{15}^* \tag{3.74}$$

$$q_2 = q_{12}, q_3 = q_{14}, q_4 = q_{13}, q_5 = q_{15} \tag{3.75}$$

By using the further chroma information, the reconstructed q_2 to q_5 will be more accurate than the non-adaptive algorithm. The luma usually will be calculated by subtracting all 16 modulated chromas from the CFA image. Using more precise chroma information will enhance the quality of luma and quality of the reconstructed image as a result. In our revised demosaicking method, we calculated the value of q_2 to q_5 based on the filtered value for q_{14}, which is further from the luma, using equations 3.74 and 3.75. The results will be discussed in the following section. As we discussed before, the reconstructed color image contains three different color components which are R, G and B. In this pattern there are one luma and three groups of chroma components in the frequency domain analysis. The remaining components can be reconstructed using those basic components as we formulate in the following equations.

$$P_1 = Luma \tag{3.76}$$

$$P_2 = q_2 = {q_3}^* = -q_4 = -{q_5}^* = q_{12} = -q_{13} = q_{14}^* = -q_{15}^* \tag{3.77}$$

$$P_3 = q_6 = -q_7 \tag{3.78}$$

$$P_4 = q_{16} \tag{3.79}$$

Due to the similarity between the chromas in each group, all of the chroma components in both adaptive and non-adaptive algorithm have been extracted using three different types of Gaussian filter. The first filter has been designed for the sets of components in P_2. The second filter is filtering q_6 and q_7, and the last filter is only filtering the q_{16}.

Results and discussion

In this research, we have reconstructed the 24 Kodak images using the RGBW-Kodak pattern to compare them with the RGB-Bayer pattern. As we stated previously, the Kodak

dataset are white balanced and gamma corrected, so we only apply the demosaicking algorithm on the input Kodak images, and the results compare the reconstructed images with the input images as ground truth images.

Tables 3.3 and 3.4 show the PSNR and S-CIELAB comparison between the least-squares luma- chroma demultiplexing (LSLCD) method using the Bayer CFA, and the revised and non-adaptive demosaicking schemes using the RGBW-Kodak pattern over Kodak dataset as well as the average PSNR over 24 Kodak images.

According to the presented results, the proposed revised demosaicking scheme using the RGBW-Kodak pattern largely improved the results of the non-adaptive algorithm using the same pattern. The tables also show the comparison between the least-squares optimized method using RGB-Bayer pattern and our revised method using RGBW-Kodak pattern. Also Figure 3.8 provides the reconstructed images using the mentioned patterns and the original images. The results show some improvements mostly in horizontal and vertical axes using RGBW-Kodak. The reconstructed images contain fewer false colors in different axes using our algorithm compared to the RGB-Bayer pattern, while the least-squares method using the Bayer pattern reconstructs the edge details more accurately.

(a) Original image (b) Reconstructed using RGB-Bayer (c) Reconstructed using RGBW-Kodak

Figure 3.8: Comparison between the revised method using RGBW-Kodak and LSLCD method using RGB-Bayer

Kodak image number	RGB LSLCD method	RGBW-Kodak(Revised demosaicking)	RGBW-Kodak(Non-Adaptive demosaicking)
1	37.92	36.33	27.12
2	40.65	36.10	33.55
3	42.22	36.67	34.74
4	41.09	35.86	34.10
5	37.92	31.90	29.06
6	39.95	38.56	29.55
7	42.52	36.35	33.83
8	35.32	34.02	24.56
9	42.57	37.93	32.25
10	42.63	38.74	33.83
11	39.81	36.36	30.84
12	43.14	39.13	33.27
13	34.20	33.02	27.54
14	36.77	30.83	29.37
15	39.83	35.76	33.21
16	43.63	41.25	33.01
17	41.63	38.68	34.54
18	37.28	34.01	30.46
19	40.53	38.06	28.52
20	40.97	37.45	32.06
21	38.79	36.69	30.02
22	38.57	34.82	31.01
23	42.98	36.40	34.29
24	35.34	35.27	30.12
Average over 24 images	39.8	36.3	31.3

Table 3.3: PSNR of Kodak images using RGB-Bayer (least-square method) and RGBW-Kodak (Non-adaptive and Revised method) and the average PSNR over 24 Kodak images

Kodak image number	RGB LSLCD method	RGBW-Kodak(Revised demosaicking)	RGBW-Kodak(Non-Adaptive demosaicking)
1	1.19	2.24	4.96
2	0.66	1.28	1.94
3	0.66	1.27	1.87
4	0.66	1.57	2.03
5	1.07	3.45	4.09
6	0.78	1.49	3.44
7	0.55	1.70	2.20
8	1.47	2.63	5.99
9	0.58	1.37	2.41
10	0.54	1.24	2.06
11	0.75	1.67	2.80
12	0.48	1.07	2.18
13	1.62	3.28	4.95
14	1.00	2.60	3.38
15	0.64	1.47	2.04
16	0.53	1.10	2.34
17	0.51	1.16	1.71
18	0.99	2.44	3.13
19	0.77	1.57	3.15
20	0.57	1.17	2.29
21	0.91	1.89	3.28
22	0.93	2.23	3.16
23	0.49	1.44	1.81
24	0.98	2.06	3.30
Average over 24 images	0.79	1.81	2.94

Table 3.4: S-CIELAB of Kodak images using RGB-Bayer (least-square method) and RGBW-Kodak (Non-adaptive and Revised method) and the average S-CIELAB over 24 Kodak images

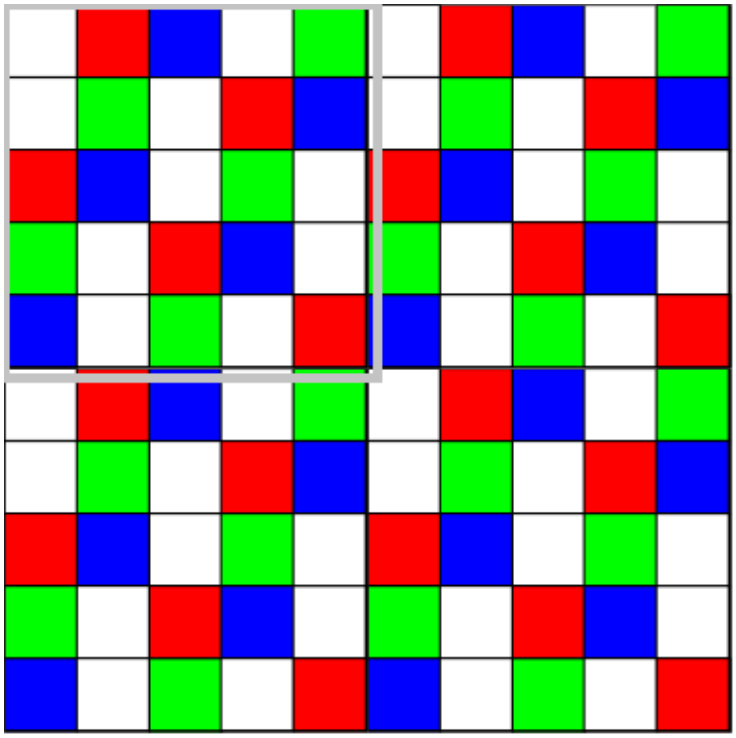

Figure 3.9: RGBW(5×5)[45] (four periods)

3.4.2 RGBW - 5×5 pattern

The 5×5 RGBW CFA has been proposed in [45] and the demosaicking algorithm presented in [29] has been implemented on it. We are presenting some improvement on the result of the reconstructed images using this pattern with the same demosaicking algorithm. Figure 3.9 shows a new proposed RGBW CFA in [45]. This CFA is a 5×5 template containing 10 white pixel and equal number of red, green and blue filters.

Demosaicking algorithm

As we can see in Figure 3.10 a smaller pattern containing five pixels is repeated in this CFA. Using the smaller pattern, the CFA signal is sampled on lattice $\Lambda = Z^2$ with reciprocal lattice $\Lambda^* = Z^2$. The periodicity lattice and corresponding reciprocal lattice are

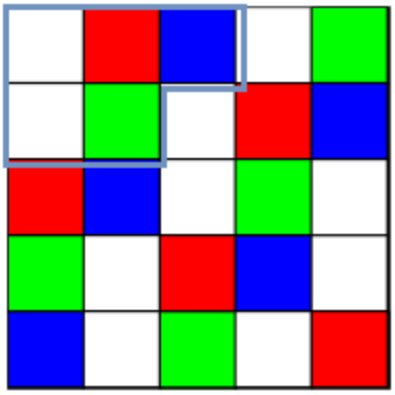

Figure 3.10: The smaller repeated pattern in RGBW(5×5)

given by:

$$V_\Gamma = \begin{bmatrix} 2 & -1 \\ 1 & 2 \end{bmatrix}, V_{\Gamma^*} = \begin{bmatrix} \frac{2}{5} & \frac{-1}{5} \\ \frac{1}{5} & \frac{2}{5} \end{bmatrix} \tag{3.80}$$

Using these lattices, we can model the CFA signal as a sum of luma and chroma components. The demosaicking model is presented in Chapter 2, and it is modified here for this pattern.

$$f_{\text{CFA}}[\mathbf{x}] = \sum_{i=1}^{K} q_i[\mathbf{x}] \exp(j2\pi(\mathbf{x} \cdot \mathbf{d}_i)), \tag{3.81}$$

$$K = 5 \tag{3.82}$$

As we discussed in Chapter 2, matrix $\boldsymbol{B}$ and matrix $\boldsymbol{D}$ for this CFA pattern are as follows.

$$\boldsymbol{B} = \begin{bmatrix} 0 & 1 & 2 & 0 & 1 \\ 0 & 0 & 0 & 1 & 1 \end{bmatrix}, \tag{3.83}$$

$$\boldsymbol{D} = \frac{1}{5} \times \begin{bmatrix} 0 & 2 & -2 & -1 & 1 \\ 0 & 1 & -1 & 2 & -2 \end{bmatrix}, \tag{3.84}$$

Also matrix $\boldsymbol{M}$ will be calculated using the following equations.

$$\boldsymbol{q}[\mathbf{x}] = \boldsymbol{M}\boldsymbol{f}[\mathbf{x}] \tag{3.85}$$

$$\boldsymbol{f} = \begin{bmatrix} f_1, & f_2, & f_3 \end{bmatrix}^T \tag{3.86}$$

$$\boldsymbol{q} = \begin{bmatrix} q_1, & q_2, & \dots & , & q_5 \end{bmatrix}^T$$

$$K = 5 \tag{3.87}$$

$$\boldsymbol{M}_{(RGBW5\times5)} = \begin{bmatrix} 0.2 & 0.2 & 0.2 & 0.4 \\ -0.1618 - 0.1176j & -0.1618 + 0.1176j & 0.0618 + 0.1902j & 0.2618 - 0.1902j \\ -0.1618 + 0.1176j & -0.1618 - 0.1176j & 0.0618 - 0.1902j & 0.2618 + 0.1902j \\ 0.0618 + 0.1902j & 0.0618 - 0.1902j & -0.1618 + 0.1176j & 0.0382 - 0.1176j \\ 0.0618 - 0.1902j & 0.0618 + 0.1902j & -0.1618 + 0.1176j & 0.0382 - 0.1176j \end{bmatrix} \tag{3.88}$$

The matrix $\boldsymbol{J}$ is a 5×4 matrix, as we explained in Chapter 2, and it defines four input channels: R, G, B and W. The values of the white filter in the CFA image will be calculated as $W = \frac{1}{3}R + \frac{1}{3}G + \frac{1}{3}B$.

$$\boldsymbol{J}_{RGBW5\times5} = \begin{bmatrix} 0 & 0 & 0 & 1 \\ 1 & 0 & 0 & 0 \\ 0 & 0 & 1 & 0 \\ 0 & 0 & 0 & 1 \\ 0 & 1 & 0 & 0 \end{bmatrix}^T \tag{3.89}$$

$$W = \frac{1}{3}(R + B + G) \tag{3.90}$$

In the frequency domain, the Fourier transform of the CFA signal is:

$$F_{\text{CFA}}(\mathbf{u}) = \sum_{i=1}^{K} Q_i(\mathbf{u} - \mathbf{d}_i) \quad \text{Where} \quad Q_i(\mathbf{u}) \triangleq \mathcal{F}\{q_i[\mathbf{x}]\} \tag{3.91}$$

The chroma components are extracted with bandpass filters centered at the frequencies $\mathbf{d}_i$. The next step in the non-adaptive demosaicking algorithm is reconstructing the full RGB color image using the pseudo inverse matrix $\boldsymbol{M}^{\dagger}$. Figure 3.11 shows the position of 5 extracted component in one unit cell of Λ^*. Since we reduce the number of repeated color filters from 25 to 5, there is four chroma components with the same Euclidean distance of the luma in one unit cell. Thus, there is no other way to isolate the chromas from the luma, and enhance the quality of the reconstructed chromas with an adaptive algorithm.

Results and discussion

The demosaicking method has been applied on the input Kodak images as previous sections, and the PSNR results calculate the difference between reconstructed images and

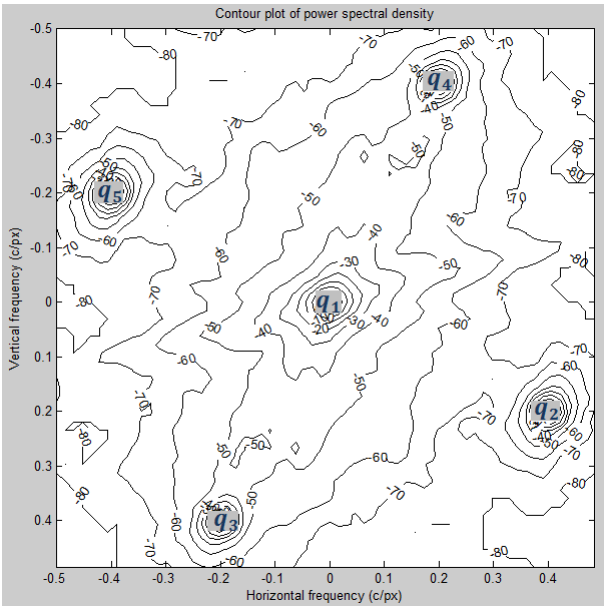

Figure 3.11: Luma- Chroma position in one unit cell-RGBW(5×5)

the input images. Although the method discussed in [45] is using the same demosaicking approach, our implemented algorithm improved the PSNR slightly and the visual results also shows some improvement in color estimation. Table 3.5 shows the comparison between our method and the proposed method in [45] using RGBW 5×5 as well as the non-adaptive demosaicking algorithm using RGBW-Bayer that will be discuss in the next section.

Image number in dataset	RGBW(5×5) proposed Non-Adaptive demosaicking)	RGBW(5×5) reconstructed in [45] using Dubois Method
1	36.56	35.23
2	37.05	37.49
3	37.46	37.46
4	37.21	37.32
5	33.47	32.96
6	38.88	36.56
7	37.94	38.22
8	34.35	33.28
9	38.84	38.78
10	37.77	36.63
11	37.01	36.13
12	40.39	40.18
13	32.93	30.91
14	31.87	32.24
15	36.65	36.29
16	40.98	39.58
17	39.24	37.90
18	34.79	33.87
19	38.58	37.53
20	37.58	36.71
21	37.31	36.14
22	35.81	35.59
23	38.04	38.86
24	35.27	31.90
Average over 24 images	36.9	35.4

Table 3.5: PSNR of proposed Non-Adaptive demosaicking method using RGBW(5×5) pattern and the presented method in [45] for Kodak dataset

3.4.3 RGBW-Bayer pattern

Figure 3.12 shows the RGBW-Bayer pattern. The RGBW-Bayer period contains four pixels, and is the same as the RGB-Bayer pattern where one of the green filters has been replaced with a white pixel.

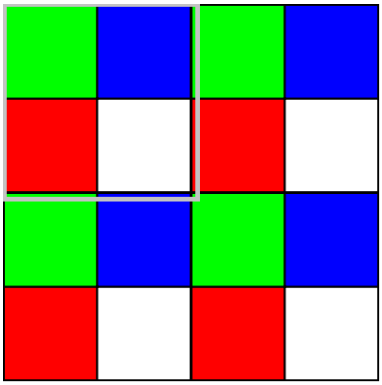

Figure 3.12: RGBW-Bayer pattern

Demosaicking algorithm

The CFA signal is sampled on lattice $\Lambda = Z^2$ with reciprocal lattice $\Lambda^* = Z^2$. The periodicity lattice and corresponding reciprocal lattice are given by:

$$V_\Gamma = \begin{bmatrix} 2 & 0 \\ 0 & 2 \end{bmatrix}, V_{\Gamma^*} = \begin{bmatrix} \frac{1}{2} & 0 \\ 0 & \frac{1}{2} \end{bmatrix} \tag{3.92}$$

Using the mentioned lattices, we can model the CFA signal as a sum of luma and chroma components. The demosaicking model described in [18] has been used and modified here.

$$f_{\text{CFA}}[\mathbf{x}] = \sum_{i=1}^{K} q_i[\mathbf{x}] \exp(j2\pi(\mathbf{x} \cdot \mathbf{d}_i))), \tag{3.93}$$

$$K = 4 \tag{3.94}$$

According to [18], $\mathbf{b}_i$ refers to the columns of matrix $\boldsymbol{B}$ which gives the coset representative of Γ in Λ. Also $\mathbf{d}_i$ refers to the columns of matrix $\boldsymbol{D}$ and they are coset representatives of

Λ^* in Γ^*.

$$\boldsymbol{B} = \begin{bmatrix} 0 & 1 & 0 & 1 \\ 0 & 0 & 1 & 1 \end{bmatrix}, \tag{3.95}$$

The matrix $\boldsymbol{D}$ is a $2 \times K$ matrix where K is the number of components in one period of the lattice, which is equal to 4 in RGBW-Bayer.

$$\boldsymbol{D} = \frac{1}{2} \times \begin{bmatrix} 0 & 1 & 0 & 1 \\ 0 & 0 & 1 & 1 \end{bmatrix}, \tag{3.96}$$

The luma and chroma components can be extracted from the CFA image, so we can calculate the $\boldsymbol{M}$ using the following equation.

$$\boldsymbol{q}[\mathbf{x}] = \boldsymbol{M}\boldsymbol{f}[\mathbf{x}] \tag{3.97}$$

$$\boldsymbol{f} = \begin{bmatrix} f_1, & f_2, & f_3 \end{bmatrix}^T \tag{3.98}$$

$$\boldsymbol{q} = \begin{bmatrix} q_1, & q_2, & q_3, & q_4 \end{bmatrix}^T$$

The calculated matrices $\boldsymbol{M}$ for each CFA are as follow.

$$\boldsymbol{M}_{Bayer} = \begin{bmatrix} 0.25 & 0.25 & 0.25 & 0.25 \\ -0.25 & 0.25 & 0.25 & -0.25 \\ 0.25 & 0.25 & -0.25 & -0.25 \\ -0.25 & 0.25 & -0.25 & 0.25 \end{bmatrix} \tag{3.99}$$

The matrix $\boldsymbol{J}$ is defining the four input channels: R, G, B and W, while each column of the matrix represents one of the colors in this pattern. As we discussed before, we assume that the white filter should pass all three colors and does not absorb any color spectrum. So the value of the white pixels in CFA image can be estimated as the summation of R, G and B divided by three. The value that has been captured by the white filter usually contains less noise compared the other three color filters and the optimized results of this study can be used for noise reduction purposes in the future.

$$\boldsymbol{J}_{Bayer} = \begin{bmatrix} 0 & 1 & 0 & 0 \\ 1 & 0 & 0 & 0 \\ 0 & 0 & 1 & 0 \\ 0 & 0 & 0 & 1 \end{bmatrix}^T \tag{3.100}$$

The chroma components are filtered using bandpass filters centered at the frequencies $\mathbf{d}_i$. The full color image will be reconstructed using matrix $\boldsymbol{M}^{\dagger}$ in the non-adaptive demosaicking algorithm. Figure 3.13 shows the luma-chroma position in one unit cell.

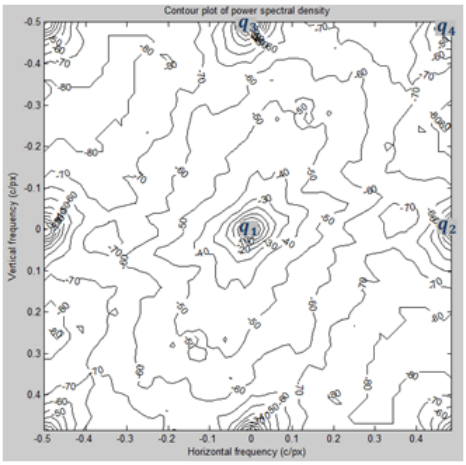

Figure 3.13: Luma- Chroma position in one unit cell for RGBW-Bayer

Adaptive demosaicking algorithm for RGBW-Bayer pattern

Note that with our first assumption about $W = \frac{1}{3}(R + B + G)$, we can simplify our initial implementations as follows:

$$f_4(\mathbf{x}) = \frac{1}{3}(f_1(\mathbf{x}) + f_2(\mathbf{x}) + f_3(\mathbf{x})) \tag{3.101}$$

So we can recalculate all chromas.

$$q_1(\mathbf{x}) = \frac{1}{3}(f_1(\mathbf{x}) + f_2(\mathbf{x}) + f_3(\mathbf{x})) \tag{3.102}$$

$$q_2(\mathbf{x}) = \frac{1}{3}(f_1(\mathbf{x}) + \frac{1}{2}f_2(\mathbf{x}) + \frac{1}{2}f_3(\mathbf{x})) \tag{3.103}$$

$$q_3(\mathbf{x}) = \frac{1}{3}(\frac{1}{2}f_1(\mathbf{x}) + \frac{1}{2}f_2(\mathbf{x}) - f_3(\mathbf{x})) \tag{3.104}$$

$$q_4(\mathbf{x}) = \frac{1}{3}(-\frac{1}{2}f_1(\mathbf{x}) + f_2(\mathbf{x}) - \frac{1}{2}f_3(\mathbf{x})) \tag{3.105}$$

In matrix form

$$\begin{bmatrix} q_1(\mathbf{x}) \\ q_2(\mathbf{x}) \\ q_3(\mathbf{x}) \\ q_4(\mathbf{x}) \end{bmatrix} = \begin{bmatrix} \frac{1}{3} & \frac{1}{3} & \frac{1}{3} \\ -\frac{1}{3} & \frac{1}{6} & \frac{1}{6} \\ \frac{1}{6} & \frac{1}{6} & -\frac{1}{3} \\ -\frac{1}{6} & \frac{1}{3} & -\frac{1}{6} \end{bmatrix} \begin{bmatrix} f_1(\mathbf{x}) \\ f_2(\mathbf{x}) \\ f_3(\mathbf{x}) \end{bmatrix} \tag{3.106}$$

where the coefficient matrix called $\mathbf{M}$. Also we have:

$$f_{CFA}(x,y) = q_1(x,y) + q_2(x,y)(-1)^x + q_3(x,y)(-1)^y + q_4(x,y)(-1)^{x+y} \tag{3.107}$$

$$= r_1(x,y) + r_2(x,y) + r_3(x,y) + r_4(x,y) \tag{3.108}$$

As we can see in the matrix $\mathbf{M}$, 4^{th} row of matrix M is sum of 2^{nd} and 3^{rd} rows. So:

$$q_2(x,y) + q_3(x,y) = q_4(x,y) \tag{3.109}$$

For the adaptive algorithm, first we need to estimate $\hat{r_2}$, $\hat{r_3}$, $\hat{r_4}$ with three bandpass filters at $(\frac{1}{2},0)$, $(0,\frac{1}{2})$, $(\frac{1}{2},\frac{1}{2})$ respectively. Then demodulate them as follows:

$$\hat{q_2}(x,y) = \hat{r_2}(x,y)(-1)^x \tag{3.110}$$

$$\hat{q_3}(x,y) = \hat{r_3}(x,y)(-1)^y \tag{3.111}$$

$$\hat{q_4}(x,y) = \hat{r_4}(x,y)(-1)^{x+y} \tag{3.112}$$

Then we need to find the average energy, as we discussed before. Assuming the calculated energy near $(f_m,0)$, $(0,f_m)$ is e_x and e_y, we can set

$$w = \frac{e_x}{e_x + e_y} \tag{3.113}$$

When $w \approx 1$, then q_2 is more reliable, and when $w \approx 0$, then q_3 is more reliable. Therefore, if $w \approx 1$, we leave q_2 as it is, and replace q_3 with $q_4 - q_2$ using equation 3.109. If $w \approx 0$, we leave q_3 as it is, and replace q_2 with $q_4 - q_3$.

In general, the reconstructed chromas can be express as:

$$\hat{q_2}(\mathbf{x}) = w(\mathbf{x})\hat{q_2}(x) + (1 - w(\mathbf{x}))(\hat{q_4}(x) - \hat{q_3}(x)) \tag{3.114}$$

$$\hat{q_3}(\mathbf{x}) = (1 - w(\mathbf{x}))\hat{q_3}(x) + w(\mathbf{x})(\hat{q_4}(x) - \hat{q_2}(x)) \tag{3.115}$$

$$\hat{q_4}(\mathbf{x}) = \hat{q_4}(x), \qquad \text{no change} \tag{3.116}$$

Using the new value of the reconstructed chromas, we can estimate luma.

$$\hat{q_1}(x,y) = f_{CFA}(x,y) - \hat{q_2}(x,y)(-1)^x - \hat{q_3}(x,y)(-1)^y - \hat{r_4}(x,y) \tag{3.117}$$

So, the $\mathbf{M}^\dagger$ matrix will be as follows:

$$\mathbf{M}^\dagger = \begin{bmatrix} 1 & -\frac{4}{3} & \frac{2}{3} & -\frac{2}{3} \\ 1 & \frac{2}{3} & \frac{2}{3} & \frac{4}{3} \\ 1 & \frac{2}{3} & -\frac{4}{3} & -\frac{2}{3} \end{bmatrix} \tag{3.118}$$

And we can reconstruct the RGB image using $M^\dagger$ matrix.

Results and discussion

In this section the results of adaptive demosaicking using RGBW-Bayer have been compared with the least square method using RGB-Bayer. The Kodak dataset is used as the input images, and the CFA is reconstructed using them. Then the proposed demosaicking algorithm will be applied on the CFA images afterward. The PSNR ans S-CIELAB metrics are applied to compare the input Kodak images and the reconstructed images using the proposed demosaicking algorithm. Table 3.6 and 3.7 shows the comparison between three-channel and four-channel Bayer patterns in term of PSNR and S-CIELAB. The results are very close in both CFAs for the noise-free images.

Image number in dataset	Bayer-RGBW (Adaptive demosaicking)	RGB-Bayer (LSLCD method)[29]
1	37.90	37.92
2	39.22	40.65
3	40.82	42.22
4	40.02	41.09
5	36.93	37.92
6	43.64	39.95
7	41.21	42.52
8	34.92	35.32
9	41.48	42.57
10	41.84	42.63
11	39.29	39.81
12	42.92	43.14
13	34.87	34.20
14	34.82	36.77
15	39.16	39.83
16	43.80	43.63
17	41.31	41.63
18	36.73	37.28
19	40.13	40.53
20	40.17	40.97
21	38.65	38.79
22	37.46	38.57
23	41.12	42.98
24	39.36	35.34
Average over 24 images	39.49	39.8

Table 3.6: Comparison between the PSNR of Adaptive demosaicking method using RGBW-Bayer CFA and Least Square method using RGB-Bayer for Kodak dataset

Image number in dataset	Bayer-RGBW (Adaptive demosaicking)	RGB-Bayer (LSLCD method)[29]
1	1.25	1.19
2	0.74	0.66
3	0.62	0.51
4	0.76	0.66
5	1.34	1.07
6	0.44	0.78
7	0.69	0.55
8	1.59	1.47
9	0.69	0.58
10	0.65	0.54
11	0.85	0.75
12	0.53	0.48
13	1.69	1.62
14	1.21	1.00
15	0.75	0.64
16	0.58	0.53
17	0.56	0.51
18	1.19	0.99
19	0.87	0.77
20	0.64	0.57
21	1.01	0.91
22	1.08	0.93
23	0.62	0.49
24	0.56	0.98
Average over 24 images	0.87	0.79

Table 3.7: Comparison between the S-CIELAB of Adaptive demosaicking method using RGBW-Bayer and Least Square method using RGB-Bayer for Kodak dataset

3.4.4 Comparison between RGBW patterns

In this research we decided to develop a demosaicking algorithm for RGBW CFAs, and study on the effect of clear/panchromatic pixels in reconstructed image quality. Three different four channel CFAs have been studied, and a demosaicking algorithm has been developed for each case. The Kodak data set is used to evaluate and compare the results.

Table 3.8 and 3.9 show the PSNR and S-CIELAB comparison between non-adaptive demosaicking algorithm for each CFA as well as the results of PSNR of the previous work using RGBW 5×5 [45] on Kodak images and the average over 24 Kodak dataset. Also Table 3.10 illustrates the PSNR comparison between adaptive demosaicking results for RGBW-Bayer and RGBW-Kodak [39] for the same sample images. The results have been compared with the results of Least-Square method on the RGB-Bayer [29].

The results of Table 3.8 and 3.9 show the non-adaptive demosaicking method that we proposed for RGBW(5×5) improved the PSNR and S-CIELAB comparing to the method in [45]. Also the result of non-adaptive method using RGBW-Bayer is also working slightly better among three discussed RGBW patterns.

(a) Original image

(b) Non-adaptive RGBW-Kodak

(e) Non-Adaptive RGBW-Bayer

(c) RGBW CFA(5×5)

(f) Adaptive RGBW-Bayer

(d) Adaptive RGBW-Kodak

(g) Least Square RGB-Bayer [16]

Figure 3.14: Comparison between The adaptive and non-adaptive demosaicking method for different four channel CFAs

Image number in dataset	Bayer-RGBW (Non-Adaptive demosaicking)	Kodak-RGBW (Non-Adaptive demosaicking)	RGBW(5×5) proposed Non-Adaptive demosaicking)	RGBW(5×5) reconstructed in [45] using Dubois Method
1	36.14	27.12	36.56	35.23
2	36.74	33.55	37.05	37.49
3	37.88	34.74	37.46	37.46
4	37.25	34.10	37.21	37.32
5	34.20	29.06	33.47	32.96
6	39.15	29.55	38.88	36.56
7	37.92	33.83	37.94	38.22
8	32.27	24.56	34.35	33.28
9	38.51	32.25	38.84	38.78
10	39.58	33.83	37.77	36.63
11	37.17	30.84	37.01	36.13
12	39.58	33.27	40.39	40.18
13	35.09	27.54	32.93	30.91
14	31.85	29.37	31.87	32.24
15	37.07	33.21	36.65	36.29
16	40.26	33.01	40.98	39.58
17	40.34	34.54	39.24	37.90
18	35.62	30.46	34.79	33.87
19	37.09	28.52	38.58	37.53
20	38.24	32.06	37.58	36.71
21	37.21	30.02	37.31	36.14
22	35.49	31.01	35.81	35.59
23	37.80	34.29	38.04	38.86
24	37.06	30.12	35.27	31.90
Average over 24 images	37.06	31.3	36.9	35.42

Table 3.8: PSNR for Non-Adaptive demosaicking method using different RGBW patterns and the average PSNR over 24 Kodak images

Image number in dataset	Bayer-RGBW (Non-Adaptive demosaicking)	Kodak-RGBW (Non-Adaptive demosaicking)	RGBW(5×5) proposed Non-Adaptive demosaicking)
1	1.96	4.96	2.03
2	1.09	1.94	1.04
3	0.96	1.87	1.17
4	1.07	2.03	1.19
5	1.95	4.09	2.40
6	1.18	3.44	1.32
7	1.14	2.20	1.22
8	2.46	5.99	2.37
9	1.04	2.41	1.09
10	0.93	2.06	1.18
11	1.32	2.80	1.40
12	0.94	2.18	0.88
13	1.98	4.95	2.88
14	1.79	3.38	2.15
15	1.02	2.04	1.13
16	1.15	2.34	1.07
17	0.70	1.71	0.89
18	1.55	3.13	1.95
19	1.35	3.15	1.28
20	0.92	2.29	1.05
21	1.41	3.28	1.52
22	1.56	3.16	1.68
23	0.98	1.81	1.02
24	1.06	3.30	1.62
Average over 24 images	1.31	2.94	1.48

Table 3.9: S-CIELAB of some sample images for Non-Adaptive demosaicking method using different RGBW patterns and the average S-CIELAB over 24 Kodak images

The Tables 3.10 and 3.11 provide the results of adaptive demosaicking algorithm in terms of PSNR and S-CIELAB, and show some improvement on the proposed adaptive demosaicking algorithm using the RGBW-Bayer comparing to the adaptive algorithm using RGBW-Kodak. The results have also been compared with the least-square method results on RGB-Bayer pattern.

Usually adaptive demosaicking method reconstruct more isolated chroma and luma signals and works better than non adaptive methods, and the reconstructed images prove this fact. As we can see in Figure 3.14, among non-adaptive methods, the RGBW(5×5) is more successful to estimate colors correctly while RGBW-Bayer reconstruct the edges and image details better.

Comparing adaptive algorithms, the RGBW-Kodak fully estimated the colors. The proposed weighted algorithm for RGBW-Bayer reconstructs the image details better while it contains some false color. We can conclude that the CFA templates with more white filters estimate less false color and an appropriate adaptive demosaicking algorithm is needed to restore the edges perfectly.

Image number in dataset	Bayer-RGBW (Adaptive demosaicking)	Kodak-RGBW (Adaptive demosaicking)	RGB-Bayer (LSLCD method)[1]
1	37.90	36.33	37.92
2	39.22	36.10	40.65
3	40.82	36.67	42.22
4	40.02	35.84	41.09
5	36.93	31.90	37.92
6	43.64	38.56	39.95
7	41.21	36.35	42.52
8	34.92	34.02	35.32
9	41.48	37.93	42.57
10	41.84	38.74	42.63
11	39.29	36.36	39.81
12	42.92	39.13	43.14
13	34.87	33.02	34.20
14	34.82	30.83	36.77
15	39.16	35.76	39.83
16	43.80	41.25	43.63
17	41.31	38.68	41.63
18	36.73	34.01	37.28
19	40.13	38.06	40.53
20	40.17	37.45	40.97
21	38.65	36.69	38.79
22	37.46	34.82	38.57
23	41.12	36.40	42.98
24	39.36	35.27	35.34
Average over 24 images	39.4	36.3	39.8

Table 3.10: Comparison between the PSNR of Kodak images for adaptive demosaicking method using RGBW CFAs and least-square method using RGB-Bayer

Image number in dataset	Bayer-RGBW (Adaptive demosaicking)	Kodak-RGBW (Adaptive demosaicking)	RGB-Bayer (LSLCD method)[1]
1	1.25	2.24	1.19
2	0.74	1.28	0.66
3	0.62	1.27	0.51
4	0.76	1.57	0.66
5	1.34	3.45	1.07
6	0.44	1.49	0.78
7	0.69	1.70	0.55
8	1.59	2.63	1.47
9	0.69	1.37	0.58
10	0.65	1.24	0.54
11	0.85	1.67	0.75
12	0.53	1.07	0.48
13	1.69	3.28	1.62
14	1.21	2.60	1.00
15	0.75	1.47	0.64
16	0.58	1.10	0.53
17	0.56	1.16	0.51
18	1.19	2.44	0.99
19	0.87	1.57	0.77
20	0.64	1.17	0.57
21	1.01	1.89	0.91
22	1.08	2.23	0.93
23	0.62	1.44	0.49
24	0.56	2.06	0.98
Average over 24 images	0.87	1.81	0.79

Table 3.11: Comparison between the S-CIELAB of Kodak images for demosaicking method using RGBW CFAs and least-square method using RGB-Bayer

3.4.5 White filter estimation

The method described in previous sections was based on $W = \frac{1}{3}R + \frac{1}{3}G + \frac{1}{3}B$. We optimized the white color component calculation assuming that there is a linear relationship between white component and the three primary color components (red, green, blue). The following method describes the closest way that we can linearly model white color components similar to the digital cameras based on two different sensor characteristics. VEML6040 is an available sensor released in 2015 from Vishay company [10], and KAI-Kodak110002 [9] is a color sensor presented by Eastman Kodak company in 2004. We will calculate the optimized coefficients separately for each sensor. Figure 3.15 shows a typical non-normalized responsivity of red, green, blue and white filter spectral responses, according to the VEML6040 sensor [10]. Also, Figure 3.16 shows responsivity curves of red, green and blue filters for KAI-Kodak110002 [9], and Figure 3.17 is the responsivity curve for white filter for the same sensor.

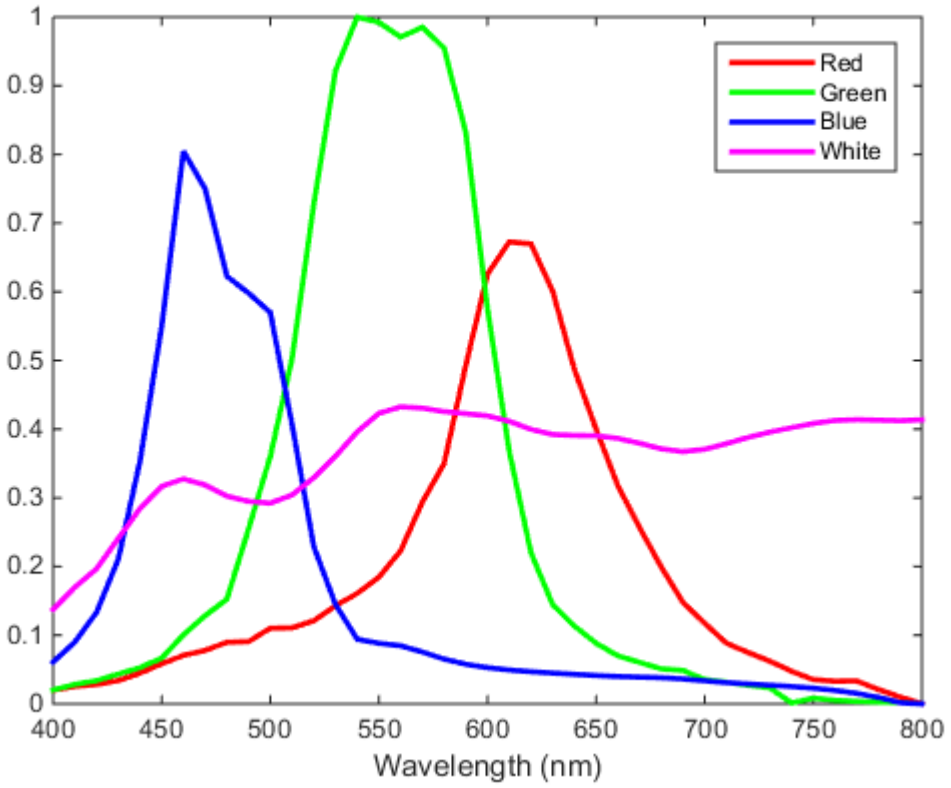

Figure 3.15: Non-normalized spectral response of red, green, blue and white color filters for VEML6040 sensor (400nm-800nm)

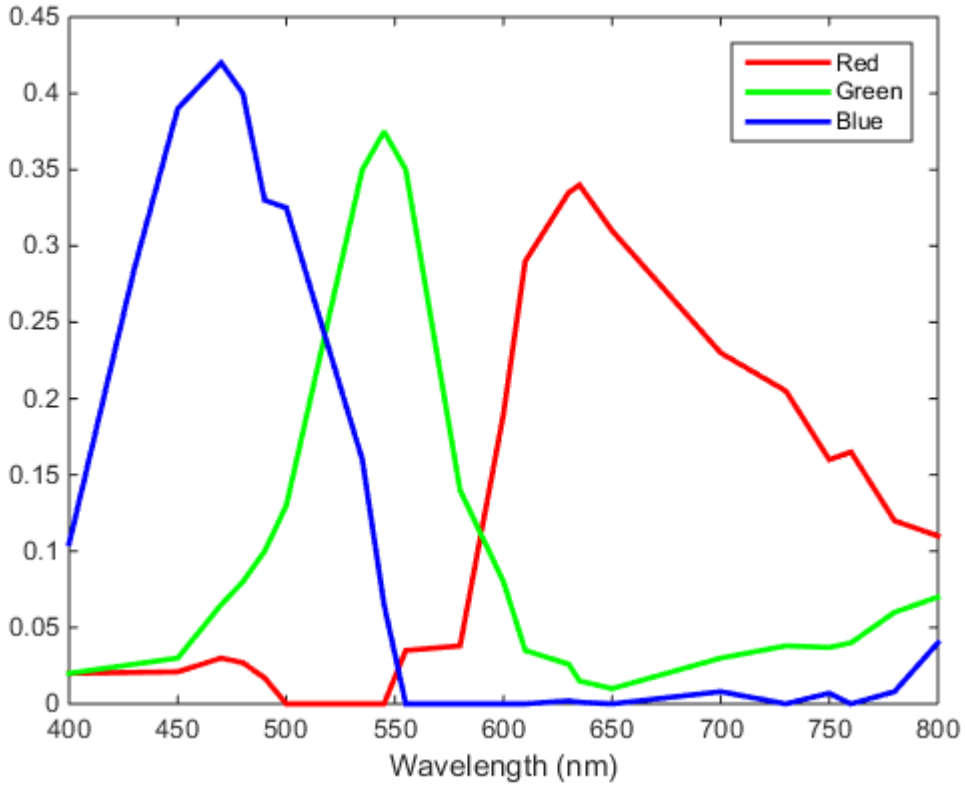

Figure 3.16: Non-normalized spectral response of red, green and blue color filters for KAI-Kodak11002 sensor (400nm-800nm)

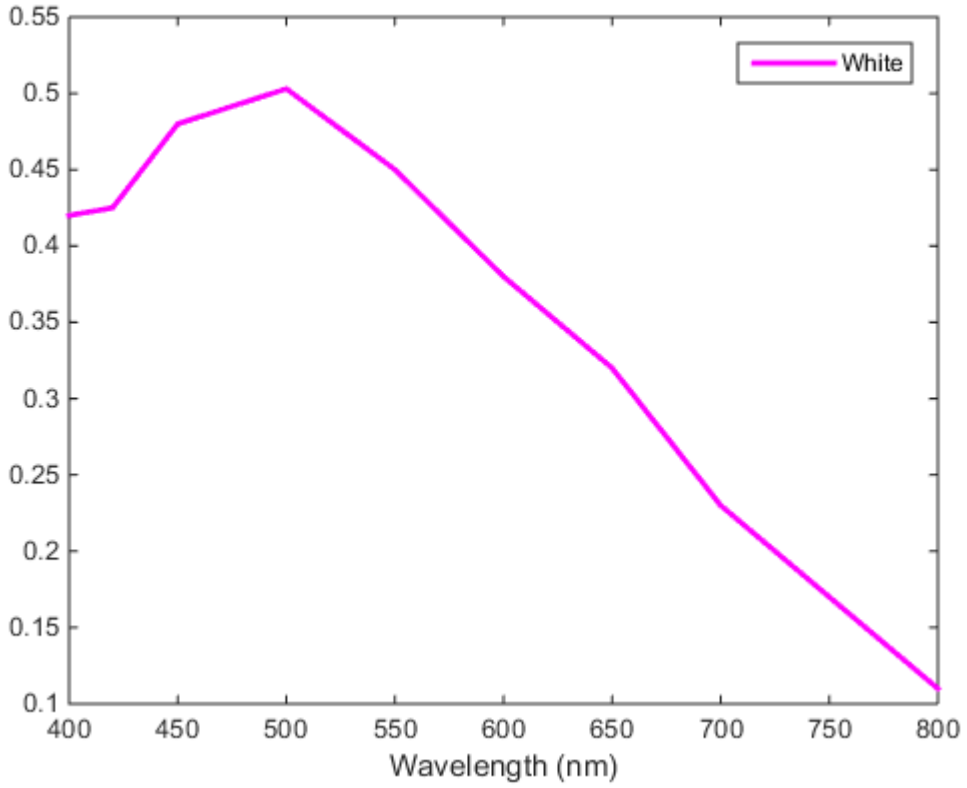

Figure 3.17: Non-normalized spectral response of white filter for KAI-Kodak11002 sensor (400nm-800nm)

Assuming a constant patch of light with power density spectrum $C(\lambda)$, we make the following four measurements over the range of wavelengths from 400 to 650 nm:

$$C_R = \int_v r(\lambda)C(\lambda)d\lambda \tag{3.119}$$

$$C_B = \int_v b(\lambda)C(\lambda)d\lambda \tag{3.120}$$

$$C_G = \int_v g(\lambda)C(\lambda)d\lambda \tag{3.121}$$

$$C_W = \int_v w(\lambda)C(\lambda)d\lambda \tag{3.122}$$

$r(\lambda)$, $g(\lambda)$, $b(\lambda)$ and $w(\lambda)$ are the spectral sensitivity curves of an RGBW CFA sensor. Assume that $r(\lambda)$, $g(\lambda)$, $b(\lambda)$ and $w(\lambda)$ have been scaled, so that if $C(\lambda) = D_{65}(\lambda)$ with luminance equal to 1, then $D_R = D_B = D_G = D_W = 1$. So the values of red, green, blue and white components will be normalized by multiplying them to the spectrum of $D65$, as a constant power density spectrum, on a specific range of wavelength. We wish to estimate C_W as a linear combination of C_R, C_G, C_B:

$$\hat{C}_W = a_R C_R + a_G C_G + a_B C_B, \qquad where \qquad a_R + a_G + a_B = 1 \tag{3.123}$$

Then using a database of typical spectral densities of light, we can calculate and minimize the mean square error between the real white components and the calculated one. We calculate and normalized the values of red (C_R), green (C_G), blue (C_B) and white (C_W) over the Macbeth color checker database [37].

Common light sources deliver light that has a very broad spectral output, reaching beyond the visible, so many visual and detector-based applications use an infrared filter that is designed to pass only light within the visible spectrum. Thus, there is an IR cut-off filter inside digital cameras that eliminates the effects of infrared light, and cuts off the frequencies over 650 nm. Therefore we filtered the values over 650 nm in our simulation.

The MSE will be calculated for both sensors separately, using the Quadratic programming subject to $a_R + a_B + a_G = 1$.

$$Error = \sum_{i=1}^{N} (C_{Wi} - (a_R C_{Ri} + a_G C_{Gi} + a_B C_{Bi}))^2 \tag{3.124}$$

N = number of samples in the database

Using Lagrange multiplier method, we can minimize error function subject to $a_R+a_B+a_G = 1$. We set β as Lagrange multiplier variable, and find the local minimum of the ε function.

$$\varepsilon = \sum_{i=1}^{N}(C_{Wi} - (a_R C_{Ri} + a_G C_{Gi} + a_B C_{Bi}))^2 + \beta(a_R + a_B + a_G) \tag{3.125}$$

$$\nabla_{a_R} = \frac{\partial \varepsilon}{\partial a_R} = \sum_{i=1}^{N} 2(C_{Wi} - (a_R C_{Ri} + a_G C_{Gi} + a_B C_{Bi}))(-C_{Ri}) + \beta = 0 \tag{3.126}$$

$$\nabla_{a_G} = \frac{\partial \varepsilon}{\partial a_R} = \sum_{i=1}^{N} 2(C_{Wi} - (a_R C_{Ri} + a_G C_{Gi} + a_B C_{Bi}))(-C_{Gi}) + \beta = 0 \tag{3.127}$$

$$\nabla_{a_B} = \frac{\partial \varepsilon}{\partial a_R} = \sum_{i=1}^{N} 2(C_{Wi} - (a_R C_{Ri} + a_G C_{Gi} + a_B C_{Bi}))(-C_{Bi}) + \beta = 0 \tag{3.128}$$

We can show all three equations in matrix form.

$$\begin{bmatrix} 2\sum_{i=1}^{N} {C_{Ri}}^2 & 2\sum_{i=1}^{N} C_{Ri}C_{Gi} & 2\sum_{i=1}^{N} C_{Ri}C_{Bi} \\ 2\sum_{i=1}^{N} C_{Gi}C_{Ri} & 2\sum_{i=1}^{N} {C_{Gi}}^2 & 2\sum_{i=1}^{N} C_{Gi}C_{Bi} \\ 2\sum_{i=1}^{N} C_{Bi}C_{Ri} & 2\sum_{i=1}^{N} C_{Bi}C_{Gi} & 2\sum_{i=1}^{N} {C_{Bi}}^2 \end{bmatrix} \begin{bmatrix} a_R \\ a_G \\ a_B \end{bmatrix} = \begin{bmatrix} 2\sum_{i=1}^{N} C_{Wi}C_{Ri} \\ 2\sum_{i=1}^{N} C_{Wi}C_{Gi} \\ 2\sum_{i=1}^{N} C_{Wi}C_{Bi} \end{bmatrix} - \beta \begin{bmatrix} 1 \\ 1 \\ 1 \end{bmatrix} \tag{3.129}$$

Assuming

$$Q = \begin{bmatrix} 2\sum_{i=1}^{N} {C_{Ri}}^2 & 2\sum_{i=1}^{N} C_{Ri}C_{Gi} & 2\sum_{i=1}^{N} C_{Ri}C_{Bi} \\ 2\sum_{i=1}^{N} C_{Gi}C_{Ri} & 2\sum_{i=1}^{N} {C_{Gi}}^2 & 2\sum_{i=1}^{N} C_{Gi}C_{Bi} \\ 2\sum_{i=1}^{N} C_{Bi}C_{Ri} & 2\sum_{i=1}^{N} C_{Bi}C_{Gi} & 2\sum_{i=1}^{N} {C_{Bi}}^2 \end{bmatrix} \tag{3.130}$$

and

$$b = \begin{bmatrix} 2\sum_{i=1}^{N} C_{Wi}C_{Ri} \\ 2\sum_{i=1}^{N} C_{Wi}C_{Gi} \\ 2\sum_{i=1}^{N} C_{Wi}C_{Bi} \end{bmatrix} \tag{3.131}$$

we can simplify the equation as:

$$\begin{bmatrix} a_R \\ a_G \\ a_B \end{bmatrix} = Q^{-1}(b - \beta \begin{bmatrix} 1 \\ 1 \\ 1 \end{bmatrix}) \tag{3.132}$$

Using the constraint, we can find β, and apply it to the problem. The local minimum values for a_R, a_B and a_G will be estimated.

$$\begin{bmatrix} 1 & 1 & 1 \end{bmatrix} \begin{bmatrix} a_R \\ a_G \\ a_B \end{bmatrix} = 1 \tag{3.133}$$

$$\beta = \frac{\begin{bmatrix} 1 & 1 & 1 \end{bmatrix} Q^{-1} b - 1}{\begin{bmatrix} 1 & 1 & 1 \end{bmatrix} Q^{-1} \begin{bmatrix} 1 \\ 1 \\ 1 \end{bmatrix}} \tag{3.134}$$

The calculated a_R, a_B and a_G will be replaced in equation 3.90 as coefficients for red, green and blue components. The calculated values based on VEML6040 sensor are $a_R = 0.3870$, $a_G = 0.2571$ and $a_B = 0.3560$. Note that these coefficients will be applied to a camera using the filters shown in Figure 3.15.

$$\hat{W}_{\text{VEML6040}} = 0.3870(R) + 0.2571(G) + 0.3560(B) \tag{3.135}$$

Same coefficients have been calculated for KAI-Kodak11002 sensor as $a_R = 0.1783$, $a_G = 0.3864$ and $a_B = 0.4353$, and these coefficients will be applied to a camera using filters as Figure 3.16 and 3.17.

$$\hat{W}_{\text{KAI-Kodak11002}} = 0.1783(R) + 0.3864(G) + 0.4353(B) \tag{3.136}$$

Updated demosaicking algorithm for RGBW-Bayer

In this section, the presented adaptive demosaicking algorithm will be updated using the new sets of coefficients for both sensors. For VEML6040 sensor as the white filter values in the CFA have been updated using equation 3.135, the adaptive demosaicking algorithm for RGBW-Bayer pattern has been designed based on the new white values.

$$f_4(\mathbf{x}) = 0.3870 f_1(\mathbf{x}) + 0.2571 f_2(\mathbf{x}) + 0.3560 f_3(\mathbf{x}) \tag{3.137}$$

So we can recalculate all chromas as follows:

$$q_1(\mathbf{x}) = \frac{1}{4}((1+a_R)f_1(\mathbf{x}) + (1+a_G)f_2(\mathbf{x}) + (1+a_B)f_3(\mathbf{x})) \tag{3.138}$$

$$q_2(\mathbf{x}) = \frac{1}{4}((-1-a_R)f_1(\mathbf{x}) + (1-a_G)f_2(\mathbf{x}) + (1-a_B)f_3(\mathbf{x})) \tag{3.139}$$

$$q_3(\mathbf{x}) = \frac{1}{4}((1-a_R)f_1(\mathbf{x}) + (1-a_G)f_2(\mathbf{x}) + (-1-a_B)f_3(\mathbf{x})) \tag{3.140}$$

$$q_4(\mathbf{x}) = \frac{1}{4}((-1+a_R)f_1(\mathbf{x}) + (1+a_G)f_2(\mathbf{x}) + (-1+a_B)f_3(\mathbf{x})) \tag{3.141}$$

In matrix form

$$\begin{bmatrix} q_1(\mathbf{x}) \\ q_2(\mathbf{x}) \\ q_3(\mathbf{x}) \\ q_4(\mathbf{x}) \end{bmatrix} = \begin{bmatrix} 0.3234 & 0.3726 & 0.3040 \\ -0.3234 & 0.1274 & 0.1960 \\ 0.1766 & 0.1274 & -0.3040 \\ -0.1766 & 0.3726 & -0.1960 \end{bmatrix} \begin{bmatrix} f_1(\mathbf{x}) \\ f_2(\mathbf{x}) \\ f_3(\mathbf{x}) \end{bmatrix} \tag{3.142}$$

As matrix **M'** has been updated with equation 3.137, we can call the updated coefficients matrix as **N**.

We will use the same weighting scheme described in the previous section. The updated reconstructed chromas using weighting scheme can be express as

$$\hat{q}_{2_{\text{weighted}}}(\mathbf{x}) = w(\mathbf{x})\hat{q}_2(\mathbf{x}) + (1-w(\mathbf{x}))(\frac{0.4348}{0.6028}\hat{q}_4(\mathbf{x}) - \frac{0.6690}{0.6028}\hat{q}_3(\mathbf{x})) \tag{3.143}$$

$$\hat{q}_{3_{\text{weighted}}}(\mathbf{x}) = (1-w(\mathbf{x}))\hat{q}_3(\mathbf{x}) + w(\mathbf{x})(\frac{0.4348}{0.6690}\hat{q}_4(\mathbf{x}) - \frac{0.6028}{0.6690}\hat{q}_2(\mathbf{x})) \tag{3.144}$$

$$\hat{q}_4(\mathbf{x}) = \hat{q}_4(\mathbf{x}), \qquad \text{no change} \tag{3.145}$$

Also, according to KAI-Kodak11002 sensor specification the white filter values in the CFA is updated using equation 3.136, and the adaptive demosaicking algorithm for RGBW-Bayer pattern captured by a camera using this sensor will be updated as follows:

$$f_4(\mathbf{x}) = 0.1783 f_1(\mathbf{x}) + 0.3864 f_2(\mathbf{x}) + 0.4353 f_3(\mathbf{x}) \tag{3.146}$$

and the matrix **N** will be calculated as the updated form of **M'**

$$\begin{bmatrix} q_1(\mathbf{x}) \\ q_2(\mathbf{x}) \\ q_3(\mathbf{x}) \\ q_4(\mathbf{x}) \end{bmatrix} = \begin{bmatrix} 0.2946 & 0.3466 & 0.3588 \\ -0.2946 & 0.1534 & 0.1412 \\ 0.2054 & 0.1534 & -0.3588 \\ -0.2054 & 0.3466 & -0.1412 \end{bmatrix} \begin{bmatrix} f_1(\mathbf{x}) \\ f_2(\mathbf{x}) \\ f_3(\mathbf{x}) \end{bmatrix} \tag{3.147}$$

The weighting method will be updated using the new coefficient matrix. The updated reconstructed chromas will be

$$\hat{q}_{2_{\text{weighted}}}(\mathbf{x}) = w(\mathbf{x})\hat{q}_2(\mathbf{x}) + (1 - w(\mathbf{x}))(\frac{0.5241}{0.7019}\hat{q}_4(\mathbf{x}) - \frac{0.4824}{0.7019}\hat{q}_3(\mathbf{x})) \tag{3.148}$$

$$\hat{q}_{3_{\text{weighted}}}(\mathbf{x}) = (1 - w(\mathbf{x}))\hat{q}_3(\mathbf{x}) + w(\mathbf{x})(\frac{0.5241}{0.4824}\hat{q}_4(\mathbf{x}) - \frac{0.7019}{0.4824}\hat{q}_2(\mathbf{x})) \tag{3.149}$$

$$\hat{q}_4(\mathbf{x}) = \hat{q}_4(x), \qquad \text{no change} \tag{3.150}$$

As we discussed before, we can find luma by subtracting updated $\hat{q}_2(\mathbf{x})$,$\hat{q}_3(\mathbf{x})$ and $\hat{q}_4(\mathbf{x})$ from CFA image. The RGB image will be reconstructed using matrix $M^{\dagger}$.

We can apply the designed adaptive demosaicking algorithm based on equation 3.90 on the calculated CFA using equation 3.135, and the PSNR results will be less than the updated adaptive demosaicking algorithm using equation 3.135, as we can see in the Table 3.12 and 3.13.

Table 3.12 and 3.13 show the comparison between the total PSNR and S-CIELAB values over the 24 Kodak images using the ideal estimation for white value using equation 3.90 and the initial estimation for white filters using equation 3.135. The estimated values for white filters using equation 3.135 show the closest white values to the received values in white filters in digital cameras. The results show that the PSNR and S-CIELAB values

improve using the updated adaptive demosaicking algorithm. The results show that when the demosaicking algorithm is adapted to the true relation between W and R, G and B is 2.75 db higher than that when it is not adapted.

Image number in dataset	(a)	(b)	(c)
1	37.90	36.58	37.95
2	39.22	39.05	39.29
3	40.82	33.96	41.02
4	40.02	37.76	40.23
5	36.93	35.49	37.12
6	43.64	36.11	43.43
7	41.21	37.54	41.51
8	34.94	34.50	34.90
9	41.48	38.90	41.57
10	41.84	40.43	41.87
11	39.29	37.56	39.25
12	42.92	36.48	43.15
13	34.87	33.27	34.67
14	34.82	32.85	34.92
15	39.16	36.66	39.29
16	43.80	40.89	43.74
17	41.31	40.49	41.19
18	36.73	35.20	36.65
19	40.13	37.84	40.10
20	40.17	37.44	40.13
21	38.65	37.77	38.56
22	37.46	35.26	37.54
23	41.12	32.41	41.24
24	39.36	37.51	39.15
Average over 24 images	39.49	36.75	39.52

Table 3.12: PSNR Kodak images and average total PSNR over 24 images. (a) Results of applying adaptive demosaicking method designed using equation 3.90 for the CFA modeled using equation 3.90, (b) Results of applying adaptive demosaicking method designed using equation 3.90 for the CFA modeled using equation 3.135, (c) Results of applying adaptive demosaicking method designed using equation 3.135 for the CFA modeled using equation 3.135

Image number in dataset	(a)	(b)	(c)
1	1.32	2.01	1.31
2	0.75	0.83	0.74
3	0.65	2.22	0.64
4	0.78	1.40	0.76
5	1.38	1.83	1.30
6	0.48	3.39	0.53
7	0.71	2.36	0.67
8	1.67	1.96	1.67
9	0.73	1.24	0.72
10	0.68	1.12	0.68
11	0.89	1.87	0.90
12	0.57	2.82	0.56
13	1.81	2.89	1.88
14	1.26	2.68	1.25
15	0.77	1.17	0.74
16	0.63	1.36	0.64
17	0.59	0.75	0.62
18	1.24	1.99	1.24
19	0.91	1.80	0.90
20	0.67	1.41	0.65
21	1.06	1.36	1.09
22	1.12	2.40	1.09
23	0.64	3.31	0.62
24	0.59	1.43	0.66
Average over 24 images	0.91	1.90	0.90

Table 3.13: S-CIELAB for Kodak images and average total S-CIELAB over 24 images. (a) Results of applying adaptive demosaicking method designed using equation 3.90 for the CFA modeled using equation 3.90, (b) Results of applying adaptive demosaicking method designed using equation 3.90 for the CFA modeled using equation 3.135, (c) Results of applying adaptive demosaicking method designed using equation 3.135 for the CFA modeled using equation 3.135

3.4.6 Least-square method optimization algorithm

Least square filter design

Since we are using $\hat{q_4}$ to reconstruct $\hat{q_2}$ and $\hat{q_3}$, the optimized extracted $\hat{q_4}$ improves the quality of $\hat{q_2}$ and $\hat{q_3}$. Hence, we decided to design least square filter to extract q_4.

The least-square method will be explained in the following steps. We can call the design filter h_4 for $\hat{q_4}$.

$$\hat{r}_4[\mathbf{x}] = (f_{CFA} * h_4)[\mathbf{x}] \tag{3.151}$$

$$\hat{q}_4[\mathbf{x}] = \hat{r}_4[\mathbf{x}] \exp(-j2\pi \mathbf{d}_4 \cdot \mathbf{x}) \tag{3.152}$$

Assume $W^{(i)}$ is the region of support of the i^{th} training image, $i = 1, ..., P$. We set $P = 24$, as we are using Kodak dataset for training. Then the least-square filter will be modeled as:

$$h_4 = \arg\min_h \sum_{i=1}^{P} \sum_{\mathbf{x} \in W^{(i)}} \left| (r_4^{(i)} - h * f_{CFA}^{(i)})[\mathbf{x}] \right|^2 \tag{3.153}$$

Assuming S as the region of support of h_4, $|S| = N_B$, then

$$(h * f_{CFA}^{(i)})[n_1, n_2] = \sum_{(k_1,k_2) \in S} h[k_1, k_2] f_{CFA}^{(i)}[n_1 - k_1, n_2 - k_2] \tag{3.154}$$

It can also be expressed in matrix form as follows. We arrange the filter coefficients into an $N_B \times 1$ column matrix, taking the coefficients of h column by column from left to right.

$$\mathbf{h}_{1D} = \begin{bmatrix} \mathbf{h}(:,1) \\ \mathbf{h}(:,2) \\ \vdots \\ \mathbf{h}(:,N_{filt}) \end{bmatrix} \tag{3.155}$$

where $N_B = N_{filt}^2$ Let $N_w = \left|W^{(i)}\right|$, assumed the same for all i. Arrange $r_4^{(i)}$ into an $N_B \times 1$ column matrix in the same way.

$$\mathbf{r}_{1D,4}^{(i)} = \begin{bmatrix} \mathbf{r}_4^{(i)}(:,1) \\ \mathbf{r}_4^{(i)}(:,2) \\ \vdots \\ \mathbf{r}_4^{(i)}(:,N_W) \end{bmatrix} \tag{3.156}$$

Then

$$\hat{r}_{1D,4} = Z^{(i)} h_{1D} \tag{3.157}$$

where $\mathbf{Z}^{(i)}$ is an $N_W \times N_B$ matrix. Each column of $\mathbf{Z}^{(i)}$ is a reshaped version of $f_{CFA}^{(i)}[n_1 - k_1, n_2 - k_2]$ for some k_1 and k_2, rearranged in the order of $\mathbf{h}_{1D}$.

$$\mathbf{Z}^{(i)}(:, m[k_1, k_2]) = \begin{bmatrix} f_{CFA}^{(i)}[n_1 - k_1, n_2 - k_2](:, 1) \\ f_{CFA}^{(i)}[n_1 - k_1, n_2 - k_2](:, 2) \\ \vdots \\ f_{CFA}^{(i)}[n_1 - k_1, n_2 - k_2](:, N_W) \end{bmatrix} \tag{3.158}$$

where $h_{1D}[m[k_1, k_2]] = h[k_1, k_2]$. Z is real value, and r is complex, so we have:

$$\mathbf{h}_{1D,4} = [\sum_{i=1}^{p} \mathbf{Z}^{(i)T} \mathbf{Z}^{(i)}]^{-1} [\sum_{i=1}^{p} \mathbf{Z}^{(i)T} r_{1D,4}^{(i)}] \tag{3.159}$$

$$\mathbf{h}_4 = \begin{bmatrix} h_4(1,1) & \cdots & h_4(N_{filt}, 1) \\ \vdots & \ddots & \vdots \\ h_4(1, N_{filt}) & \cdots & h_4(N_{filt}, N_{filt}) \end{bmatrix} \tag{3.160}$$

Using the h_4, we can extract $\hat{q}_4$ more accurately, and reconstruct the $\hat{q}_2$ and $\hat{q}_3$ through equations 3.148 to 3.150. The updated $\hat{q}_2$ to $\hat{q}_4$ also leads to better luma estimation.

Results

Tables 3.14 and 3.15 provide the results of updated demosaicking algorithm with least-square method using RGBW-Bayer for both sensors, and compare them with the results of least-square demosaicking method using RGB-Bayer in terms of PSNR and S-CIELAB. The tables show that the average overall PSNR and S-CIELAB for least-square method using RGBW-Bayer over 24 images are very close to the average of least-square method using RGB-Bayer.

Image number in dataset	Bayer-RGBW using VEML6040 (LSLCD method)	Bayer-RGBW using KAI-Kodak11002 (LSLCD method)	RGB-Bayer (LSLCD method)[1]
1	38.93	37.52	37.92
2	39.26	39.25	40.65
3	40.56	41.09	42.22
4	39.85	40.25	41.09
5	36.80	37.07	37.92
6	43.52	42.82	39.95
7	41.03	41.50	42.52
8	35.64	34.62	35.32
9	41.71	41.62	42.57
10	41.91	41.84	42.63
11	39.40	39.07	39.81
12	43.25	43.07	43.14
13	35.19	34.34	34.20
14	34.29	34.88	36.77
15	39.08	39.41	39.83
16	43.87	43.30	43.63
17	41.20	41.08	41.63
18	36.57	36.57	37.28
19	40.45	39.86	40.53
20	40.14	39.92	40.97
21	38.86	38.33	38.79
22	37.63	37.44	38.57
23	41.06	41.29	42.98
24	39.09	39.13	35.34
Average over 24 images	39.56	39.39	39.8

Table 3.14: Comparison between the PSNR of Kodak images for Least-Square demosaicking method using Bayer-RGBW CFA and VEML6040 and KAI-Kodak11002 sensors and Least Square method using RGB-Bayer

Image number in dataset	Bayer-RGBW using VEML6040 (LSLCD method)	Bayer-RGBW using KAI-Kodak11002 (LSLCD method)	RGB-Bayer (LSLCD method)[1]
1	1.24	1.42	1.19
2	0.76	0.76	0.66
3	0.66	0.65	0.66
4	0.79	0.79	0.66
5	1.32	1.31	1.07
6	0.54	0.59	0.78
7	0.70	0.68	0.55
8	1.60	1.81	1.47
9	0.72	0.74	0.58
10	0.68	0.70	0.54
11	0.88	0.95	0.75
12	0.55	0.58	0.48
13	1.82	1.96	1.62
14	1.30	1.31	1.00
15	0.75	0.75	0.64
16	0.64	0.69	0.53
17	0.62	0.63	0.51
18	1.25	1.27	0.99
19	0.91	0.96	0.77
20	0.71	0.73	0.57
21	1.08	1.16	0.91
22	1.08	1.11	0.93
23	0.63	0.64	0.49
24	0.66	0.66	0.98
Average over 24 images	0.91	0.95	0.79

Table 3.15: Comparison between the S-CIELAB of Kodak images for Least-Square demosaicking method using Bayer-RGBW CFA and VEML6040 and KAI-Kodak11002 sensors and Least Square method using RGB-Bayer

3.5 Four-channel CFA reconstruction using hyperspectral images

In this section, we will estimate the four-channel image using hyperspectral image information. We are trying to validate the white filter estimation process that has been presented in previous section. A recent hyperspectral dataset will be used to make a real RGBW CFA. The RGB images will be reconstructed using updated least-square demosaicking algorithm based on white filter estimation, and the reconstructed image quality will be compared with the original RGB image.

As we know, color images will be reconstructed based on three primary color components (red, green, and blue). The spectral imaging divides the light spectrum into many more bands (usually 31). The hyperspectral sensors collect information as a set of images. Each image represents a narrow wavelength range of a spectral band.

3.5.1 Spectral image dataset

A set of hyperspectral images presented in [33] has been used in this work. These images have been taken using a liquid crystal tunable filter (LCTF) based capturing system. The target-based characterization methods used for particular lighting geometry, color target material and surface structure to minimize the lighting geometry on target apparence. The images have been captured using LCTF system in $[400 - 700]$ interval (every 10 nm). There will be 31 spectral images in each case. Additional corrections also applied to compensate angular dependency of LCTF transmission and geometry dissimilarities. To convert the hyperspectral images into RGB images, we have filtered out the values over 650 nm, assuming there usually should be an IR-cut off filter inside camera. Figure 3.18 shows some sample images of the spectral dataset.

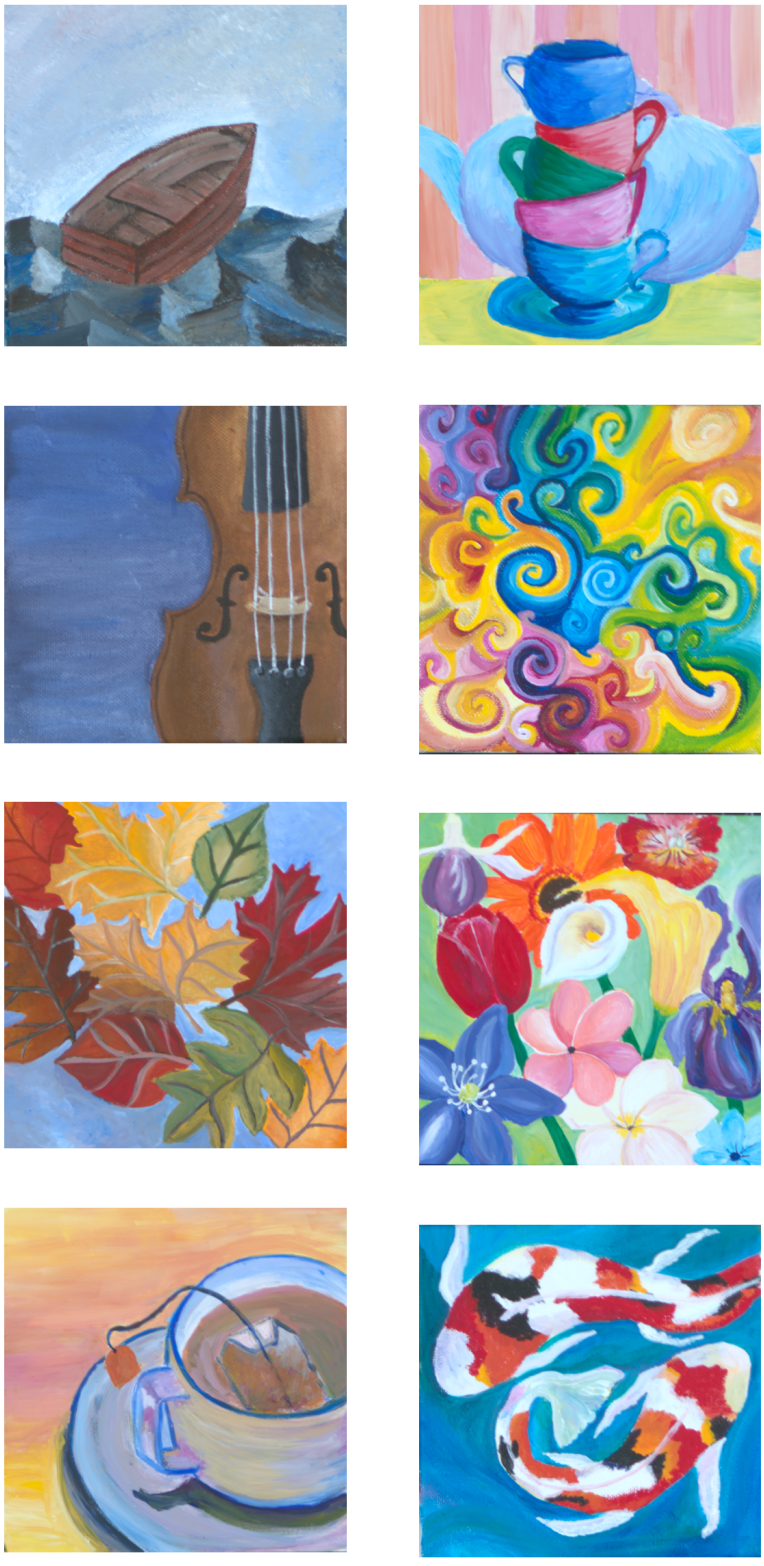

Figure 3.18: Sample spectral images from [33]

3.5.2 RGBW CFA reconstruction using hyperspectral images

To create RGBW CFA image we need to reconstruct red, green, blue and white images separately using the available 31 spectral images. According to a typical non-normalized responsivity of red, green, blue and white filters that has been shown in Figure 3.15 and presented by Vishay company [10], we have:

$$C_R = \int_v r(\lambda)C(\lambda)d\lambda \tag{3.161}$$

$$C_B = \int_v b(\lambda)C(\lambda)d\lambda \tag{3.162}$$

$$C_G = \int_v g(\lambda)C(\lambda)d\lambda \tag{3.163}$$

$$C_W = \int_v w(\lambda)C(\lambda)d\lambda \tag{3.164}$$

$C(\lambda)$ is a constant patch of light with power density spectrum, and $r(\lambda)$,$g(\lambda)$, $b(\lambda)$ and $w(\lambda)$ are the spectral sensitivity curves of an RGBW CFA sensor. These curves will be white balanced when we multiply them to $C(\lambda) = D_{65}(\lambda)$ with luminance equal to 1, then set $D_R = D_B = D_G = D_W = 1$. First, we should white balance the red, green, blue and white spectrum of Figure 3.15, then hyperspectral images will be multiplied to the white balanced values of red, green, blue and white. Assuming hyperspectral image as $S(i, j, k)$, and S_R,S_G,S_B and S_W, are the three dimensional red, green, blue and white images.

$$S_R = \sum_{k=1}^{N_3} S(i, j, k)C_R \tag{3.165}$$

$$S_B = \sum_{k=1}^{N_3} S(i, j, k)C_B \tag{3.166}$$

$$S_G = \sum_{k=1}^{N_3} S(i, j, k)C_G \tag{3.167}$$

$$S_W = \sum_{k=1}^{N_3} S(i, j, k)C_W \tag{3.168}$$

We sum up values over the third dimension. The results will be two dimensional red, green, blue and white images. The final images will be scaled and gamma corrected as well. Using these images, the RGBW CFA will be calculated.

White balancing and gamma correction will be applied before demosaicking. A white balance channel has a response equal to one to the reference white spectrum. In order to white balance different channels, we have to multiply them to a constant value in each case. Gamma correction step is needed to correct the image brightness/ luminance in different displays. This problem cause due to the nonlinear relationship between received light and image brightness in human eye. So, it needs to be corrected with gamma correction function, and raise image brightness to the power of $\frac{1}{\sqrt{2}}$.

3.5.3 Results

In this section the results of least-square demosaicking algorithm using RGBW-Bayer and RGB-Bayer CFA images on hyperspectral image dataset [33] will be provided. The RGBW CFAs have been created using both VEML6040 and KAI-Kodak11002 sensors. As we are simulating the digital camera processing system, we have to include the white balancing and gamma correction steps on the captured image. Then the CFA images will be reconstructed using the white balanced gamma corrected image. The output images will be reconstructed using the proposed demosaicking process, and the reconstructed images will be compared with the input (Captured) images. The PSNR and S-CIELAB results calculate the differences between the reconstructed images and the input images as ground truth images.

Table 3.16 shows the average PSNR of reconstructed images using RGBW-Bayer and VEML6040 sensor over the whole dataset is $1.4db$ higher than RGB-Bayer. Table 3.17 compare the PSNR of RGBW-Bayer using KAI-Kodak11002 sensor and the RGB-Bayer. The average PSNR of RGBW-Bayer reconstructed images over the whole dataset is $1.1db$ higher than RGB-Bayer for KAI-Kodak11002 sensor.

Image number in dataset	RGBW-Bayer (LSLCD)	RGB-Bayer (LSLCD method)
1	45.28	44.13
2	39.22	38.12
3	40.72	39.66
4	44.70	43.29
5	44.15	42.78
6	38.90	37.65
7	44.61	43.15
8	40.41	38.63
9	38.41	37.22
10	43.49	42.20
11	43.85	42.20
12	40.05	39.03
13	46.39	44.91
14	42.86	41.06
15	46.11	44.43
16	39.14	37.68
17	45.10	43.59
18	41.35	39.73
19	44.78	43.31
20	43.11	41.66
21	44.54	43.05
22	40.82	38.98
23	45.81	44.48
24	45.30	43.91
25	46.68	45.68
26	41.25	40.31
27	45.78	44.29
28	45.73	45.19
29	43.61	42.73
30	44.90	43.48
Average over 30 images	43.24	41.88

Table 3.16: Comparison between the PSNR of hyperspectral images [33] for Least Square demosaicking method using RGBW-Bayer using VEML6040 sensor and Least Square method using RGB-Bayer

Image number in dataset	RGBW-Bayer (LSLCD)	RGB-Bayer (LSLCD method)
1	42.93	42.01
2	36.82	35.87
3	38.38	37.44
4	42.71	41.84
5	41.02	39.63
6	36.28	35.22
7	42.28	41.19
8	37.94	36.30
9	35.78	34.79
10	41.34	40.39
11	41.82	40.61
12	37.50	36.79
13	43.95	43.00
14	40.80	39.29
15	44.18	42.93
16	36.79	35.71
17	43.35	42.34
18	38.78	37.41
19	42.39	41.36
20	40.41	39.17
21	42.24	41.01
22	38.56	36.85
23	43.50	42.47
24	43.08	42.02
25	44.42	43.63
26	38.62	37.82
27	43.62	42.38
28	43.07	42.49
29	40.82	40.06
30	42.45	41.24
Average over 30 images	40.86	39.78

Table 3.17: Comparison between the PSNR of hyperspectral images [33] for Least Square demosaicking method using RGBW-Bayer using KAI-Kodak 11002 sensor and Least Square method using RGB-Bayer

We also evaluate the accuracy of estimated white pixels, as we optimized the estimation process in Section 3.4.5 using the hyperspectral dataset. First, we reconstructed the RGB images using hyperspectral images and estimated the white filter values using equation 3.135. Then, we reconstructed the W (white) images using hyperspectral dataset and calculated the PSNR of the estimated white values versus the calculated white values from dataset on the 30 images. The following table shows the comparison of estimated white and the actual white values using hyperspectral data in term of PSNR. Tables 4.7 and 3.19 show the PSNR of estimated white and actual white images over the hyperspectral dataset using VEML6040 and KAI-Kodak11002 sensors in order. The average result over the whole dataset prove that the provided optimized white filter estimation equation in Section 3.4.5 is accurate.

Image number	Comparison between the actual and the estimated white image(PSNR)
1	41.96
2	46.37
3	47.32
4	43.09
5	44.83
6	44.65
7	41.92
8	39.75
9	43.45
10	42.55
11	46.10
12	41.10
13	37.16
14	38.40
15	39.66
16	40.19
17	40.58
18	37.35
19	37.71
20	44.44
21	41.20
22	37.30
23	44.56
24	42.01
25	49.60
26	45.70
27	48.73
28	42.96
29	47.50
30	47.13
Average over 30 images	42.84

Table 3.18: PSNR of estimated white using equation (3.135) pixels and actual white pixels for 30 hyperspectral images using VEML6040 sensor

Image number	Comparison between the actual and the estimated white image(PSNR)
1	44.20
2	48.19
3	47.59
4	44.62
5	44.27
6	41.03
7	39.35
8	35.87
9	40.16
10	41.59
11	40.62
12	41.92
13	37.55
14	36.37
15	38.54
16	35.43
17	37.63
18	32.30
19	34.03
20	41.88
21	36.15
22	32.40
23	46.50
24	38.01
25	54.06
26	47.80
27	53.44
28	43.91
29	49.07
30	50.50
Average over 30 images	41.83

Table 3.19: PSNR of estimated white using equation (3.136) pixels and actual white pixels for 30 hyperspectral images using KAI-Kodak11002 sensor

Chapter 4

Demosaicking of noisy CFA images

In this chapter we will account for the received noise in camera CFA sensors. The received noise in CFAs impacts the performance of the demosaicking algorithm. We are estimating the value of noise in red, green, blue and white filters in this chapter. We will also propose a joint noise reduction-demosaicking algorithm for RGBW CFAs and evaluate the quality of the reconstructed image, and we compare the results with the previous works in this field.

Based on the noise level that have been estimated through noise estimation process, an appropriate set of least-square filters will be looked up. The demosaicking algorithm using least-square filters will be applied on CFA image as we discussed in the previous chapter.

4.1 Noise in CFA images

Due to the physical limits of current cameras, there is photon noise captured in camera sensors. The source of noise can be either an array of electronic noise like variance in amplifier gains or photon shot noise developed in the light measuring process. Noise in CCD sensors after gamma correction can be assumed as additive and signal independent as described in [25].

$$f_{CFAN}[n_1, n_2] = f_{CFA}[n_1, n_2] + v[n_1, n_2] \tag{4.1}$$

The noise signal in the images will be modeled as identically distributed and stationary zero-mean noise. We can approximate noise in the white-balanced, gamma-corrected signal as signal-independent white Gaussian noise, with channel dependent variances [25]

$$\sigma_R{}^2 : \sigma_G{}^2 : \sigma_B{}^2 : \sigma_W{}^2 = \alpha_R : \alpha_G : \alpha_B : \alpha_W. \tag{4.2}$$

We will model the noise in each color channel as white Gaussian noise with variances $\sigma_R{}^2$, $\sigma_G{}^2$, $\sigma_B{}^2$ and $\sigma_W{}^2$. These values are calculated by the gain needed to achieve white balance for red, green and blue. We estimate the variance for white color in the same way. The variance values for red, green and blue channel for Canon $10D$ with three channel sensor have been calculated as 1.86, 0.69 and 1 in order [17]. In this research the channel dependent variances for two different four channel sensors will be calculated, as it has been calculated for three channel sensors previously.

Using the non-normalized filter absorption curve $C_R(\lambda)$, $C_G(\lambda)$, $C_B(\lambda)$, $C_W(\lambda)$ as we had in Figure 3.15, and assuming that if the cutoff filter is included, the raw output of a sensor element will be

$$F_i = \int_{\lambda_{min}}^{\lambda_{max}} f(\lambda) C_i(\lambda) d\lambda \tag{4.3}$$

$i \in R, G, B, W$.

Assume $f(\lambda)$ is reference white, $D65$, as $f_{65}(\lambda)$

$$(F_{65,i})^{(raw)} = \int_{\lambda_{min}}^{\lambda_{max}} f_{65}(\lambda) C_i(\lambda) d\lambda \tag{4.4}$$

$i \in R, G, B, W$.

For white balance, we multiply all the $F_{65,i}^{(raw)}$ by constants α_i

$$F_{65,i} = \alpha_i F_{65,i}^{(raw)} \tag{4.5}$$

such that all $F_{65,i}$ are equal, $i \in R, G, B, W$. If $\alpha_B = 1$, then we need

$$\alpha_i F_{65,i}^{(raw)} = F_{65,B}^{(raw)} \tag{4.6}$$

$$\alpha_i = \frac{F_{65,B}^{(raw)}}{F_{65,i}^{(raw)}} \tag{4.7}$$

$i \in R, G, B, W$.

The variances for different channels for VEML6040 [10] sensor have been calculated as $\alpha_R = 1.2163$, $\alpha_G = 0.6371$, $\alpha_B = 1$ and $\alpha_W = 0.8053$, and for Kodak-KAI-11000 sensor [9] are $\alpha_R = 2.2169$, $\alpha_G = 1.2885$, $\alpha_B = 1$ and $\alpha_W = 0.3690$.

4.2 Noise estimation

In the previous chapter we optimized the demosaicking method for RGBW CFAs using least-square filters, and we applied it to the noise-free Kodak dataset and a noise-free hyperspectral dataset. We are implementing the denoising-demosaicking algorithm based on the LS method that has been described in Section 3.4. The image quality using RGBW-Bayer was the best among the presented RGBW CFAs in previous chapter, and we designed the joint denoising-demosaicking algorithm for RGBW-Bayer in this chapter.

In this chapter, we simulate Gaussian noise with different variances for each color filter for both sensors considered, and artificially add them to the input data set. These images will be used as noisy input images. Since the real noise level is unknown, we will simulate the noise effect by adding several different levels of noise to the input image. A set of least-square filters for each noise level will be designed using the noisy datasets. A noise estimator will be applied to the system to find the variance of the input image noise.

The noise for R, G, B and W components will be estimated using the Amer and Dubois noise estimation method [4]. The proposed noise estimation method in [4] is not designed for CFA images, however, it was adapted to RGB-Bayer in [25]. We assume the image as a combination of four color images, and we are using this method on four subimages of red, green, blue and white. In this method, the images are partitioned into a set of intensity homogeneous blocks, and we find the local variance in each block of the image. In each block, the signals assumed to be constant, and the variance of the noise is σ^2.

Using the Amer and Dubois method, we select intensity homogeneous blocks in a subimage of R,G,B and W. A subimage should not contain blocks with line structure. The noise

level estimation method consists of detection of intensity homogeneous blocks and calculating

$$\sigma_i = \sqrt{\alpha_i}\sigma_A \tag{4.8}$$

for color $i \in R, G, B, W$ of the selected blocks. For each subimage, we define square $\omega \times \omega$ blocks ${B_{kl}}^{(j)}$, centered at each location (k, l) in the subimage, $j \in R, G, B, W$. We denote the sample mean and sample variance for each block by $\mu_{Bkl}(j)$ and ${\sigma_{Bkl}}^2(j)$. Therefore, for the most homogeneous block in the image, $\mu_{Bkl}(j)$ shows the signal value and the variance ${\sigma_{Bkl}}^2(j)$ can be representative of the noise in the corresponding channel, and gives us a good estimation of the noise variance in a specific channel.

Intensity homogeneous block will be calculated for each block as a homogeneity measure, $\varepsilon_{Bkl}(j)$ as described in [4] and [25]. Comparing the homogeneity measure for each block, we will choose the most intensity homogeneous blocks. The following figure shows different directions that the homogeneity measures will be calculated on the blocks. As Figure 4.1 shows, eight directional homogeneity measures will be assumed from eight edge directions, where ${\zeta_{Bkl}}^{(m)}(j)$ is the absolute value of the output of a one dimensional high pass filter applied on mask contour m, evaluated at the center of the block. We assume that blocks with the smallest sum of all directional homogeneity measures,

$$\varepsilon_{Bkl}(j) = \sum_{1 \le m \le 8} {\zeta_{Bkl}}^{(m)}(j), \tag{4.9}$$

may be identified as intensity homogeneous blocks. We can assume the window size ω. ω is an odd number, and has been set to $\omega \geq 5$ empirically. We use a high pass filter with size of $1 \times \omega$ on the image. The high-pass filter has been set as

$${f_{HP}}^5 = [-1, -1, 4, -1, -1]. \tag{4.10}$$

In this method the ideal intensity homogeneous block will be the one with lowest sum of all homogeneity measures. To find the more accurate estimation of noise level, we do not rely on only one block homogeneity measure, and we use three blocks in each subimage to calculate the noise variance. Assume $V^{(j)}$ to be the set of locations of the centers of three blocks in subimage j with the lowest aggregate homogeneity measure. The corresponding

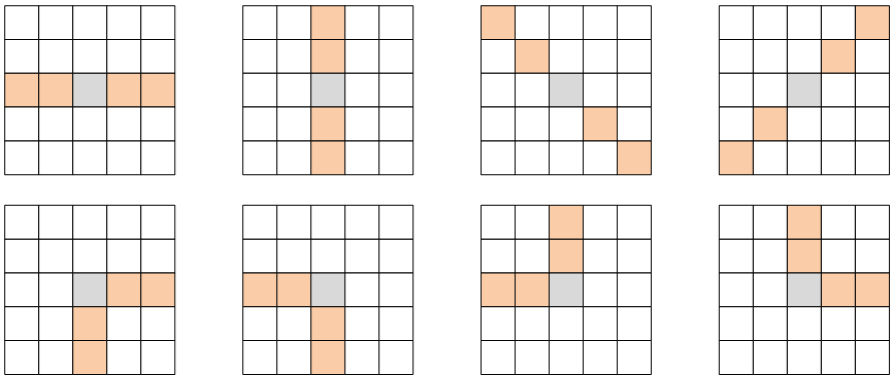

Figure 4.1: Eight different masks for homogeneity measures with the size $\omega = 5$

sample variances are ${\sigma_{Bkl}}^2(j)$, $(k,l) \in V^{(j)}$ for $j \in R, G, B, W$, and the estimate of the variance for each phase is

$${\sigma_{e,j}}^2 = \frac{1}{3} \sum_{(k,l)\in V^{(j)}} {\sigma_{Bkl}}^2(j). \tag{4.11}$$

If we know the exact ratio of $\alpha_R : \alpha_G : \alpha_B : \alpha_W$ that was used to obtain f_{CFAN}, we select ${\sigma_e}^{T\alpha}$ as,

$${\sigma_e}^{T\alpha} = median[\frac{\sigma_{e,R}}{\sqrt{\alpha_R}}, \frac{\sigma_{e,G}}{\sqrt{\alpha_G}}, \frac{\sigma_{e,B}}{\sqrt{\alpha_B}}, \frac{\sigma_{e,W}}{\sqrt{\alpha_W}}] \tag{4.12}$$

where $T\alpha$ stands for true alpha ratio, which means we apply the known alpha values for estimating the noise standard deviation.

However, as we describe in Section 4.1, the ratio $\alpha_R : \alpha_G : \alpha_B : \alpha_W$ can be different depending on camera models. Therefore we may have to estimate the $\alpha_R : \alpha_G : \alpha_B : \alpha_W$ ratio first before we determine σ_e. From equation 4.6 we know

$${\sigma_R}^2 : {\sigma_G}^2 : {\sigma_B}^2 : {\sigma_W}^2 = \alpha_R : \alpha_G : \alpha_B : \alpha_W, \tag{4.13}$$

so we assume

$$\frac{\sigma_{e,R}}{\sqrt{\alpha_R}} \approx \frac{\sigma_{e,G}}{\sqrt{\alpha_G}} \approx \frac{\sigma_{e,B}}{\sqrt{\alpha_B}} \approx \frac{\sigma_{e,W}}{\sqrt{\alpha_W}}. \tag{4.14}$$

If we arbitrarily set $\alpha_B = 1$, then α_R, α_G and α_W will be calculated.

The homogeneity in each block will be calculated using local uniformity analyzer, using high-pass operators on a 5×5 mask in eight different directions. The results of the

local uniformity analyzer will be zero in the homogeneous area, and it is non-zero in non-uniform areas. The sum of absolute values over the eight directions will be assumed as the homogeneity factor. Using the homogeneity factor over the blocks, we find the average variance of noise over the whole image.

Assuming there are 11 representative levels of noise, we will estimate the noise level of input image, and select an appropriate set of filters to extract the color components and demosaicking algorithm.

4.3 Demosaicking of noisy CFA images

The least-square demosaicking method has been proposed in Section 3.4 for RGBW CFAs, and will be used for noise reduction. The noisy images will be used as a training set for the least-square method. Different levels of Gaussian noise with parameter σ will be added to the input CFA images. In the training phase, noise will be added to the gamma-corrected R, G, B and W components with the given ratio of variances. The standard deviation of noise for each color channel will be assumed as $\sqrt{\alpha_R}\sigma$, $\sqrt{\alpha_G}\sigma$, $\sqrt{\alpha_B}\sigma$ and $\sqrt{\alpha_W}\sigma$, and $\sigma \in 0, 2, ..., 20$ for eleven noise levels. Then, an appropriate least-square demosaicking system will be designed for each set of noisy images. So we designed several demosaicking systems, adapted to different levels of noise. In the proposed noise reduction algorithm, the noise level of input image will be estimated, and an appropriate set of filters for demosaicking will be chosen. The following block diagram 4.2 shows the demosaicking and denoising algorithm.

Since the value of the estimated noise level is a continuous value and the added noise level is a discrete value, we need to map the estimated value to one of the added noise levels $\sigma \in 0, 2, ..., 20$, then the least square filter will be assigned. Assuming the noise level $2(p-1)$, the color mean square error will be calculated and the best set of least square filter σ_{MS} will be determined. We will select the nearest even noise level $\sigma_{discrete}$

$$\sigma_{discrete} = 2 \times round(\frac{\sigma_{MS}}{2}). \tag{4.15}$$

The following plot Figure 4.3 shows the estimated noise variance versus the added noise level over the 24 images of Kodak dataset using VEML sensor. The results illustrate that the estimated noise level is close to the actual added noise value, and the appropriate least square filter set has been chosen for each image.

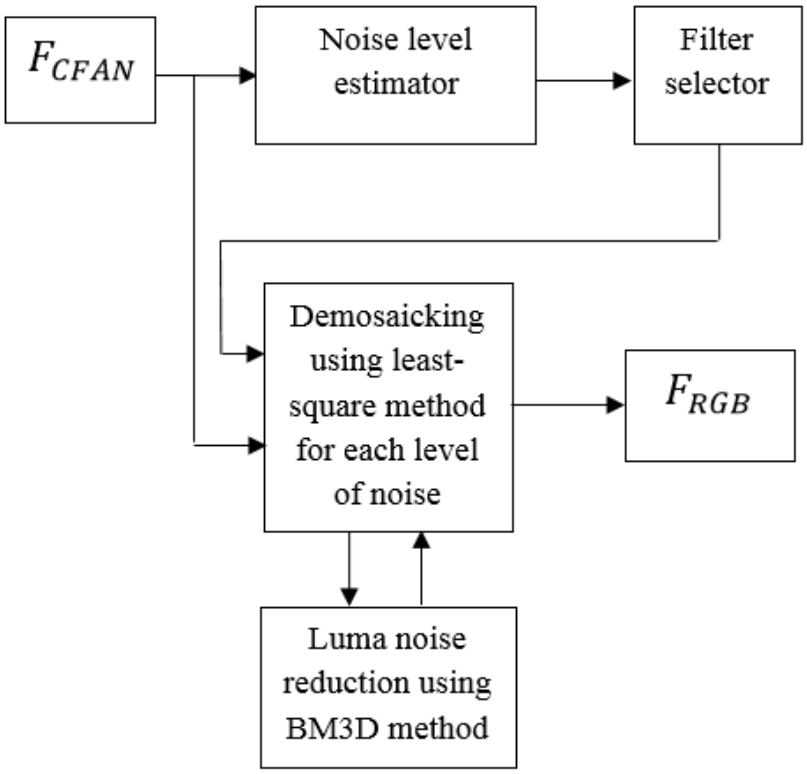

Figure 4.2: Demosaicking-denoising system

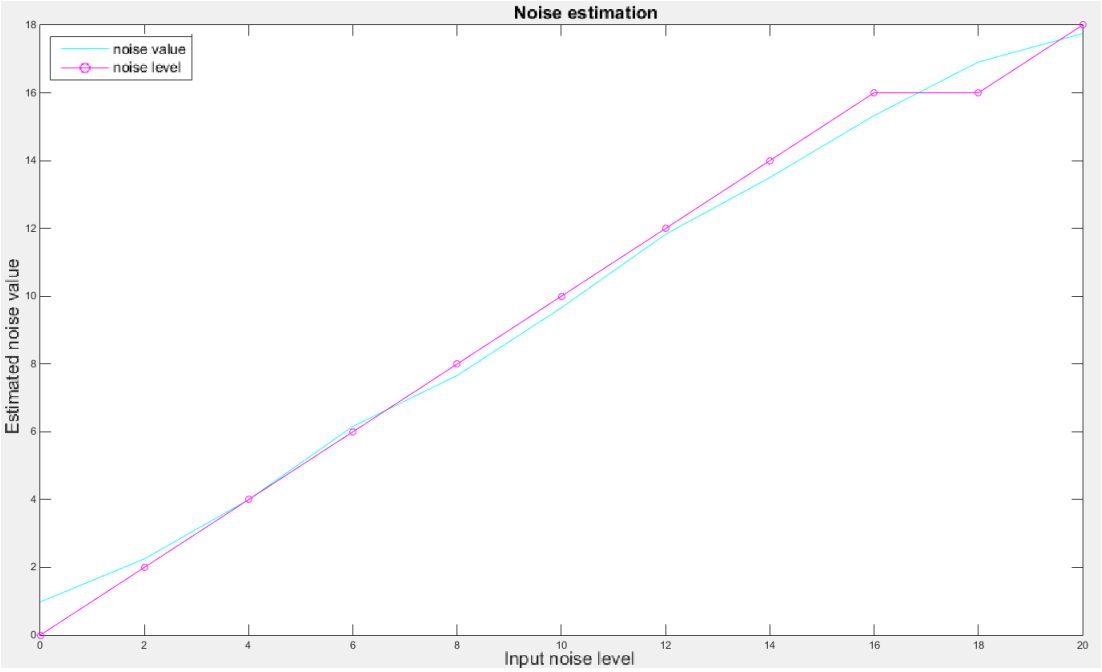

Figure 4.3: Added noise level versus estimated noise level on Kodak image dataset using VEML6040

4.3.1 Luma noise reduction using BM3D

In the demosaicking algorithm, reconstructing the more accurate luma components is crucial, and results in better quality of the reconstructed image. As we explained before, during the demosaicking process the luma component will be calculated by subtracting all chromas from the CFA. Since we are extracting chromas using noisy input images, the estimated chromas will not be accurate, and it leads to the poor estimation of the luma component. Using a state of art denoising method for gray scale images gives us a better estimation of luma. We will apply the Block Matching $3D$ ($BM3D$) denoising algorithm [12] in this stage, which is one of the state of the art denoising method.

4.4 Results

In this section, we designed and implemented the joint demosaicking-denoising algorithm. As we discussed in this chapter, we added different levels of noise artificially to the Kodak dataset. There will be ten different levels of white Gaussian noise with the variance of $\sigma = 0, 2, 4, ..., 20$. Then the noise estimator will estimate the noise level and set the suitable demosaicking algorithm for the estimated noise level to reconstruct the image.

The value of clear/panchromatic pixels have been estimated based on the equations 3.135 and 3.136 provided in Section 3.4.5 on the Kodak dataset. The results will be compared with the hyperspectral image dataset with actual value of white pixels as well.

Tables 4.1, 4.2, 4.3 and 4.4 show the results of demosaicking-denoising method and least-square method for Kodak dataset noisy images using RGBW-Bayer CFA in terms of PSNR and S-CIELAB for VEML6040 and Kodak-KAI-11000 sensors. These tables contain the average results over 24 images of Kodak data set in each case. The average results over 24 images for different noise level show the proposed algorithm robustness in different noise level, and let us compare the average results for RGBW-Bayer with the average results of previous work for RGB-Bayer. According to the provided results in the following tables the demosaicking-denoising algorithm is working better than regular demosaicking algorithm without noise reduction method. A comparison between the state

of the art joint denoising-demosaicking method applied on RGB-Bayer is provided as well. The denoising-demosaicking method on RGB-Bayer is working better than previous works on this topic as discussed in [25].

Tables 4.1 and 4.3 show the results of regular least-square demosaicking method using RGB-Bayer and RGBW-Bayer for Kodak dataset noisy images for both sensors. The average PSNR of demosaicking-denoising method over 11 noise levels using RGBW-Bayer is higher than the average PSNR using RGB-Bayer for both sensors. It shows that the RGBW-Bayer pattern containing clear/ panchromatic filter receives higher signal to noise ratio, and works better in presence of noise. We can conclude the same result based on the S-CIELAB results as shown in Tables 4.2 and 4.4.

Noise level (Noise variance)	LS method on RGBW	LS method on RGB	Demosaicking-denoising on RGBW	Demosaicking-denoising on RGB
1(0)	39.69	40.22	39.08	40.26
2(2)	37.77	37.96	37.59	37.51
3(4)	34.75	34.68	35.46	34.91
4(6)	32.18	32.00	34.11	32.90
5(8)	30.08	29.85	32.95	31.41
6(10)	28.35	28.10	32.03	30.27
7(12)	26.88	26.64	31.11	29.37
8(14)	25.62	25.38	30.26	28.69
9(16)	24.51	24.28	29.56	28.03
10(18)	23.52	23.31	28.96	27.51
11(20)	22.63	22.44	28.38	27.06
Average over 11 noise levels	29.63	29.53	32.68	31.62

Table 4.1: Average PSNR over 24 Kodak images using least-Square (LS) method and demosaicking-denoising method on RGBW-Bayer using VEML6040 sensor and RGB-Bayer for different noise levels

.

Noise level (Noise variance)	LS method on RGBW	Demosaicking-denoising on RGBW
1(0)	0.85	1.01
2(2)	1.14	1.24
3(4)	1.65	1.62
4(6)	2.21	2.00
5(8)	2.81	2.38
6(10)	3.43	2.76
7(12)	4.05	3.16
8(14)	4.69	3.56
9(16)	5.33	3.95
10(18)	5.97	4.33
11(20)	6.62	4.72
Average over 11 noise levels	3.52	2.79

Table 4.2: Average S-CIELAB over 24 Kodak images using least-Square(LS) method and demosaicking-denoising method on RGBW-Bayer using VEML6040 sensor for different noise levels

.

Noise level (Noise variance)	LS method on RGBW	LS method on RGB	Demosaicking-denoising on RGBW	Demosaicking-denoising on RGB
1(0)	39.39	40.22	38.87	40.26
2(2)	37.14	37.96	36.89	37.51
3(4)	33.86	34.68	34.60	34.91
4(6)	31.17	32.00	33.55	32.90
5(8)	29.01	29.85	32.44	31.41
6(10)	27.25	28.10	31.17	30.27
7(12)	25.76	26.64	30.39	29.37
8(14)	24.49	25.38	29.50	28.69
9(16)	23.37	24.28	28.36	28.03
10(18)	22.38	23.31	27.92	27.51
11(20)	21.48	22.44	27.37	27.06
Average over 11 noise levels	28.66	29.53	31.91	31.62

Table 4.3: Average PSNR over 24 Kodak images using least-Square(LS) method and demosaicking-denoising method on RGBW-Bayer using Kodak-KAI-11000 sensor and RGB-Bayer for different noise levels

.

Noise level (Noise variance)	LS method on RGBW	Demosaicking-denoising on RGBW
1(0)	0.95	1.11
2(2)	1.30	1.41
3(4)	1.89	1.87
4(6)	2.57	2.24
5(8)	3.27	2.66
6(10)	3.99	3.16
7(12)	4.73	3.58
8(14)	5.47	4.04
9(16)	6.22	4.52
10(18)	6.98	4.93
11(20)	7.74	5.39
Average over 11 noise levels	4.10	3.17

Table 4.4: Average S-CIELAB over 24 Kodak images using least-Square(LS) method and demosaicking-denoising method on RGBW-Bayer using Kodak-KAI-11000 sensor for different noise levels

.

The following figures show the noisy CFA images for two sample images and two different noise levels in each case ($\sigma = 6, 14$), as well as the reconstructed image using least-square demosaicking method (presented in previous chapter) and demosaicking-denoising algorithm. As we can see visually in Figures 4.4 and 4.5, the quality of reconstructed images using demosaicking-denoising algorithm are better than the quality of reconstructed images using LS method in different input noise levels. The CFA images are not meant to be displayed, and they do not have a good quality. We present them here to show the effect of noise in different noise level in the CFA images.

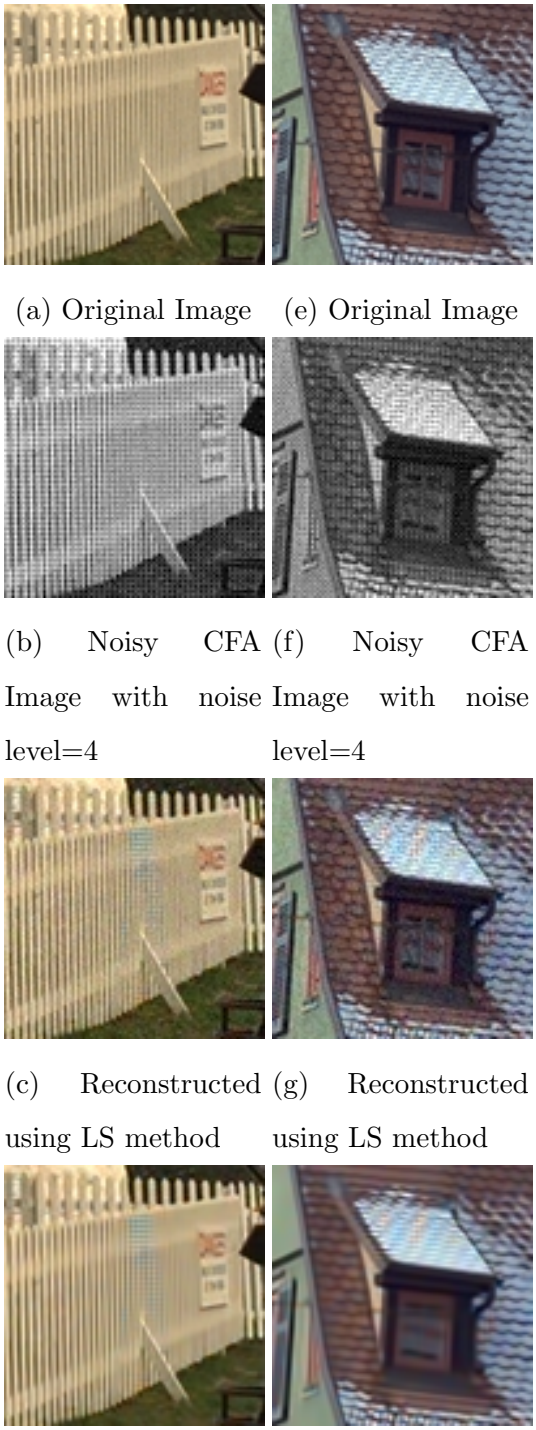

(a) Original Image (e) Original Image

(b) Noisy CFA Image with noise level=4 (f) Noisy CFA Image with noise level=4

(c) Reconstructed using LS method (g) Reconstructed using LS method

(d) Reconstructed using demosaicking-denoising method (h) Reconstructed using demosaicking-denoising method

Figure 4.4: Reconstructed noisy image with $\sigma = 6$ using regular least-square demosaicking method and denoising-demosaicking method with RGBW-Bayer CFA

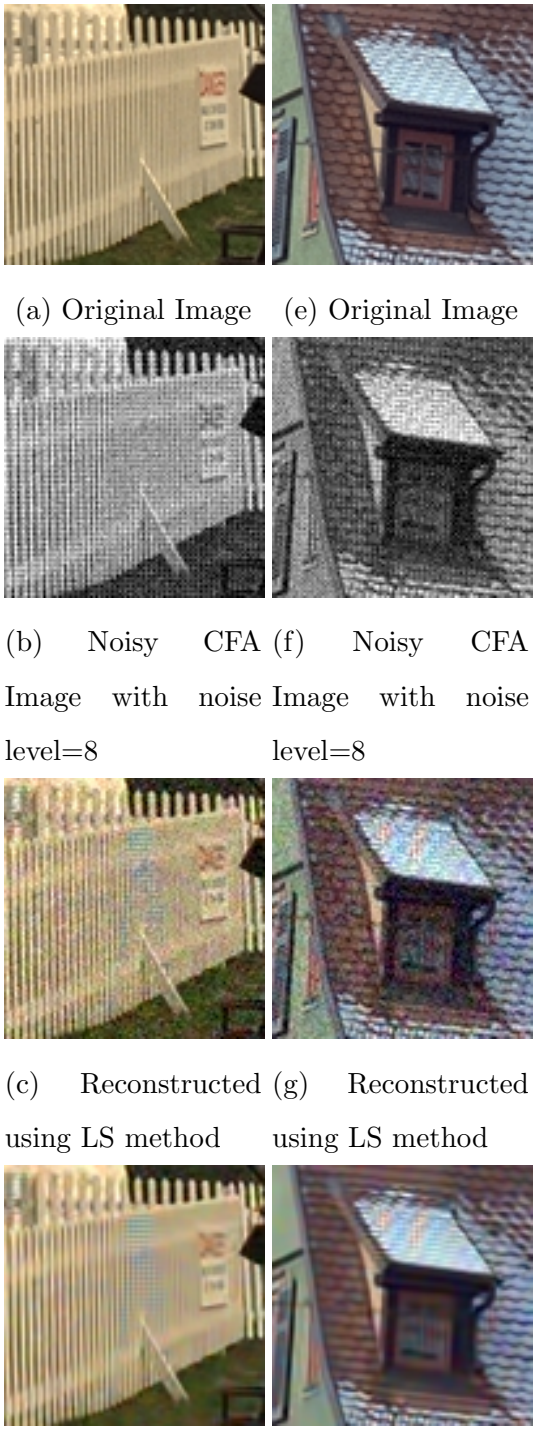

(a) Original Image (e) Original Image

(b) Noisy CFA Image with noise level=8 (f) Noisy CFA Image with noise level=8

(c) Reconstructed using LS method (g) Reconstructed using LS method

(d) Reconstructed using demosaicking-denoising method (h) Reconstructed using demosaicking-denoising method

Figure 4.5: Reconstructed noisy image with $\sigma = 14$ using regular least-square demosaicking method and denoising-demosaicking method with RGBW-Bayer CFA

All the provided results above have been simulated and tested on RGB Kodak data set. The following tables show the result of demosaicking-denoising algorithm with least-square method on a hyperspectral dataset [33] for both sensors. The RGB and RGBW images have been calculated based on the hyperspectral images, and the RGB and RGBW CFAs have been reconstructed for each image. Therefore, we are simulating the actual captured white values from the clear/panchromatic filters using hyperspectral images and we are comparing the results with reconstructed images using the RGB-Bayer on the same dataset.

Tables 4.5 and 4.6 provide the average PSNR over the 30 images of dataset for both sensors. The noisy RGBW CFA have been reconstructed by adding different noise level to the CFA image, as we discussed before. Using the average results over 30 hyperspectral images for different noise level we will be able to compare the proposed algorithm robustness in different noise level, and let us compare the average results for RGBW-Bayer with the average results of Kodak dataset for RGBW-Bayer.

Since we are using two different datasets, we will not be able to compare the average PSNR over the whole dataset with the previous results. The provided results are showing that the proposed demosaicking-denoising algorithm is working very well on hyperspectral images as a sample of received image with RGBW CFAs in presence of noise.

It shows that the demosaicking-denoising algorithm is working better than regular demosaicking algorithm without noise reduction method. A comparison between the state of art joint denoising-demosaicking method applied on RGBW-Bayer on Kodak dataset is provided as well. The results shows that the RGBW CFA is more robust to noise than the RGB CFA as we hypothesized in this research.

Noise level (Noise variance)	Demosaicking-denoising on RGBW	Demosaicking-denoising on RGB
1(0)	43.16	43.15
2(2)	40.59	40.47
3(4)	38.34	38.38
4(6)	36.78	36.56
5(8)	35.52	35.22
6(10)	34.42	34.15
7(12)	33.28	33.00
8(14)	32.44	31.96
9(16)	31.56	31.13
10(18)	30.80	30.32
11(20)	29.95	29.51
Average over 11 noise levels	35.17	34.85

Table 4.5: Average PSNR over 30 hyperspectral images using demosaicking-denoising method on RGBW-Bayer using VEML6040 and RGB-Bayer for different noise levels

.

Noise level (Noise variance)	Demosaicking-denoising on RGBW	Demosaicking-denoising on RGB
1(0)	40.64	40.61
2(2)	38.68	38.03
3(4)	36.21	35.94
4(6)	35.24	35.05
5(8)	33.98	33.81
6(10)	32.67	32.43
7(12)	31.63	31.23
8(14)	30.60	30.23
9(16)	29.70	29.28
10(18)	28.90	28.43
11(20)	28.16	27.64
Average over 11 noise levels	33.31	32.97

Table 4.6: Average PSNR over 30 hyperspectral images using demosaicking-denoising method on RGBW-Bayer using Kodak-KAI-11000 and RGB-Bayer for different noise levels .

The following Figures 4.6 and 4.7 show the average PSNR over 30 hyperspectral images using demosaicking-denoising method on RGBW-Bayer and RGB-Bayer for different noise levels. Figure 4.6 shows the results of RGBW-Bayer using VEML6040 and figure 4.7 shows the results of RGBW-Bayer using Kodak-KAI-11000. The results shows that the RGBW-Bayer works better comparing the RGB-Bayer in presence of noise for both sensors.

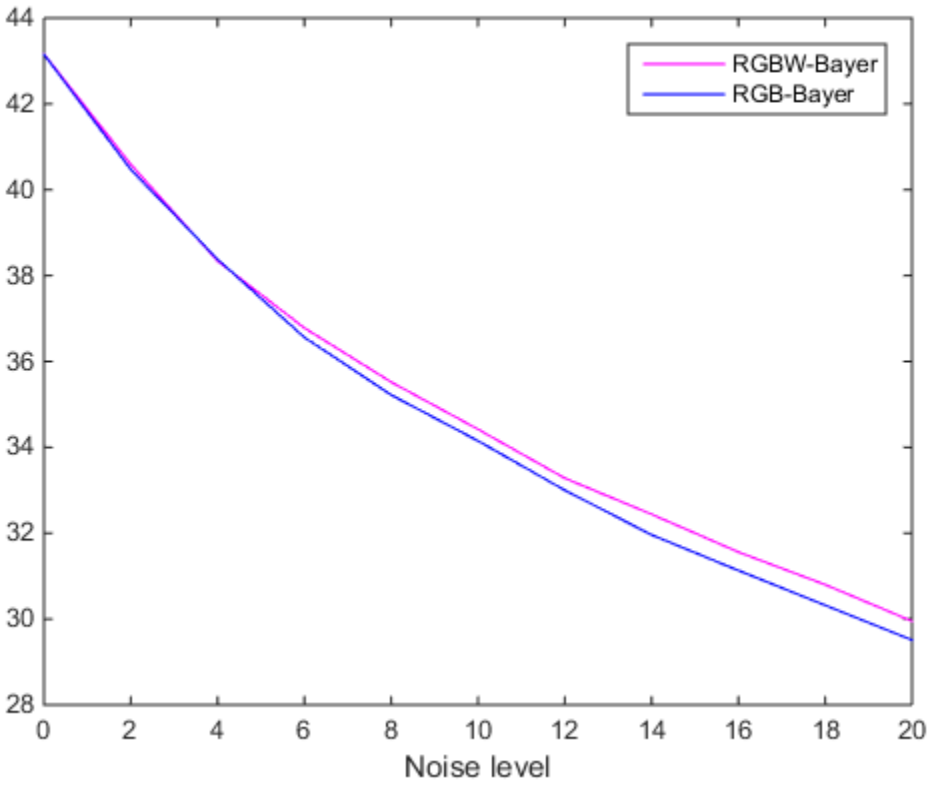

Figure 4.6: Comparison between the average PSNR over 30 hyperspectral images using demosaicking-denoising method on RGBW-Bayer with VEML6040 and RGB-Bayer for different noise levels

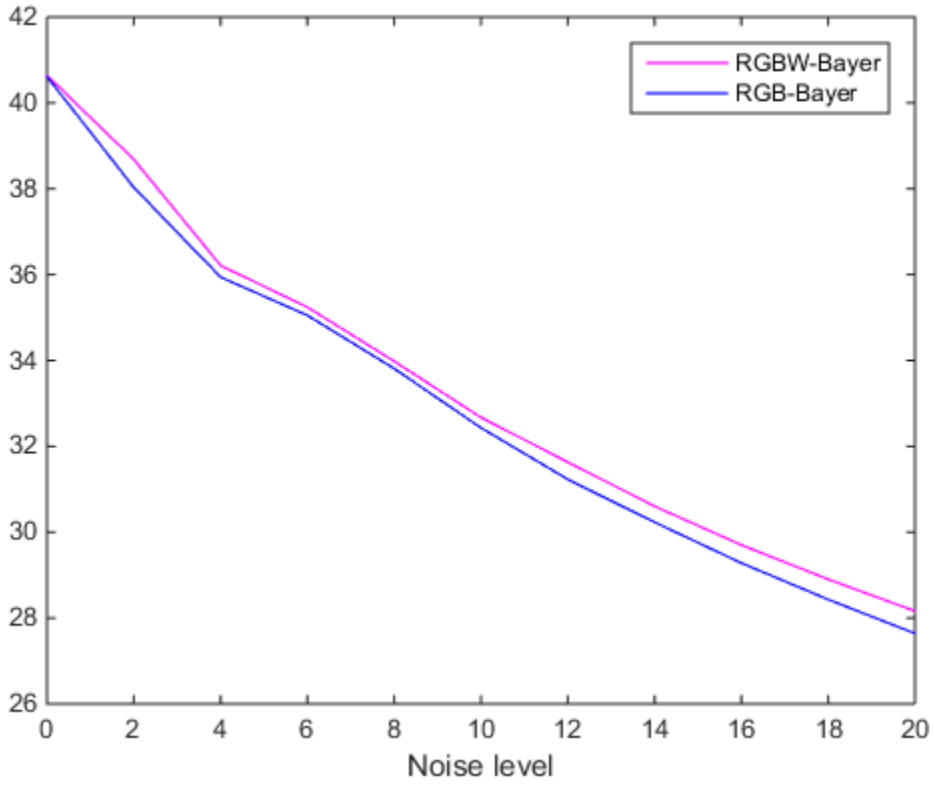

Figure 4.7: Comparison between the average PSNR over 30 hyperspectral images using demosaicking-denoising method on RGBW-Bayer with Kodak-KAI11000 and RGB-Bayer for different noise levels

Also, the following tables 4.7, 4.8 show the average S-CIELAB results of 30 hyperspectral images using demosaicking-denoising method on RGBW-Bayer and RGB-Bayer for different noise levels for both sensors. The average SCIELAB show the similarity between the original image and the reconstructed image in presence of noise using denoising-demosaicking algorithm over the whole data set for each noise level. The comparison between RGB-Bayer and RGBW-Bayer shows that the RGBW-Bayer is working better for noisy input images.

Noise level (Noise variance)	Demosaicking-denoising on RGBW	Demosaicking-denoising on RGB
1(0)	0.53	0.46
2(2)	0.84	0.85
3(4)	1.25	1.27
4(6)	1.66	1.66
5(8)	2.08	2.12
6(10)	2.50	2.58
7(12)	2.93	3.02
8(14)	3.35	3.50
9(16)	3.78	3.92
10(18)	4.20	4.37
11(20)	4.64	4.82
Average over 11 noise levels	2.52	2.59

Table 4.7: Average S-CIELAB over 30 hyperspectral images using demosaicking-denoising method on RGBW-Bayer using VEML6040 and RGB-Bayer for different noise levels

.

Noise level (Noise variance)	Demosaicking-denoising on RGBW	Demosaicking-denoising on RGB
1(0)	0.66	0.64
2(2)	1.063	1.07
3(4)	1.58	1.65
4(6)	2.08	2.17
5(8)	2.60	2.66
6(10)	3.13	3.26
7(12)	3.66	3.76
8(14)	4.20	4.27
9(16)	4.74	4.79
10(18)	5.27	5.35
11(20)	5.80	5.83
Average over 11 noise levels	3.16	3.22

Table 4.8: Average S-CIELAB over 30 hyperspectral images using demosaicking-denoising method on RGBW-Bayer using Kodak-KAI-11000 and RGB-Bayer for different noise levels .

The following Figure 4.8 shows the similarity of added noise level versus the estimated noise variance using noise estimation process over the hyperspectral dataset using VEML6040 sensor. The results shows the estimated noise level is close to the actual added noise level and the filter selection and demosaicking-denoising algorithm works well on these dataset.

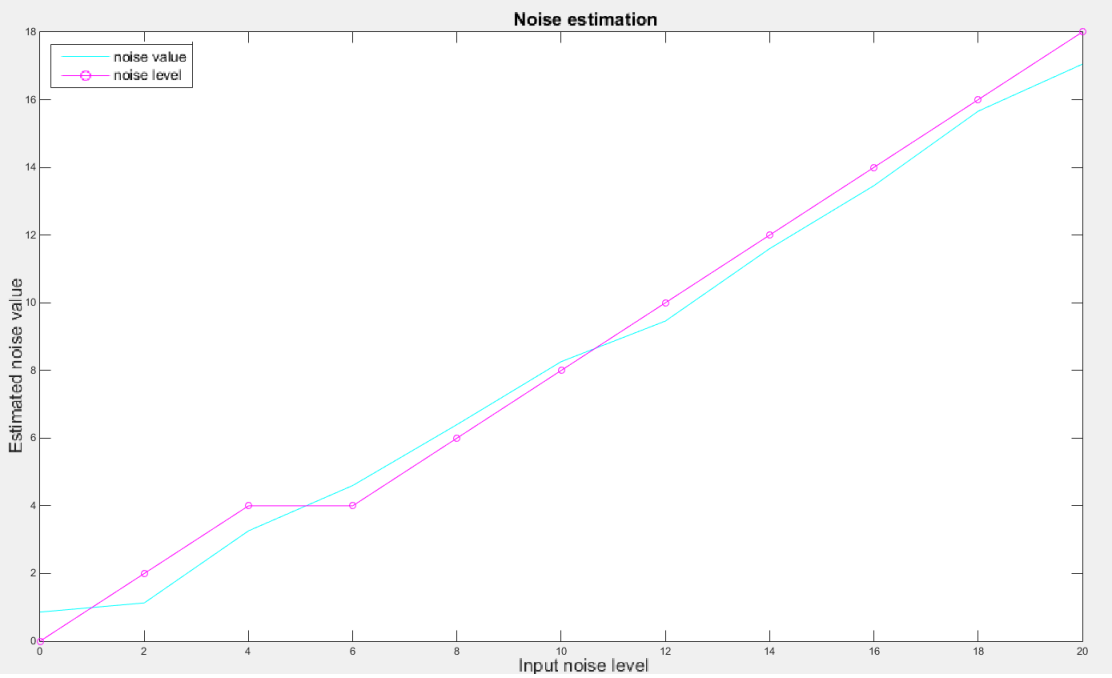

Figure 4.8: Added noise level versus estimated noise level on hyperspectral image dataset using VEML6040

Chapter 5

Conclusion

5.1 Conclusions

A novel demosaicking-denoising method for RGBW CFAs has been introduced in this research. According to the results, the presented method led to a noticeable improvement in received signal to noise ratio compared to the existing methods in the literature. The presented methods included a demosaicking algorithm on a three channel CFA and three four channel CFAs. The contributions were as follows:

- Due to the complexity of the Fujifilm X-Trans pattern, it has been chosen to study among three-channel CFAs, and adaptive and non-adaptive and least-square demosaicking algorithms have been developed for it. Since there is no available literature on Fujifilm X-Trans pattern demosaicking, the results have been compared with the state of the art demosaicking method on RGB-Bayer. The Fujifilm X-Trans pattern has a large number of color filters, and it provides more accurate color estimation through demosaicking process, but it is not work as good as Bayer pattern in high frequency areas. The results have been presented at the International Conference of Image Processing (ICIP)-2014 [38].

- The RGBW-Kodak pattern has been modeled, and adaptive and non-adaptive demosaicking algorithms have been proposed for it. It has been published in SPIE/ IS&T

Electronic Imaging-2015 conference [39]. Also, a recently developed RGBW pattern presented in [45] has been reviewed in this work and a demosaicking algorithm has been implemented for this pattern. The RGBW-Bayer CFA has been discussed, and adaptive and non-adaptive demosaicking algorithms have been presented for it. Also the adaptive demosaicking algorithm for three-channel and four-channel CFAs has been presented in a structured and organized method, and it can be applied on different CFAs.

In our initial assumption, we simulate the white filters output as a combination of red, green and blue filters. The best estimation of white filter output has been calculated using the other three primary color components by quadratic programming. The adaptive demosaicking algorithm for RGBW-Bayer has been optimized using least-squares method. The comparison between different RGBW patterns has been presented in this research, and it has been published in SPIE/ IS&T Electronic Imaging-2016 conference [40].

Initially, the Kodak data set has been used for comparing the results. The results shows less color artifacts for Fujifilm X-Trans pattern compared to the RGB-Bayer. The results of demosaicking algorithms for all three RGBW patterns have been compared. The visual results and the PSNR show that RGBW-Bayer was the best among the discussed patterns. The least-square method results for RGBW-Bayer have been compared with the least-square method using RGB-Bayer pattern.

- The effect of noise has been simulated on red, green, blue and white filters, and an appropriate demosaicking-denoising algorithm on RGBW-Bayer pattern has been developed using a new set of coefficients for noise in different channel. The demosaicking-denoising algorithm results on Bayer-RGBW CFA with demosaicking-denoising algorithm on RGB-Bayer results have been compared. Thus the results of noise reduction on white color filters has been evaluated. The proposed algorithm has been applied on Kodak dataset and a hyperspectral dataset. Also the white filter estimation results have been validated using hyperspectral images. The results have been white balanced and gamma corrected, and the SCIELAB and PSNR values for each developed

demosaicking algorithm have been measured.

The results of four channel CFA have been evaluated on a hyperspectral data set [33] as well. The results of demosaicking-denoising algorithm using both hyperspectral and Kodak images shows improvement using RGBW-Bayer CFA comparing to the RGB-Bayer CFA. The comparison between the white filter estimation using the optimized equation 3.135 based on the value of three primary color filters (red,green and blue) and the actual white filter values of hyperspectral images shows the estimated values are very accurate.

5.2 Future work

The proposed algorithms for RGB and RGBW color filter arrays led to a new demosaicking-denoising algorithm for RGBW CFAs. The results of this research can be expanded to different aspects. Some suggested future works are as follows:

- As this research showed the signal to noise ratio has higher value using RGBW CFAs, studying and creating CFAs containing more white filters can improve the reconstructed image quality.
- A case study is applying the presented adaptive, non-adaptive, and least-square demosaicking method, on different CFAs. Since, there might be a better RGBW CFA to reconstruct the color images, the proposed demosaicking-denoising algorithm can be applied on other RGBW CFAs.
- The modeled white filter based on red, green and blue filters value, can be utilized to replace color filters with white filters. Designing new CFA patterns with two color filters and more white filters can be another research direction in future.

References

[1] J. E. Adams. Design of practical color filter array interpolation algorithms for digital cameras. *IEEE International Conference On Image Processing (ICIP)*, 1(8):518–533, 1998.

[2] J. E. Adams, A. Deever, J. F. Hamilton Jr, M. Kumar, R. Palum, and B. H. Pillman. Single capture image fusion with motion consideration. In Rastislav Lukac, editor, *Computational Photography: Methods and Applications*, chapter 2, page 63. CRC Press, 2010.

[3] D. Alleysson, S. Susstrunk, and J. Herault. Linear demosaicing inspired by the human visual system. *IEEE transaction on Image Processing*, 14(4), 2005.

[4] A. Amer and E. Dubois. Fast and reliable structure-oriented video noise estimation. *IEEE Transactions on Circuits and Systems for Video Technology*, 15(1):113–118, 2005.

[5] A. Buades, Y. Lou, J. Morel, and Z. Tang. Multi image noise estimation and denoising. *https://hal.archives-ouvertes.fr/hal-00510866/file/Burst$_H$al.pdf*, (*hal*−00510866), 2010.

[6] H. C. Burger, C. J. Schuler, and S. Harmeling. Image denoising: Can plain neural networks compete with BM3D. In *IEEE Conference on Computer Vision and Pattern Recognition (CVPR)*, pages 2392–2399, 2012.

[7] P. Chatterjee, N. Joshi, Sing Bing Kang, and Y. Matsushita. Noise suppression in low-light images through joint denoising and demosaicing. In *IEEE Conference on*

Computer Vision and Pattern Recognition, CVPR '11, pages 321–328. IEEE Computer Society, 2011.

[8] D. R. Cok. Signal processing method and apparatus for producing interpolated chrominance values in a sampled color image signal. *U.S. Patent No. 4 642 678*, 1987.

[9] Eastman Kodak Company. Kodak, KAI-11002 image sensor.[online]. website:. https://www.pco.de/fileadmin/user_upload/db/download/KAI-11000CMLongSpec.pdf, 2006.

[10] Vishay Company. VEML Sensor-Vishay.[online]. website:. http://www.vishay.com/docs/84276/veml6040.pdf.

[11] S. Courroux, S. Guyetant, S. Chevobbe, and M. Paindavoine. A wavelet-based demosaicking algorithm for embedded applications. In *Conference on Design and Architectures for Signal and Image Processing (DASIP)*, 2010.

[12] K. Dabov, A. Foi, V. Katkovnik, and K. Egiazarian. Image denoising by sparse 3-D transform-domain collaborative filtering. *IEEE Transactions on Image Processing*, 16(8):2080–2095, 2007.

[13] W. Dong, X. Li, L. Zhang, and G. Shi. Sparsity-based image denoising via dictionary learning and structural clustering. In *IEEE Conference on Computer Vision and Pattern Recognition (CVPR)*, pages 457–464, 2011.

[14] J. Driesen and P. Scheunders. Wavelet-based color filter array demosaicking. In *IEEE International Conference on Image Processing (ICIP)*, volume 5, 2004.

[15] E. Dubois. Lslcd algorithm performance on different sampling structures.[online]. website:. http://www.site.uottawa.ca/~edubois/SingleSensorImaging/Structure_comparison/.

[16] E. Dubois. Frequency-domain methods for demosaicking of Bayer-sampled color images. *IEEE Signal Processing Letters*, 12(12):847, 2005.

[17] E. Dubois. *The Structure and Properties of Color Spaces and the Representation of Color Images*. Morgan & Claypool Publishers, 1st edition, 2009.

[18] E.Dubois. Color filter array sampling of color images: Frequency-domain analysis and associated demosaicking algorithms. In Rastislav Lukac, editor, *Single-Sensor Imaging Methods and Applications for Digital Cameras*, chapter 7, pages 183–212. CRC Press, 2008.

[19] Fujifilm. FUJIFILM X-Pro1. [online]. website:. http://www.fujifilmusa.com/products/digital-cameras/x/fujifilm-x-pro1/features.

[20] B. K. Gunturk, Y. Altunbasak, and R. M. Mersereau. Color plane interpolation using alternating projections. *IEEE transaction on Image Processing*, 11(9):997–1013, 2002.

[21] B. K. Gunturk, J. Glotzbach, Y. Altunbasak, R. W. Schafer, and R. M. Mersereau. Demosaicking: color filter array interpolation. *IEEE Signal Processing Magazine*, 22(1):44–54, Jan 2005.

[22] J.F. Hamilton and J.T. Compton. Processing color and panchromatic pixels. *U.S. Patent No.: US8274715B2*, 2012.

[23] K. Hirakawa and T. W. Parks. Adaptive homogeneity-directed demosaicing algorithm. *IEEE transaction on Image Processing*, 14(3), 2005.

[24] M. Hirakawa, K. Xiao-Li and P. J. Wolfe. A framework for wavelet-based analysis and processing of color filter array images with applications to denoising and demosaicing. In *IEEE International Conference on Acoustics, Speech and Signal Processing (ICASSP)*, volume 1, 2007.

[25] G. Jeon and E. Dubois. Demosaicking of noisy Bayer-sampled color images with least-squares luma-chroma demultiplexing and noise level estimation. *IEEE Transactions on Image Processing,*, 22(1):146–156, 2013.

[26] G. M. Johnson and M. D. Fairchild. A top down description of S-CIELAB and ciede2000. *Color Research Application*, 28(6):425–435, 2003.

[27] R. W. B. Kolta, H. A. Aly, and W. Fakhr. A hybrid demosaicking algorithm using frequency domain and wavelet methods. In *International Conference on Image Information Processing (ICIIP)*, 2011.

[28] B. Leung, G. Jeon, and E. Dubois. Demosaicking of noisy Bayer-sampled color images with Least-Squares luma-chroma demultiplexing and noise level estimation: Additional results.[online]. website:. http://www.site.uottawa.ca/~edubois/lslcd/.

[29] B. Leung, G. Jeon, and E. Dubois. Least-squares luma chroma demultiplexing algorithm for Bayer demosaicking. *IEEE Transactions on Image Processing*, 20(7):1885–1894, 2011.

[30] X. Li, B. K. Gunturk, and L. Zhang. Image demosaicing: A systematic survey. *International Society for Optics and Photonics*, pages 68221J–68221J, 2008.

[31] R. Lukac and K. N. Plataniotis. Single-sensor camera image processing. In Rastislav Lukac, editor, *Color image processing: methods and applications*, chapter 16, pages 363–392. CRC press, 2006.

[32] D. Menon and G. Calvagno. Color image demosaicking: an overview. *Signal Processing: Image Communication*, 26(8):518–533, 2011.

[33] F. Moghareh Abed. Pigment identification of paintings based on Kubelka-Munk theory and spectral images. *PhD Thesis. Rochester Institute of Technology*, 2014.

[34] T. K. Moon and W. C. Stirling. *Mathematical methods and algorithms for signal processing*. Prentice Hall, Upper Saddle River, NJ, 2000.

[35] M. Nawrath and J. Jakel. Deriving color images from noisy Bayer data using local demosaicking and non-local denoising. In *International Conference on Image and Signal Processing (CISP)*, volume 2, pages 668–672, 2011.

[36] R. Niruban, T. Sree Renga Raja, and T. Sree Sharmila. Novel color filter array demosaicing in frequency domain with spectral refinement. *Jurnal of Computer Science*, 10:1591–1599, 2014.

[37] Ch. Poynton. Macbeth Color Checker.[online]. website:. http://www.poynton.com/notes/color/GretagMacbeth-ColorChecker.html.

[38] M. Rafinazari and E. Dubois. Demosaicking algorithm for the fujifilm X-Trans color filter array. In *IEEE International Conference on Image Processing (ICIP)*, 2014.

[39] M. Rafinazari and E. Dubois. Demosaicking algorithm for the Kodak-RGBW color filter array. *in Proc. Color Imaging XXI: Displaying, Processing, Hardcopy, and Applications,Electronic Imaging-SPIE*, 9395, 2015.

[40] M. Rafinazari and E. Dubois. Demosaicking algorithms for different RGBW color filter arrays. *in Proc. Color Imaging XXI: Displaying, Processing, Hardcopy, and Applications,Electronic Imaging-SPIE*, 9395:COLOR–312.1–6, 2016.

[41] S. Sari, H. Roslan, and T. Shimamura. Noise estimation by utilizing mean deviation of smooth region in noisy image. *International Conference on Computational Intelligence, Modelling and Simulation*, 2012.

[42] Sony. Sony-RGBE. [online]. website:. http://www.dpreview.com/articles/1471104084/sonyrgbeccd.

[43] H. P. Sung, S. K. Hyung, S. Lansel, M. Parmar, and B. A. Wandell. A case for denoising before demosaicking color filter array data. In *Asilomar Conference on Signals, Systems and Computers*, pages 860–864, Nov 2009.

[44] C. Tomasi and R. Manduchi. Bilateral filtering for gray and color images. *International Conference on Computer Vision*, 1998.

[45] J. Wang, Ch. Zhang, and P. Hao. New color filter arrays of high light sensitivity and high demosaicking performance. *IEEE International Conference on Image Processing (ICIP)*, pages 3153–3156, 2011.